High Spin States Excited by (α,d) Reactions on 1f-2p Shell Nuclei

Kenji Okada

//

Abstract:

The high spin states in the 1f-2p shell doubly-odd nuclei have been investigated by (α,d) reactions on ^{50}Ti, ^{52}Cr, ^{54}Fe (N=28) and ^{56}Fe (N=30) by using 23.9 MeV alpha particles provided from the OULNS cyclotron. Outgoing particles from the reaction were detected by a counter telescope consisting of a ΔE(60 μm) and an E(700 μm) silicon surface barrier detectors. Angular distributions of deuterons were measured from 15° to 85° for the ^{50}Ti target, from 15° to 100° for the ^{52}Cr target and from 15° to 110° for the iron targets in 5° step.

The (α,d) reactions induced by medium energy (E_α=40~50 MeV) alpha particles are known to excite preferentially stretched configuration states with $(j_p j_n)_{J_{max}}$. In all the present (α,d) reactions two levels at Ex~0.5 and ~4.5 MeV were populated intensely. Thus the present work showed that the striking selectivity of the (α,d) reaction mentioned above is still maintained even with the relatively low energy projectiles (E_α≈25 MeV). Their excitation energies are 0.020 ±0.020 and 4.32 ±0.03 MeV in ^{52}V, 0.363 ±0.010 and 4.72 ±0.02 MeV in ^{54}Mn, 0.576 ±0.010 and 4.99 ±0.02 MeV in ^{56}Co and 0.020 ±0.02 MeV in ^{58}Co. The angular distributions have been analyzed by a zero-range DWBA calculation to assign a transferred orbital angular momentum(L) and to obtain an absolute cross section for a $[\pi(\ell_p j_p)\nu(\ell_n j_n)]_{LJ}$ transfer. The states with the lower excitation energies have been identified to have a common configuration of $[\pi f_{7/2}^n \nu p_{3/2}]$ with the spin 5^+ resulting from the stretched coupling of the $1f_{7/2}$ proton with the $2p_{3/2}$ neutron. The states with the higher excitation energies have been newly assigned to be 8^- states with a common $[\pi f_{7/2}^n \nu g_{9/2}]$ configuration. The assignments were based on the DWBA fits

of L=4 and L=7 transfers for the two members, respectively, and the absolute cross sections. The (α,d) reaction Q-values and the cross sections for these strongly excited states at the lower and higher excitation energies decrease with increasing the atomic numbers. The DWBA calculations and the shell model analyses for these states revealed that the proton transfer into the $1f_{7/2}$ shell orbit was essential for both the lower and higher states to explain these systematics.

The preferential excitation of the high spin states at 23.9 MeV projectiles have been explained in terms of an angular momentum matching condition (L_m=4~7 $\hbar$) among the participants of the reaction and a large geometrical factor for the stretched angular momentum coupling in the (α,d) reaction.

A two-body residual interaction energy for the state with J=8 and an average interaction energy of the $[\pi f_{7/2}{}^{\nu}g_{9/2}]_J$ configuration are deduced to be -0.76 and -0.73 MeV, respectively. The results are compared with calculations employing a δ-force interaction including a spin exchange term (-1.42 and -0.69 MeV) and with matrix elements of other configurations calculated by Kuo and Brown (~-0.90 and ~-0.70 MeV). The somewhat small value of -0.76 MeV may be due to unaccurate $1g_{9/2}$ single neutron energies in the N=29 odd mass nuclei.

Contents

		page
§ 1.	Introduction	1
§ 2.	Review of previous works	6
§ 3.	Experimental procedures	12
§ 4.	Experimental results	16
4-1)	$^{54}Fe(\alpha,d)^{56}Co$ reaction	16
4-2)	High spin states	17
§ 5.	DWBA analysis	19
5-1)	Configurations of levels excited by the (α,d) reaction	19
5-2)	DWBA theory for (α,d) reaction	22
5-3)	Comparison with experiments	26
5-4)	Other excitation processes	30
§ 6.	Discussion for $^{54}Fe(\alpha,d)^{56}Co$ reaction	34
§ 7.	Highest spin states with configurations of $[\pi f_{7/2}^{n}\nu(\ell j)]$	43
7-1)	General considerations	43
7-2)	Excitation energies of the high spin states	46
7-3)	Angular distributions and cross sections	49
	(i) 5^+ states	49
	(ii) 8^- states	56
7-4)	Residual interaction energy of $[\pi f_{7/2}\nu g_{9/2}]_{8^-}$	65
§ 8.	Summary and conclusions	74
	Acknowledgements	79
	References	80
	Appendix	85
	Figure captions	88
	Figures	
	Tables	

§ 1. Introduction

Various types of direct nuclear reactions have been used to study nuclear structures and nuclear reaction mechanisms. The reactions are conventionally classified into several groupes depending on a number of transferred nucleons. They are inelastic scattering, charge exchange, one-nucleon transfer, two-nucleon transfer and three or more- nucleon transfer reactions. The transfer reactions are normally subdivided into stripping and pick-up reactions. It has been known that each of these reactions has its own characteristics in a way to excite a nuclear state. Therefore, levels excited strongly by a given reaction must have the property which is characteristic of the reaction.

Levels populated by one-nucleon transfer reactions have, as a main component, a single particle or a single hole nature of a shell model depending on a stripping or a pick-up reaction, respectively. An angular distribution of the one-nucleon transfer reaction is characterized essentially by the orbital angular momentum carried by the transferred nucleon. A distorted wave Born approximation (DWBA) analysis[1)] has successfully explained the shapes and the magnitudes of the differential cross section. Then, valuable spectroscopic properties such as spins, parities and spectroscopic factors have been extracted for a vast number of nuclear levels in odd mass nuclei.

On the other hand, two-nucleon transfer reactions have recieved relatively little attention up to about ten years before. The reasons are considered to be due to some difficulties in analysis

and interpretation of the experimental results and an experimental difficulty to measure small reaction cross sections. Since formulations of the theory of direct two-nucleon transfer reactions have been given by several authors[2,3,4], however, the two-nucleon transfer reactions have become a powerful tool to investigate a nuclear structure as similar as the one-nucleon transfer reactions. The two-nucleon transfer reactions generally have following features. The reactions can excite nuclear levels which can hardly be studied by other reactions. The reaction excites selectively characteristic levels compared with the one-nucleon transfer reaction. The selective nature is due to strict selection rules of the reaction and also to correlations introduced by an angular momentum coupling between the transferred two nucleons.

The most extensively studied and well analyzed reactions are two neutron transfer (p,t)[5,6] and (t,p)[7] reactions. From these reactions a pairing correlation was found to be important in even-even nuclei. Proton-neutron transfer reactions such as (^{3}He,p)[8,9], (p,^{3}He)[10,11], (α,d)[12,13] and (d,α)[14,15] reactions have mainly been used to investigate nuclear structures of doubly-odd nuclei, because the doubly-odd nuclei can easily be reached by the p-n pair transfer into even mass nuclei of spin zero. Although a strong collectivity as seen in the (p,t) and (t,p) reactions, has not been observed in the p-n pair transfer reactions so far, some interesting behaviors have been found in the (^{3}He,p) and (α,d) reactions. Both the (^{3}He,p) and (α,d) reactions transfer a p-n pair to a target nucleus and both reaction mechanisms are considered to be similar with each other,

however, levels excited by the two reactions are not always the same [12,16,17,18]. Usually the (^{3}He,p) reactions have been used to search for 1^+ and 0^+ levels which were formed by an L=0 orbital angular momentum transfer[9,16,19]. States with spins higher than $J \geq 4$ have only weakly excited in these (^{3}He,p) reactions. While (α,d) reactions have excited preferentially high spin states[20,21,22,23]. The pioneering study on the (α,d) reaction performed by Rivet et al[21]. have suggested that the most strongly populated states are those in which the captured proton and neutron enter the same shell states and couple to the maximum angular momentum. In our previous study on ^{51}V(α,d)^{53}Cr reaction[24] a $g_{9/2}$ single particle state has been excited strongly via a $[\pi f_{7/2} \nu g_{9/2}]$ transfer.

Just as for single nucleon transfer reactions, the angular distribution for two-nucleon transfer reactions is also characterized by an orbital angular momentum carried by the nucleon pair. In this case many different configurations of the two-nucleon pair can contribute in a given angular momentum transfer. Then the cross section of the two-nucleon transfer reaction is sensitive to the configuration mixing of the level involved. But transitions to high spin states are expected to proceed via a transfer of a pure configuration, because the configurations which can form the high spin are limitted in a given configuration space.

In the present work ^{50}Ti(α,d)^{52}V, ^{52}Cr(α,d)^{54}Mn, ^{54}Fe(α,d)^{56}Co and ^{56}Fe(α,d)^{58}Co reactions are used to study structures of doubly-odd nuclei. Except for ^{56}Fe target nucleus, all other nuclei are characterised by a neutron number N=28. These targets were chosen by following reasons. The N=28 targets and N=29 residual nuclei

of the (α,d) reactions are considered to be well described in terms of shell model wave functions. An excitation of high spin states with configurations $[\pi f_{7/2}^{n} \nu(\ell j)]$ is expected in the (α,d) reaction at even a rather low alpha particle energy of 24 MeV. Negative parity states have not been found in the 1f-2p doubly-odd nuclei. Theoretical predictions of the level structure in terms of the shell model are available for the low-lying states of these nuclei.

The porpose of the present work is summarized in following five items.

(i) To find high spin states of the doubly-odd nuclei in the 1f-2p shell region by means of the (α,d) reaction

(ii) To find negative parity states with $[\pi f_{7/2}^{n} \nu$ g,d,s] configurations

(iii) To explain a preferential excitation of high spin states in the (α,d) reaction in terms of reaction kinematics and an angular momentum coupling among the target and residual nuclei and the transferred two nucleons

(iv) To extract an effective two-body interaction energy from a systematics of excitation energies of the high spin states

(v) Finally to demonstrate an usefulness of the (α,d) reaction in a research on a nuclear spectroscopy .

An introductory review of previous works on N=29 doubly-odd nuclei is presented in next chapter. Detailes of experimental procedures are described in chapter 3. In chapter 4 experimental results of the (α,d) reactions are shown. Methods of theoretical analyses employing the DWBA calculations and two-step calculations are described in chapter 5. To demonstrate a validity of the DWBA calculations and to show a consistency of the present results with previous works, levels of ^{56}Co nucleus are discussed individually in chapter 6. In chapter 7 detailed analysis and discussion on assignments of the high spin states are presented and reasons of a preferential excitation of the high spin states by the (α,d) reactions are discussed. Also an extraction of a two-body interaction energy is presented in that chapter. Summary and conclusions are given in chapter 8.

$ 2. Review of previous works

Doubly-odd nuclei with N=29 have been investigated more by two-nucleon transfer reactions than by one-nucleon transfer reactions. This is because firstly few stable target nuclides are available to reach the doubly-odd nuclei by one-nucleon transfer reactions. Secondly because of the large spin of an odd mass target nucleus in the present mass region ($7/2^-$ for proton odd and $3/2^-$ for neutron odd nuclei), it is very difficult to determine a spin of a residual state unambiguously by one-nucleon transfer reactions. On the other hand two-nucleon transfer reactions on even mass nuclei ($J^\pi = 0^+$) can restrict a spin of a final state to a few limitted values. In some special cases, moreover, a spin-parity can uniquely be determined by selection rules of the reaction.

In this chapter experimental works on the doubly-odd nuclei with N=29 (^{50}Sc, ^{52}V, ^{54}Mn and ^{56}Co) performed so far are reviewed briefly.

^{50}Sc

The ^{50}Sc nucleus cannot be studied by one-nucleon transfer reactions because of no stable isotopes used for target. The level structure of the ^{50}Sc has been investigated by two-nucleon transfer ^{48}Ca(^{3}He,p)[16,25,26] and ^{48}Ca(α,d)[18] reactions. Ohnuma et al.[25] have studied the low-lying states of ^{50}Sc by the (^{3}He,p) reaction at 12 MeV ^{3}He particle energy and have assigned the levels up to 3.259 MeV excitation on the basis of shell model wave functions given by Kuo and Brown. Laget et al[26]. have also investigated the levels

up to 6.285 MeV excitation by the (^{3}He,p) reaction at 18.5 MeV incident energy. They have only deduced angular momentum transfers. Fleming et al.[16] have studied ^{50}Sc in order to find $J^\pi = 1^+$ states which may give information on a p-n pairing interaction. They have found seven 1^+ states up to 5 MeV excitation and have pointed out that a large 1^+ strength could not be explained by a calculation within a 1f-2p shell model configuration space. Engeland and Osnes[27] have analyzed their data on the basis of the shell model calculation including both 1f-2p and 3s-2d-1g shells, and the strength of the 1^+ levels was still below the experimental value.

The ^{48}Ca(α,d) reaction has been studied using 31 MeV alpha particles by Moazed et al.[18]. The states below 2.5 MeV excitation have been compared with a DWBA calculation. Though they have not analyzed the levels above 3 MeV excitation , they have observed the most prominent peak at 4.42 Mev which has only weakly been excited by the (^{3}He,p) reactions. This 4.42 MeV level was studied in this article.

^{52}V

An energy level scheme of the low-lying states of ^{52}V has been determined mainly by means of (d,p)[28,29,30,31] and (n,γ)[32] reactions on ^{51}V. Assignments of an orbital angular momentum transfer (ℓ_n) have been done up to 3.65 MeV excitation energy by Catala et al.[31]. Almost all levels observed have been populated through a neutron transfer with ℓ_n=1. Some levels have been fed

by a neutron transfer of ℓ_n=2 or ℓ_n=3 with small cross sections. Two negative parity states have been observed at around 3.5 MeV excitation by ℓ_n=2 transfers.

$^{50}Ti(^3He,p)^{52}V$ reactions have been performed by Hardie et al.[33] at 17 MeV ^3He energy and by Caldwell et al.[34] at 15 MeV. They have measured angular distributions of the levels up to 8.838 Mev excitation. Their attentions have been paid to the states populated through L=0 or L=0, 2 transfers to investigate the 1^+ states of ^{52}V and 0^+ isobaric analogue and anti-analogue states of ^{52}Ti ground state. In the (^3He,p) reactions states of spins larger than 3 units have not been observed except for a 4^+ state at 0.442 MeV. This selective excitation of the low-spin states is mainly come from the low-energy of the incident ^3He particles.

No (α,d) reactions on ^{50}Ti have not been done yet.

^{54}Mn

The ^{54}Mn nucleus is the most extensively examined one by various reactions among the N=29 doubly-odd nuclei. Bjerregaard et al.[30] have determined level energies of ^{54}Mn up to 2.2 MeV by a ^{56}Fe(d,α) reaction . Hjorth[13] has measured the (d,α) angular distributions for the states up to 4.33 MeV excitation and has deduced spectroscopic factors of the two-nucleon transfer reaction by DWBA analysis. Lynn et al.[35] have studied ^{54}Mn by $^{52}Cr(^3He,p)$ at 11 MeV and $^{53}Cr(^3He,d)$ at 10 MeV bombarding energies. The (^3He,d) reaction has populated levels up to an excitation energy of 5.56 MeV. Nine transitions with an ℓ_p=3 and a transition leading to 5.131 MeV

level with an ℓ_p=2 have been observed besides dominant ℓ_p= 1 transfers. A detailed study of the $^{52}Cr(^3He,p)^{54}Mn$ reaction has been performed by Betts et al.[17] at 16.5 MeV incident energy with 20 keV energy resolution. They have found eleven 1^+states up to 5.50 MeV in excitation energy and have concluded that the total transition strength to the 1^+ states is found to be about three times larger than that calculated in a configuration space of 1f-2p shells. The levels above 2.5 MeV excitation populated by the (^{3}He, p) reaction have not overlapped with the ones populated by the (d, α) reaction. This complemental excitation is quite natural because the (d,α) reaction excites hole states such as a $[\pi(f_{7/2})^5\nu(p_{3/2})^2(f_{7/2})^{-1}]$, while the (^{3}He,p) reaction excites particle states such as a $[\pi(f_{7/2})^4\pi(p_{3/2})^1\nu(p_{3/2},p_{1/2}$ or $f_{5/2})^1]$.

An investigation by $^{52}Cr(\alpha,d)$ ^{54}Mn reaction has been performed by Lu et al.[22] at an alpha particle energy of 50 MeV. They have assigned 9.47 MeV state to be 9^+ with a probable $[\pi g_{9/2}\ \nu g_{9/2}]$ configuration. Their 9^+ assignment was based on a Q value systematics of the (α,d) reactions on A=52~66 nuclei. Though a prominent peak has been observed at 4.70 MeV excitation , they have not comment on this level. The 4.70 MeV state has only weakly been seen in the (^{3}He,p) reactions. Other spectroscopic information on the low-lying states in ^{54}Mn has been extracted from $^{54}Fe(n,p)$[36] and $^{54}Cr(p,n)$[37] charge exchange reactions. Dickens[36] has investigated properties of levels in ^{54}Mn by using $^{54}Fe(n,p\gamma)$ reaction. He has proposed a set of unique J^π assignments for the lowest five excited states. Hill and Buccino[37] have also studied the lowest five states by $^{54}Cr(p,n\gamma)$ reaction.

^{56}Co

The ^{56}Co nucleus cannot be reached by single nucleon transfer reactions . However, this nucleus have been extensively studied by two-nucleon transfer reactions and charge exchange reactions, because the ^{56}Co is a very interesting nucleus from a shell model point of view. The levels of ^{56}Co is expected to be formed by a particle-hole coupling to a doubly magic nucleus ^{56}Ni.

Earlier studies on ^{56}Co have been restricted to measurements of gamma-rays from the 1.718 MeV state following to an electron capture in ^{56}Ni.[38,39,40,41,42] Therefore, information on states above the 1.718 MeV level have not been obtained. These experimental results led a necessity to consider a configuration mixing of two-particle two-hole components in the 1.718 MeV state.[43] Low-spin states in ^{56}Co have been studied by means of ^{54}Fe(^{3}He,p) reactions[8,9,14,44,45] at ^{3}He particle energies ranging from 12 MeV to 18 MeV. Laget et al.[44] have measured 28 angular distributions up to 5.495 excitation and have analyzed them by a DWBA calculation. The 3.613 and 4.451 MeV states which were strongly excited by the (^{3}He,p) reaction have been tentatively assigned to be members of multiplets belonging to a $[\pi f_{7/2}^{-2}\ \pi p_{3/2}\nu p_{3/2}]_{T=2}$ configuration. Caldwell et al.[9] have also measured (^{3}He,p) angular distributions for the states up to 6.545 MeV excitation and have made new 1^{+} assignments for several states above 3 MeV excitation. The 5.337 and 5.471 MeV states have been populated very strongly by the (^{3}He,p) reactions[9,44] but they have not been analyzed in their works. Either of the 5.337 or the 5.471 MeV state is probably the same

state that Lu et al.[22] have observed at 5.44 MeV excitation by ^{54}Fe (α,d) reaction at 50 MeV alpha particle energy. In the work they have found a very strong peak at 8.92 MeV excitation and have assigned to be 9^+, which is the highest spin formed from a $[\pi g_{9/2} \nu g_{9/2}]$ configuration. This 8.92 MeV state is one of the 9^+ members found in a series of (α,d) reactions on A= 52~ 66 nuclei[22].
Other strong transitions leading to the 4.98 and 6.56 MeV levels have not been referred at all. The former level is concerned in this article.

Another useful reaction to investigate the ^{56}Co nucleus is a ^{58}Ni(d,α) reaction. Many (d,α) works have been reported up to now[8,13,14,30,44,46]. Schneider et al.[14] have most extensively investigated this nucleus by using 17 MeV deuterons. They have determined excitation energies accurately for 80 levels in ^{56}Co and have proposed unique or possible two or three candidates of J^π value for 46 positive parity states up to 4.4 MeV excitation. Frascaria et al.[46] have studied maximum spin states excited by the (d,α) reaction at 80 MeV incident deuterons. They have identified 2.28 and 5.08 MeV states to be 7^+ with a $[f_{7/2}^{-2} p_{3/2}^{2}]$ configuration and to be 3^+ with a dominant $[d_{3/2}^{-2} p_{3/2}^{2}]$ configuration, respectively. This 5.08 MeV state should not be identical with the state strongly populated by the (α,d) reaction at 4.98 MeV excitation.

$ 3. Experimental procedures

The alpha particle beam of 24 MeV was provided from the 110 cm cyclotron at Osaka University. The layout of the beam transport line is shown in Fig.3-1. The beam extracted from the cyclotron was focussed by magnetic quadrupole lenzes and then deflected 35° by a switching magnet (SM). A beam energy analysing magnet (AM) with 90° deflecting angle led the beam to a 100 cm diameter scattering chamber. Two beam defining slits posisioned at a middle point between the SM and the AM (S3) and at just in front of the center of the scattering chamber (S4) defined beam energy within 50 keV FWHM. The widths of the S3 and the S4 were 1.6 mm and 2.0 mm, respectively.

Strength of the magnetic field in the AM was monitored by a proton resonance signal. The beam through a target was stopped in a Faraday cup in which a magnetic field was applied by a permanent magnet. The magnet suppressed escape of secondary emitted electrons from the Faraday cup. The beam current was integrated by a precision current integrator to obtain an absolute charge.

Targets used in the present work were ^{50}Ti, ^{52}Cr, ^{54}Fe and ^{56}Fe. All isotopically enriched samples were obtained from the Stable Isotope Division, Oak Ridge National Laboratory in the form of oxide powder. The titanium target was prepared by sputtering a mixture of a Ti_2O_3 powder and a tantalum powder by an electron bombardment. The tantalum powder served as a reducing agent. The chromium and the iron targets were prepared from Cr_2O_3 and Fe_2O_3 powders, respectively. A mixture of the Cr_2O_3 powder and a carbon powder which served as a reducing agent was heated in a graphite crucible in a vacuum. The

chemical process goes in the following way;

$$Cr_2O_3 + 3C \longrightarrow 2Cr + 3CO \ .$$

Grains of the chromium metal thus obtained was evaporated on a slide glass. The chromium foil on the slide glass was floated on deionized water and was scooped by a target frame. The iron oxide powder was reduced by carbon powder in the same way as the chromium. Then the metallic grade was evaporated on a thin carbon backing (30 $\mu g/cm^2$).

Thicknesses of these targets were determined from elastic scattering yields of 5.6 MeV protons at angles of 15°,20° and 25°, assuming the Rutherford scattering cross section there. Though the elastic protons scattered by the metallic target nucleus could not be resolved from those scattered by carbon and oxigen contaminant nuclei at the forward angles, the yields of the contaminants were estimated as follows and then they were subtracted. In order to obtain differential cross sections of the elastic scattering from C(p,p) and O(p,p) separately, we measured proton yields from a carbon and a myler targets at the same angle and the same energy as the metallic targets. Proton yields were also measured at 90°, where the elastic peaks from the metallic chromium, the carbon and the oxigen were well separated from each other. Then from these values we could subtract the elastic yields from the contaminant nuclei. It was found that the contributions to the yields from the contaminants were only 10 % at most. The target thicknesses thus determined are listed in Table 3-I. together with an isotopic purity of each target.

In the (α,d) reactions on 1f-2p shell nuclei, reaction Q-values are about -10 MeV and the Q-values for ^{12}C, ^{16}O and ^{14}N nuclei are -13.57, -16.32 and -3.11 MeV, respectively. So only deuteron peaks from the ground state transitions for ^{12}C and ^{16}O contaminants disturbed the present (α,d) reactions at some angles. Since the ground state Q-value of the (α,d) reaction on ^{14}N is not large negative and cross sections are quite large, the deuteron groupes from the very small amounts of nitrogen contaminant appeared overlapping with the peaks of the present concern at several angles. In order to subtract the contributions from the nitrogen contaminant the $^{14}N(\alpha,d)^{16}O$ reaction cross sections were measured at every angles in separate runs. The nitrogen target was prepared from adenine($C_5H_5N_5$) by evaporating on a thin alminum foil. Actually, the contributions of the nitrogen contaminant to the yields from the metallic nuclei were less than 10 % for all angles.

The $^{12}C(\alpha,d)^{14}N$ and the $^{14}N(\alpha,d)^{16}O$ reactions were used for a determination of excitation energies of the residual nuclei in the f-p shell since the Q-values and level energies of the ^{14}N and the ^{16}O are well known. The excitation energies of low-lying levels in all the residual nuclei thus obtained agreed with the values of previously reported within $\pm$30 keV.[14,17)]

Outgoing particles from the reaction were detected by a ΔE-E counter telescope consisting of a totally depleted 60 μm silicon ΔE and a 700 μm silicon surface barrier E detector. A angular width of the counter system was 1.15 degrees and a solid angle was 4.0×10^{-4}sr. A single counter of the silicon surface

barrier with 300 μm thick was placed backward by 17.5° from the telescope to obtain elastic angular distributions of alpha particles. To monitor the beam current and the target thickness, another silicon surface barrier counter was set on a wall of the scattering chamber at 30° in a laboratory angle. Any decrease of the target thickness was not observed throughout the experiment for all targets except for the adenine target.

A particle identification was made by a Goulding type particle identifier circuit[47] which employs a range-energy relation of charged particles . A typical spectrum of the identifier output is shown in Fig.3-2. Energy pulses gated by the identifier output pulses corresponding to deuterons and tritons were fed into a 4096 channels pulse height analyzer which was routed to four 1024 channel groupes. A block diagram of the circuit is shown in Fig.3-3. Overall energy resolutions of the (α,d) reactions were about 80 keV for ^{54}Mn peaks and about 90 keV for those of other nuclei.

Angular distributions of the deuterons from the (α,d) reactions were measured from 15° to 85° for the ^{50}Ti target, from 15° to 100° for the ^{52}Cr target and from 15° to 110° for the iron targets in 5° step.

§ 4. Experimental results

In this chapter experimental results obtained in the (α,d) reactions are presented. The data presented here are restricted only to those concerned with high spin states except for the ^{54}Fe(α,d)^{56}Co reaction. The angular distributions for the ^{54}Fe(α,d) reaction measured in the present work are shown for comparison with DWBA predictions.

4-1) ^{54}Fe(α,d)^{56}Co results

Fig.4-1 shows a typical energy spectrum of deuterons from the ^{54}Fe(α,d)^{56}Co reaction at θ_{LAB}= 50°. A number indicated above the peaks in the figure corresponds to a level number in Table 4-I. Measured 15 angular distributions below an excitation energy of 5.47 MeV are shown in Figs. 4-2-a,-b,-c and -d together with DWBA calculations grouped according to spin assignments. The absolute scale error in the differential cross sections was less than 15 % and was due to an uncertainty of the target thickness. Error bars shown are mainly due to statistical errors for low-lying levels, and those for higher excited states are statistical and background subtraction errors. The experimental results are summarized in Table 4-I as well as the L-value assignments from the DWBA analysis. They are also compared with the previous (d,α)[14] and (^{3}He,p)[44] results.

4-2) High spin states

Fig. 4-3 shows deuteron energy spectra for the $^{50}Ti(\alpha,d)^{52}V$, $^{52}Cr(\alpha,d)^{54}Mn$, $^{54}Fe(\alpha,d)^{56}Co$ and $^{56}Fe(\alpha,d)^{58}Co$ reactions at E_α=23.9 MeV. Peaks marked by single- and double-asterisks are levels to be treated circumstantially in the present article. Cross-hatched peaks in the spectra are impurity lines from the $^{12}C(\alpha,d)^{14}N$ reaction. The levels marked by a single-asterisk have been found in previous works[44,14] and their spins and parities have been confirmed or tentatively assigned to be 5^+. Excitation energies of these levels were 0.020 ± 0.020 Mev in ^{52}V, 0.363 ± 0.010 MeV in ^{54}Mn, 0.576 ± 0.010 MeV in ^{56}Co and 0.020 ± 0.020 MeV in ^{58}Co. For higher excitation members marked by a double asterisk, excitation energies were 4.32 ± 0.03 MeV in ^{52}V, 4.72 ± 0.02 MeV in ^{54}Mn, 4.99 ± 0.02 MeV in ^{56}Co and 3.75 ± 0.03 Mev in ^{58}Co. These higher excitation members have very weakly or not been populated by other reactions other than (α,d). In (α,d) reactions performed by Lu et al.[22] the 4.70 Mev state in ^{54}Mn, the 4.98 Mev state in ^{56}Co and 3.72 MeV state in ^{58}Co have most strongly been populated. But they have measured no angular distributions in their (α,d) works, and have not referred to these levels at all. Therefore, spins and parities of these strongly seen levels in the (α,d) reactions have not been assigned so far.

Angular distributions of deuterons leading to the lower excitation members are shown in Fig.4-4 and to the higher excitation members are shown in Fig.4-5. At the higher excitation region around $E_x \sim$ 5 MeV, where a level density is high, many peaks

weakly excited by the (α,d) reaction formed a continuum background. The cross section of higher excitation levels were obtained by desolving and subtracting unresolved peaks graphically. Here a shape of the peak was assumed to be same as the one observed for a low-lying singlet peak. Because the peaks of the present interest were very strong, errors due to the background subtraction were 10~15 % in the cross section for the ^{50}Ti(α,d) and ^{52}Cr(α,d) reactions and 15~20 % for the ^{54}Fe(α,d) and ^{56}Fe(α,d) reactions. They exceeded errors due to counting statistics considerably.

Angular distributions of elastically scattered alpha particles from ^{52}Cr and ^{54}Fe targets measured simultaneously in the (α,d) measurement are shown in Fig.4-6. These data were used to check whether optical potential parameters taken from literature can reproduce the elastic scattering cross section well or not. In separate experiment runs we measured deuteron elastic cross sections from ^{52}Cr at E_d= 11.3 MeV. The angular distribution is shown in Fig. 4-7.

§ 5. DWBA analysis

5-1) Configurations of levels excited by the (α,d) reaction

From a simple shell model point of view ground state wave functions of N=28 nuclei are described as $(1f_{7/2})^n$ proton configurations outside an inert ^{48}Ca core. Actually, experiments of single proton pick-up (d,^{3}He) reactions on N=28 nuclei[48] have revealed that the ground states of the nuclei are described quite well by the shell model wave functions except for the ^{54}Fe nucleus. For the ^{54}Fe ground state wave function, very small admixtures of $(1f_{7/2})^4(1f_{5/2})^2$ and $(1f_{7/2})^4(2p_{3/2})^2$ terms have been found besides the main $(1f_{7/2})^6$ configuration for protons. The spectroscopic factors for the $2p_{3/2}$ and the $1f_{5/2}$ states have been found to be about 4% of the total single particle strength. The (^{3}He,d) reactions have given some informations on hole components of 2s-1d shells in the N=28 nuclei. Experimental results of the reaction[49,50,51] have shown that the 2s-1d mixture in the target nuclei was very small amount and less than 2%. While a rigidity of the N=28 core has been investigated by single neutron pick-up and stripping reactions[52,53]. From the research for all N=28 nuclei, the 2p and the $1f_{5/2}$ components were less than 5% in the ground state wave functions. Therefore, it is quite good approximation to assume that the ground state of the even mass nuclei with N=28 are formed by a coupling of $(1f_{7/2})^n$ protons with the ^{48}Ca inert core.

Hence it is reasonable to expect that in the (α,d) reactions on the N=28 nuclei a proton will most likely be transferred to the $1f_{7/2}$ orbit and a neutron to one of the $2p_{3/2}$, $2p_{1/2}$ or $1f_{5/2}$ orbit.

These configurations give 12 positive parity states with spins ranging from 1^+ to 6^+. Levels formed by a coupling of a $2p_{3/2}$ proton to either a p or a f neutron may lie around 3 MeV in excitation energies. Also core excited states formed by $[(f_{7/2})^n (J) \otimes \pi(\ell j)\nu(\ell j)']$ configurations may appear as positive parity states at around 3 MeV in excitation energies. However these states are hardly excited by the direct (α,d) reactions , because the reaction does not destroy the ^{48}Ca core. If appreciable configuration mixing is realized between the single particle states and the core excited states , the (α,d) reaction can excite more levels other than those expected from the simple shell model picture. Shell model calculation based on a effective two-body interaction by Horie et al.[54] suggests that 70 levels in ^{54}Mn and 12 levels in ^{56}Co are formed in the configuration space of the $1f_{7/2}$ proton and the $2p_{3/2}$, $2p_{1/2}$ and $1f_{5/2}$ neutron shell orbits. Negative parity states in the N=29 nuclei are expected to appear at around 4 MeV excitation , though no theoretical calculations have been done to predict excitation energies of the negative parity states. Probably, they would be excited through a proton transfer to a $1f_{7/2}$ orbit and a neutron to a $1g_{9/2}$ orbit.

Allowed values of a spin and an isospin carried by the transferred two nucleons in the (α,d) reaction are

$S=1, \quad T=0.$

An n-n pair and a p-p pair in the incident alpha particle are coupled in ^{13}S state (spin singlet, isospin triplet and relative orbital angular momentum $\ell=0$) and a n-p pair in the alpha particle can couple to either ^{13}S or ^{31}S state. But only the S=1 part (spin triplet)

of the n-p pair in the alpha particle can contribute to the (α,d) reaction, since the outgoing deuteron has a spin 1 and an isospin 0. The selection rules of the direct (α,d) reaction on the 0^+ target allow at most two L (transferred angular momentum) values to contribute to an angular distribution, and specify uniquely a parity of a final state to $(-)^L$. For a transition which includes only one orbital angular momentum transfer, a spin parity J^π of a final state is $L-1 \leq J \leq L+1$, $\pi=(-)^L$, because the intrinsic spin transfer is unity in the (α,d) reaction. Therefore, natural parity states J^π with $\pi=(-)^J$ will be excited by an L=J transfer but unnatural parity states with a spin J and a parity $\pi=(-)^{J+1}$ by $L_>= J+1$ and $L_<= J-1$ transfers. If we observe the contribution of two L values ($L_<$ and $L_>$) for a single state, we can identify uniquely the final spin to $J=L_<+1$. In the most cases, however, it is difficult to uniquely assign the spin for an unknown residual level by using this characteristic feature of the (α,d) reaction, since the cross section proceeding through the lower L transfer is generally dominant. This is understood from a jj-LS transformation coefficient for relevant orbits. The values of the transformation coefficient for transfers of $[\pi f_{7/2}, \nu \ell j]_{LJ}$ pair in the reaction are listed in Table 5-I.

5-2) DWBA theory for (α,d) reaction

Here we consider a reaction of a type a+A⟶b+B , where a is an incident projectile and A is a target nucleus, while b denotes a outgoing particle and B is a residual nucleus. If a transferred cluster is symbolized by X for stripping reactions, then

$$b = a - X$$

$$B = A + X \ .$$

A transition amplitude is written by the distorted wave Born approximation theory (DWBA) as[1)]

$$T^{DW}=\int dr_{aA}\int dr_{bB}\chi_b^{(-)*}(r_{bB})\langle\phi_b\phi_B|V_{bX}|\phi_a\phi_A\rangle\chi_a^{(+)}(r_{aA}) \qquad (5\text{-}1)$$

,where $\chi^{(+)}$ and $\chi^{(-)}$ are center of mass wave functions of the incident and the outgoing particles distorted by optical potentials,respectively. The wave functions denoted by ϕ_i represents an internal motion of each nucleus i. The angular bracket means an integration over all the internal variables. V_{bX} is an interaction potential between the particles b and X. In terms of the transition amplitude, the differential cross section of the reaction is written as

$$\frac{d\sigma}{d\omega} = \frac{m_a^* m_b^*}{(2\pi\hbar^2)^2}\frac{k_b}{k_a}|T^{DW}| \qquad (5\text{-}2)$$

,where m_i^* is a reduced mass of the particle i and k_i is a wave number in channel i. For the internal wave function of the residual nucleus, a parentage expansion based on the target nucleus is introduced for the (α,d) reaction.

$$\phi_{\alpha_f I_f M_f}^{(A+2)} = \sum_{j_p j_n J} A(\alpha_f I_f; n_n \ell_n j_n n_p \ell_p j_p \ J; \alpha_i I_i)$$

$$X\ [\Psi_{(j_n j_p J)}\ \phi_{\alpha_i I_i}^{(A)}]_{\alpha_f I_f M_f} \qquad (5\text{-}3)$$

The parentage factor A(.....) can be obtained explicitly, if a shell model wave function for the residual nucleus is available. For a state with a pure configuration of the residual nucleus the parentage coefficient becomes a fractional parentage coefficient (cfp). The $\Psi_{(j_p j_n)J}$ is an antisymmetrized wave function of the transferred two nucleons. To calculate a form factor which is a center of mass motion of this wave function, the two nucleon wave function must be transformed to those of separated in the center of mass and the relative coordinates. The transformation can be made by transformation from j-j to L-S coupling schemes and then by using a Moshinsky bracket.[2)]

$$\Psi_{(j_p j_n)J} = \left(\frac{2}{1+\Delta_{j_1 j_2}}\right)^{1/2} \sum_{LS\tilde{n}\tilde{\ell}\tilde{N}\tilde{L}} \frac{1 + (-)^{\tilde{\ell}+S+\tilde{L}+1}}{2}$$

$$\times (1/2\ \ell_p(j_p)\ 1/2\ \ell_n(j_n), J | 1/2\ 1/2(S)\ \ell_p \ell_n(L), J)$$

$$\times \langle n_p \ell_p n_n \ell_n : L | \tilde{n}\tilde{\ell}\tilde{N}\tilde{L} : L \rangle \left| \left| \phi_{\tilde{n}\tilde{\ell}}(\tfrac{1}{2}\nu, r) \phi_{\tilde{N}\tilde{L}}(2\nu, R) \right|_L \chi_S \right|_{JM} \qquad (5\text{-}4)$$

Here, $\tilde{N}\tilde{L}$ and $\tilde{n}\tilde{\ell}$ are quantum numbers for the center of mass and the relative motion of the transferred pair, respectively. The radial wave function $\phi_{\tilde{N}\tilde{L}}$ of the center of mass motion is chosen to be a harmonic oscillator wave function. For the size parameter ν for a single particle state in a nucleus A use was made of the value[2)] $=0.96\ A^{-1/3}\ fm^{-2}$. $\Delta_{j\ j}$ is a Dirac delta function and $\langle \ldots | \ldots \rangle$ is a Moshinsky bracket. It is noted that adopting the zero-range DWBA theory the cross section is represented as an incoherent sum of the transferred angular momenta L and J, which can be written as

$$\frac{d\sigma}{d\omega} = \frac{2I_f+1}{2I_i+1} \frac{m_\alpha^* m_d^*}{(2\pi\hbar^2)^2} \frac{k_d}{k_\alpha} V_0^2 \qquad (5\text{-}5)$$

$$X \sum_{JLM} \left| \frac{1}{\sqrt{2L+1}} \int \chi_d^{(-)*}(k_d, \frac{A-2}{A} r) F_L(r) Y_{LM}(\hat{\theta}\phi) \chi_\alpha^{(+)}(k_\alpha, r) dr \right|^2 .$$

$F_L(r)$ is the form factor and Y_{LM} is the spherical harmonic function. In the equation (5-4), the most important term is $\ell=0$, because the relative motion between the transferred two nucleons is in S-state in the alpha particle.

The form factor in the equation 5-5) is written explicitly[2] as

$$F_L(r) = \sum_{\tilde{N}} B^*(\alpha_f I_f : S=1\ \tilde{N}\tilde{L}\tilde{n}0\ ; L, J; \alpha_i I_i)$$

$$X\ (A/(A-2))^{\tilde{N}-1+L/2}\ a_{\tilde{n}}\ \phi_{\tilde{N}\tilde{L}}(2(A-2)\nu/A, r) \ . \qquad (5\text{-}6)$$

The $a_{\tilde{n}}$ is a normarization factor when the zero-range approximation is taken for the interaction. The coefficient B is expressed as,

$$B = \sum_{\tilde{n}\tilde{N}\tilde{L}} \sqrt{N_p N_n}\ A(\alpha_f I_f; n_n \ell_n j_n n_p \ell_p j_p\ J;\ \alpha_i I_i)$$

$$X\ (1/2\ \ell_p(j_p)\ 1/2\ \ell_n(j_n), J \,|\, 1/2\ 1/2(S)\ \ell_p \ell_n(L), J)$$

$$X\ \langle n_p \ell_p n_n \ell_n : L \,|\, \tilde{N}\tilde{L}\tilde{n}0 : L \rangle \ . \qquad (5\text{-}7)$$

N_p and N_n are the number of protons and neutrons in the $(n_p \ell_p j_p)$ and $(n_n \ell_n j_n)$ orbits of a residual nuclear state. The factor $\sqrt{N_p N_n}$ comes from the antisymmetrization of the wave function.

The (α,d) specrroscopic factor for a transition of a $[\pi(\ell_p j_p)\nu(\ell_n j_n)]$ pair with angular momentum transfers of L and J is defined as

$$S(\alpha_i I_i; lLJ; \alpha_f I_f) = \sum_{\tilde{N}} \Big| \sum_{\tilde{n}} B(\alpha_i I_i : l\tilde{N}\tilde{L}\tilde{n}0 \; ; L,J; \alpha_f I_f) \left(\frac{A}{A-2}\right)^{\tilde{N}-l+L/2} a_{\tilde{n}} \Big|^2 . \tag{5-8}$$

In table 5-I the spectroscopic factors for pure configurations are tabulated together with the j-j to L-S transformation coefficients.

5-3) Comparison with experiments

The DWBA cross sections were computed with a zero-range code 'DWUCK'[55]. The two-particle form factor calculations were carried out with a code 'TWOFF'[56]. The experimental (α,d) cross section is related to the DWBA prediction as,

$$d\sigma/d\omega)_{exp.} = 4N \frac{2I_f+1}{2I_i+1} \frac{V_0^2}{10^4} \sum_{LJ} \sigma_{LJ}^{DW} /(2J+1) \quad , \qquad (5\text{-}9)$$

where a V_0 is an average interaction strength between the deuteron and transferred two nucleons.[2] A numerical factor 4 in the equation comes from a parentage expantion of a light nucleus and means a number of ways to break up an alpha particle into two deuterons. A factor 10^4 in the denominator is a square of an interaction strength employed in the code 'DWUCK'. I_i and I_f are the ground state spin of the target and the final state spin of the residual nucleus, respectively. L and J are orbital and resultant angular momenta carried by the transferred p-n pair. For reactions on spin zero nuclei (I_i=0), the relation (5-9) becomes simple, because a transferred total angular momentum should be equal to a final state spin. Then we get

$$d\sigma/d\omega)_{exp.} = 4N \frac{V_0^2}{10^4} \sum_{L} \sigma_{LJ}^{DW} \qquad (5\text{-}10)$$

Two conbinations of alpha and deuteron optical potential sets were tried as shown in Table 5-II in the present analysis. The set given by the A1 and D1 in the table is the same as used previously[60]. They are directly from the work of McFadden and Satchler for an alpha channel (A1)[57] and of Daehnick and Park for a deuteron channel (D1)[59]. Another optical potential set (A2,D2) was essentially

taken from the work of Schneider et al.[14] This set gave the best predictions in the analysis of the $^{58}Ni(d,\alpha)^{56}Co$ reaction at E_d=14 MeV, but was not the ones to reproduce the elastic scattering angular distributions best. Schneider et al.[14] suggested for reactions with a large angular momentum mismatch such as (d,α) and (^{3}He,α) reactions that the best elastic scattering parameters were not necessarily be best for those transfer reactions but one should use such potential parameters as to satisfy $V_b + V_X \approx V_{b+X}$, where b is the lighter projectile and X the transferred particle. This has been called 'well matching method '. We modified slightly the real well depth in their alpha channel parameters from 191.9 MeV to 182 MeV in order to improve DWBA fits for L=0 and 2 transfers. The optical potential parameters are listed in Table 5-II. Elastic scattering angular distributions of alpha particles obtained with the A1 and A2 parameters are shown in Fig.4-6 by solid and dashed lines, respectively. The A1 potential reproduced the experiments fairly well, while the A2 could not reproduce the deep minima of the experiments.

DWBA calculations with the A1-D1 set combined with a form factor solved in a Woods-Saxon potential of r=1.27 fm and a=0.55 fm (FF1) gave satisfactory results for L = 4, 6 and 7 transfers as shown in Fig.4-2-c by solid lines. But for small L transfers (L = 0 and 2) the A1-D1 set gave poor agreement between the predictions and the experiments. For L=0 transfers the predictions gave a too exaggerated pattern. And positions of maxima and minima of the diffraction shape shifted backward by 5°. For L=2 transfers the phase relation was good but a striking oscillatory pattern seen in the experimental

L=2 transfers could not be reproduced. This poor agreements for the L=0 and 2 may be attributed to the large angular momentum mismatch of the (α,d) reaction.

(^{3}He,α) reactions, like (α,d) , had also a large momentum mismatch. Stock et al.[61] have pointed out in their analyses of (^{3}He,α) reactions on chromium isotopes that the angular momentum mismatch make the nuclear interior contribute significantly to the reaction. To clarify this in the (α,d) case , reflection coefficients ($|\eta_\ell|$) for the alpha and deuteron partial waves at 23.9 MeV incident alpha particle energy and Q-values of -11 MeV(E_x=0.0 MeV) and -16 MeV (E_x=5 MeV) are shown in Fig.5-1. Only the partial waves in a region $|\eta_\ell| \sim$ 0.5 contribute to the elastic scattering cross section and are determined well by the elastic cross section fitting procedure. In the present case, for Q=-11 MeV the well determined partial waves were $\ell_\alpha \sim$ 11-13 ħ and $\ell_d \sim$ 6-8 ħ and for Q= -16 MeV $\ell_d \sim$ 4-5 ħ. Therefore, if the (α,d) reaction cross section of a given angular momentum transfer is mainly due to partial waves beyond this limits, the (α,d) angular distribution so obtained may not explain the experiments. In the lower part of Fig.5-1 overlap integrals for L=6 and L=0 transfers of the (α,d) reaction are shown. A radial overlap integral ($F_{SLJ}(\ell_\alpha \ell_d)$) are represented by a product of a form factor and partial waves of incident and exit channels. For simplicity, only a case of $\ell_\alpha - \ell_d$= L is shown. For the L=6 transfer, the overlap integrals of large values were located around $\ell_\alpha \sim$ 11 ħ and $\ell_d \sim$ 5 ħ, where the partial waves were well determined. While, for the L=0 transfer almost all the partial waves

in the range $0 \leq \ell_\alpha \leq 8\ \hbar$ contributed. In the latter case, the transferred p-n pair did not fill the gap between the angular momenta brought by the entrance and exit channels. In the actual cases, combinations to satisfy $\vec{\ell}_\alpha + \vec{\ell}_d = \vec{L}$ in the overlap integrals can be allowed. Then so extreme difference mentioned above did not realize.

DWBA predictions obtained with the A2-D2 set with FF2 form factor (r=1.35 fm and a=0.75 fm) are shown in Fig.4-2-a,-b,-c by dashed lines. For L=0 and 2 the A2-D2 gave considerable improvements. Particulary for an L=0 transfer to the 1.72 MeV state the agreement was almostly perfect. However, for large L transfers a slight deterioration of the predictions was seen. As a whole, the agreements between the theory and experiment were better in the A2-D2 set than in the A1-D1 set. In spite of the superiority of the A2-D2 set, we will employ the A1-D1 set for the following DWBA analysis. This is because the (α,d) normarization factor N in the equation (5-9) has been determined for the A1-D1 potentials previously by Kawa[60]. And for another, levels to be treated here are restricted to high spin states.

The empirical normarization factor of the (α,d) analysis using the Lin-Yoshida's form factor has been extracted from the previous $^{51}V(\alpha,d)^{53}Cr$ reaction[60] (N=73~130). In the Lin-Yoshida's formalism, the factor $V_0 a_{\tilde{n}}^{2}$ corresponds to the usual zero-range interaction strength D_0. The $a_{\tilde{n}}$ is an overlap integral of the wave functions for the relative motion of the two-nucleons in the incident alpha particle and of the transferred two-nucleons in the residual nucleus. For the 1f-2p shell nuclei the $a_{\tilde{n}=0}$ is about 3 $fm^{3/2}$. So the square of the empirical interaction strength thus obtained is about 10^6 $MeV^2 fm^3$. Here, we employ this value for the DWBA analysis.

5-4) Other excitation processes

In the present analysis, we assume that the (α,d) reaction proceeds via a direct one-step process. If this assumption would not right the present spectroscopic results would not be reasonable. So, we will discuss on a possibility of other reaction mechanisms of the (α,d) reaction at 23.9 MeV alpha particle energy. Possible reaction processes considered are two-step processes of sequential nucleon transfer (α-t-d) and (α-^{3}He-d) channels and a compound nuclear process besides the direct process. They are shown schematically in Fig. 5-2 by a double, dashed and solid lines, respectively.

A compound state of ^{58}Ni formed by a ^{54}Fe + alpha(23.9 MeV) system lies at 28.7 MeV in excitation energy. This is higher by 20.5 MeV and 16.5 MeV than threshold energies of a proton and a neutron emissions, respectively. While a threshold energy of a deuteron emission is 17.3 MeV and is 5.1 MeV higher than that of the neutron emission. Therefore, a proton and a neutron emission may occur in advance of a deuteron emission. Moreover, it is well known that loosely bound composite particles like a deuteron are hardly emitted from a compound nucleus. Actually following experimentally observed facts imply that a contribution to the (α,d) cross sections from a compound nuclear process is negligibly small.

(i) The angular distributions of small L transfers showed characteristic diffraction patterns,which indicate a direct process. (see Fig.4-2-a,-b)

(ii) In our previous (α,d) reaction on ^{51}V at an alpha particle energy of 22.0 MeV, angular distributions measured from 15°

to 130° in a laboratory system showed assymmetric patterns with respect to the 90° center of mass axis. They are shown in Fig.5-3.

(iii) Levels known as neutron hole states were not excited in the present (α,d) reactions at all. They have been most strongly excited by (d,α) reactions at 2.281 MeV in ^{56}Co and at 2.646 MeV in ^{58}Co reactions[14,70] and have been assigned to be 7^+ with configurations of $[\pi f_{7/2}^{-1}\ \nu f_{7/2}^{-1}]$.

(iv) In a series of (α,d) reactions on N=28 nuclei strong target dependences were observed in the cross sections to 5^+ and 8^- transitions. This will be discussed in § 7.

All the above mentioned facts come into conflict with what one would expect for the reaction proceeds via a compound process. Then a contribution to the (α,d) cross sections from the compound process was estimated to be less than a few μb/sr at most.

Two-step process

Two-step processes are much important for transitions which are forbidden by some reasons in a direct one-step process. Also for two-nucleon transfer reactions the two-step processes have a possibility to play an important role, because cross sections of the two-nucleon transfer reactions are generally small compared with those of one-nucleon transfer reactions.

In the present two-step analysis, we considered successive nucleon transfer (α-^{3}He-d) and (α-t-d) processes. We chose as intermediate states the ground state of ^{55}Co and single particle states of $p_{3/2}$ and $g_{9/2}$ shell orbits in ^{55}Fe for each process.

For the ^{55}Co intermediate states only the $f_{7/2}$ ground state was chosen because in ^{54}Fe(α,t)^{55}Co spectra which were measured at the same time with the present ^{54}Fe(α,d) measurement, only the ground state was strongly populated. Cross sections of other levels were as small as those of the (α,d) reaction.

We analyzed the present ^{54}Fe(α,d)^{56}Co reaction data of two transitions leading to 5^+ at 0.576 and 8^- state at 4.99 MeV. These transitions are allowed by the direct one-step process and were very strongly populated. Two-step calculations were carried out using a computer code 'TWOSTP' developed by Toyama and Igarashi[62]. Formalism of the two-step processes are based on a Green-function iteration method by Toyama[63,64]. The transition matrix is given separately for the one- and two-step processes as,

$$T = \langle \hat{\phi}^{(-)}_{M_f M'_f} | \left(\hat{V}_f + \hat{V}_f \frac{1}{E-H+i\varepsilon} \hat{V}_i \right) | \hat{\phi}^{(+)}_{M_i M'_i} \rangle = T^{(1)} + T^{(2)} \qquad (5\text{-}11)$$

, where suffixes M_f, M'_f, M_i and M'_i represent the magnetic quantum numbers of the residual , the emitted particle, the target and the projectile, respectively. Wave functions denoted by $\hat{\phi}^{(\pm)}_{MM'}$, mean the distorted waves including intrinsic spin function for incident and exit channels. $\hat{V}_i$ and $\hat{V}_f$ are the residual interactions which cause transitions at incident and exit channels, respectively. An operator $1/(E-H+i\varepsilon)$ describes a propagation of an intermediate particle. The first term in equation (5-11) is a transition matrix of an ordinary one-step DWBA and the second term is a second order Born approximation transition matrix element. A calculation of the second term can be carried out by using a Green function[63].

Optical potential parameters for entrance and exit channels used in the two-step calculations were the same ones employed in the direct (α,d) analysis(A1-D1). For both triton and ^{3}He channels, we used optical potential parameters with which previously measured ^{51}V(α,t)

^{52}Cr and $^{55}Mn(\alpha,t)^{56}Fe$ angular distributions have been successfully analyzed. They are listed in Table 5-II.

Calculated angular distributions of the one- and two-step processes and of the cohelent interferences are shown in Fig.5-4. In general, the cross sections via (α-t-d) processes were about 4~6 times larger than those of via (α-^{3}He-d) processes. This is due to a large Coulomb barrier in the intermediate ^{3}He channel. Cross sections of constructive and destructive interferences between (α-t-d) and (α-^{3}He-d) amplitudes are also shown. Even with the constructive interference, the two-step cross sections were factors of 8~10 weaker than the experimental cross sections. While the one-step cross sections labeled by 'D' in the figure could almostly reproduce the experiments. The predicted cross sections were modified by factors of 0.7~1.3 by the cohelent contribution of the two-step amplitudes(D+T,D-T), but the shapes of the angular distributions were little affected. It is found that for the (α,d) reactions at 23.9 MeV alpha particles leading to the highest spin states the one-step process give a dominant contribution and the sequential two-step processes play rather a minor role. However, this does not mean that the two-step processes are important for the transitions where the one-step cross sections are small and are not important for the transitions having a large one-step cross section. It must be noted that when the direct cross section is large in a given transition, also the two-step cross section becomes large and vice versa. This is mainly due to a following reason. Thansition amplitudes of the (α,d) reaction are strongly affected by a magnitude of an angular momentum transformation coefficient of the transferred two nucleons. When two-nucleons transferred sequentially into the identical orbits with the ones occupied by the one-step process, a similar transformation factor as the one-step process appears in a transition matrix of the two-step prosess also.

§ 6. Discussion for $^{54}Fe(\alpha,d)^{56}Co$ reaction

Low-lying states of ^{56}Co nucleus are considered to be formed by a coupling of one neutron and one proton hole with a doubly-closed ^{56}Ni core. Horie and Ogawa[54] have calculated the level structure of ^{56}Co in terms of an effective two-body matrix element based on shell model calculations. Where, they have assumed that low-lying states of the ^{56}Co are described by a ^{48}Ca inert core plus Z-20 protons in the $1f_{7/2}$ shell and a neutron in the $2p_{3/2}$, $2p_{1/2}$ or $1f_{5/2}$ shell orbit.

In this chapter, ^{56}Co levels are considered individually, and experimental data of the present work are compared with those of previous works, especially with high resolution $^{58}Ni(d,\alpha)^{56}Co$ work at 17 MeV performed by Schneider et al.[14] and $^{54}Fe(^{3}He,p)^{56}Co$ work at 18 MeV projectiles by Laget et al.[26] Also a comparison with DWBA calculations are made. In Table 4-I angular momentum transfers obtained by the DWBA analysis are shown in comparison with values of previous works. Normarization factors defined in equation (5-8) are also presented in column 5 ,which were deduced from integrated cross sections over an angular range 14°~ 105° in the center of mass system. For several levels the experimental results are compared with the theoretical results of Horie and Ogawa.[54] Their wave functions for corresponding levels are listed in the last column.

(1) 0.00 MeV

The ground state was only weakly excited in the present (α,d) reaction. The angular distribution was well fitted by an L=4 DWBA prediction. This L=4 assignment was consistent with the 4^+ assignment based on γ-γ correlation measurements[38,40,42]. Shell model calculations performed by Horie and Ogawa[54] have predicted a spin-parity of the ^{56}Co ground state to be 4^+ and have suggested that a $[\pi f_{7/2}\nu p_{3/2}]$ pair was a main configuration to be transferred in (α,d) reaction. Although the experimental cross section was small, it was still about twice larger than the prediction with a pure $[\pi f_{7/2}\nu p_{3/2}]_{L=4,J=4}$ transfer. A DWBA prediction employing Horie's wave function gave little change in the magnitude of the cross section because of a cancellation in transition amplitudes between remainders of $[\pi f_{7/2}\nu p_{1/2}]$ and $[\pi f_{7/2}\nu f_{5/2}]$ components.

(2) 0.157 MeV

The 0.157 MeV state was not excited so strongly. The angular distribution showed somewhat different pattern from the DWBA prediction with a pure L=2 transfer. A slight admixture of an L=4 component to the L=2 main component made the fit better. Since the 0.157 MeV state is believed to be a single level, the recognition of two L components (L=2 and 4) in the (α,d) reaction permitted an unique spin assignment of 3^+. This 3^+ assignment was consistent with previous γ-ray[42] and (d,α)[14] works. A normarization factor obtained by assuming a pure $[\pi f_{7/2}\nu p_{3/2}]_{L=2+4,J=3}$ transfer was N=74. Horie and Ogawa have predicted the first 3^+ state to be located at 0.216 MeV with a dominant configuration of $[\pi f_{7/2}^{-1}\nu p_{3/2}]$. Use of their wave function decreases the predicted cross section and yields N=90 which was close

to the (α,d) normarization factor N_0= 100.

(3) 0.576 MeV

This level was one of the most strongly seen in the (α,d) reaction. This was excited strongly in the (d,α) reactions[14,44] also, but was excited very weakly in the (^{3}He,p)[8,44] reactions. The strong transitions in both the (α,d) stripping and (d,α) pick-up reactions restrict a wave function of the level to a $[\pi f_{7/2}^{-1}\nu p_{3/2}]_J$. The (α,d) angular distribution was fairly well reproduced by an L=4 transfer. The L=4 transfer of a $[\pi f_{7/2}\nu p_{3/2}]$ pair allows spins of 3^+, 4^+ and 5^+. The 3^+ and 4^+ assignments gave N= 360 and 2140, respectively, while the 5^+ assignment gave N= 95. Comparing each N value with the normal N_0= 100, those of for the 3^+ and 4^+ were unreasonably large. Thus we adopted 5^+ assignment to the level, which was consistent with the tentative assignment in the (d,α) study by Schneider et al.[14], where the assignment was based on a cross section ratio of $\sigma(d,\alpha)/\sigma(p,^3He)$. Horie and Ogawa[54] have predicted a 5^+ at 0.408 MeV with a dominant $[\pi f_{7/2}^{-1}\nu p_{3/2}]$ plus a $[\pi f_{7/2}^{-1}\nu f_{5/2}]$ configuration. A small mixing of the $[\pi f_{7/2}^{-1}\nu f_{5/2}]$ component decreases the DWBA cross section about 20 % and gives N= 115. For this level detailed discussions will be done in chapter 7.

(4) 0.830 MeV

The 0.830 MeV state was excited very weakly in all (α,d), (d,α) (^{3}He,p) and (p,^{3}He) reactions. Therefore, we could not resolved the peak clearly from the 0.38 MeV peak of ^{58}Co caused from ^{56}Fe contamination in the target. According to the Horie's prediction, who have suggested a 4^+ at 0.840 MeV with a wave function of $0.574|\pi f_{7/2}^{-1}\nu p_{3/2}> -0.567|\pi f_{7/2}^{-1}\nu p_{1/2}> +0.734|\pi f_{7/2}^{-1}\nu f_{5/2}>$, the main $[\pi f_{7/2}^{-1}\nu f_{5/2}]$ component

of the (α,d) transition amplitude was completely canceled by the $[\pi f_{7/2}^{-1}\nu p_{3/2}]$ and $[\pi f_{7/2}^{-1}\nu p_{1/2}]$ terms.

(5) 1.00 MeV

A very strong peak populated with admixed L=2 and 4 was observed at 1.00 MeV excitation energy in the present (α,d) reaction. This state, however, has been recognized to be composed with closely spaced doublet levels at 0.970 and 1.009 MeV excitation by high resolution (^{3}He,p) and (d,α) reactions[14]. The 0.970 MeV state and the 1.009 MeV state have already been assigned to be 2^+ and 5^+, respectively, by (d,α) and β-γ studies.[14,38] The L=2 and L=4 shapes correspond to the 2^+ and the 5^+, respectively.

(6) 1.10 MeV

This level was concealed by a tail of the large 1.00 MeV peak, so an angular distribution could not be measured. The (d,α) reaction by Schneider et al.[14] has excited moderately with admixed L=2 and 4. They have assigned 3^+ to this level from the L-mixing and the σ(d,α)/σ(p,^{3}He) ratio. The 1.10 MeV state may be identical with the 1.139 MeV state predicted by Horie and Ogawa[54].

(7) 1.450 MeV

At this excitation energy no significant peaks have been seen in the present (α,d) spectra. This level is known as an anti-analogue state to the ^{56}Fe ground state and is strongly forbidden in (α,d) reaction by the selection rule $\vec{I}_f = \vec{I}_i + \vec{l}$. In (d,α) reaction the 1.450 MeV state has not been excited at all. However, in (p,^{3}He) and (^{3}He,p) it has been excited moderately by an L=0. These facts support the 0^+ assignment strongly.

(8) 1.72 MeV

This level was one of the most strongly excited in the present (α,d) reaction. The angular distribution of this level could be fitted by an L=0 DWBA curve. The L=0 transition in (α,d) and (d,α) reactions necessarily leads to an 1^+ assignment. This assignment was consistent with the original 1^+ assignment. Horie and Ogawa have predicted that the lowest 1^+ state was expected to have 3.50 MeV excitation with a $[\pi f_{7/2}^{-1}\nu f_{5/2}]$ configuration within the one-particle one-hole configuration space. The DWBA prediction assuming a pure $[\pi f_{7/2}^{-1}\nu f_{5/2}]$ configuration, however, yielded only one tenth of the experimental strength. Goode and Zamick[43] have concluded from an analysis of the ft value of ^{56}Ni β^+-decay that the configuration of the 1.72 MeV state was not an one-particle one-hole $[\pi f_{7/2}^{-1}\nu f_{5/2}]_{1^+}$ but a dominant two-particle two-hole component such as a $[\pi f_{7/2}^{-2}(0^+)$ $\pi p_{3/2}\nu p_{3/2}]_{1^+}$. The two-particle two-hole nature of this level was also supported by the result of the two-nucleon transfer cross sections. The two-particle two-hole states above mentioned can hardly be excited by two-particle pick-up reactions, but be excited preferentially by stripping reactions. In fact, (d,α)[14] and ($p,^3$He)[10] have populated this level weakly, while the present (α,d) and (^{3}He,p)[14,44] have excited strongly. A normarization factor for the DWBA calculation assuming the $[\pi f_{7/2}^{-2}(0^+)\pi p_{3/2}\nu p_{3/2}]$ configuration was N= 190 and it was still about twice as large as the ordinary value N_0= 100. Some configuration mixings of $[\pi f_{7/2}^{-2}\pi f_{5/2}$ $\nu f_{5/2}]$, $[\pi f_{7/2}^{-1}\nu f_{5/2}]$ and $[\pi f_{7/2}^{-2}\pi p_{3/2}\nu p_{1/2}]$ componente besides the main $[\pi f_{7/2}^{-2}\pi p_{3/2}\nu p_{3/2}]$ component were required to explain the experiment.

(9) 1.92 MeV

This level has been strongly seen in all two-nucleon transfer reactions. The deuteron angular distribution for this level had a characteristic L=2 shape which led a J^{π} to be one of 1^+, 2^+ and 3^+. Horie and Ogawa have predicted a $J^{\pi}= 3^+$ state at 1.905 MeV to have a dominant $[\pi f_{7/2}^{-1} \nu p_{1/2}]$ configuration. A transfer of a pure $[\pi f_{7/2} \nu p_{1/2}]$ pair leading to a 3^+ gave N = 410. The Horie's wave function led N = 220 which had been reduced by constructive interference among three components. The 1^+ and 2^+ assumption could not explain such a large experimental cross section. Although the N value was considerably larger than the N_0, the 3^+ assignment would be likely. Two-particle two-hole components may be required to explain the experimental cross section as been suggested by Schneider et al.[14)]

(10) 2.06 MeV

The 2.06 MeV state was rather weakly excited in the present (α, d) reaction. The angular distribution was tentatively identified to have an L=2 shape, although the first minimum expected to appear at 25° which characterized an L=2 shape was not clearly observed. No final conclusions could not be deduced from the present result on the 2.06 MeV state.

(11) 2.29 MeV

The experimental angular distribution of the 2.29 MeV state was well reproduced by an L=2 DWBA prediction. Schneider et al.[14)] have assigned 2.281 MeV state to be 7^+ which has been most strongly excited with an L=6 in the (d,α)reaction. They have concluded that the 2.281 MeV state has been the highest spin state belonging to a

two-particle two-hole $[\pi f_{7/2}^{-1}\nu f_{7/2}^{-1}(\nu p_{3/2})^2 0^+]_J$ multiplet. Such a state is hardly excited by (α,d) and (^{3}He,p) reactions. Schneider et al.[14] have also pointed out a possible existence of another level at Ex = 2.301 MeV excited by an L=2 transfer in (^{3}He,p) reaction. Our 2.29 MeV state was thought to be identical with latter state.

(12) 2.37 MeV

This level was excited in the present (α,d) reaction with moderate intensity. The angular distribution was well fitted with an L=6 DWBA calculation which led three possible 5^+, 6^+ or 7^+ assignments. The 7^+ assignment was unlikely because such a spin state be expected to have either a $[\pi f_{7/2}^{-1}\nu f_{7/2}^{-1}\nu p_{3/2}^{2}]$ or $[(\pi f_{7/2}^{-2})_{J\neq 0}\pi\ell j\nu\ell' j']_{J=7^+}$ could not be excited by (α,d) in first order. A 6^+ state has been predicted to be located at Ex= 2.324 MeV with a $[\pi f_{7/2}^{-1}\nu f_{5/2}]$ configuration.[54] This prediction was very close to the experimental observed excitation energy. A DWBA prediction assuming this configuration gave N = 120 , it was also close to the ordinary N_0=100. Recently, Sarantites et al.[67] have investigated the high spin states in ^{56}Co via ^{54}Fe(α,pn)^{56}Co*(γ) reaction in the energy range between 20.4 and 29.5 MeV of a projectile. They have found a sequential decay from 10^+ to 5^+ and have identified the 2.372 MeV state to be 6^+ from γ-γ coincidence measurements in conjunction with excitation functions and γ-rays angular distribution measurments. Our 6^+ identification confirmed their 6^+ assignment.

Ex ~ 3 MeV

In the excitation region around 3MeV, many closely spaced levels have been observed by the high resolution (d,α) reaction[14]. In

our (α,d) reaction many peaks were also observed but due to the poor energy resolution (FWHM ≃ 90 keV), angular distributions to the levels could not be taken except for two distinct levels. They were located at 3.08 and 3.18 MeV in excitation energies. The angular distribution of the 3.08 MeV state showed a characteristic diffraction pattern of an L=0 transfer , it suggest an 1^+ assignment. Caldwell et al.[9] have been assigned this level to be 1^+ from an L=0+2 (^{3}He,p) angular distribution, although they have not carried out DWBA calculations.

Although the experimental angular distribution of the 3.18 MeV state could not be reproduced by DWBA calculations, this state was excited probably by a small angular momentum transfer because of its structured shape. A comparizon with results of other reactions was difficult due to a high level density.

Ex ≃ 5 MeV

At a higher excitation region around 5 MeV, some prominent peaks were observed . They were located at excitation energies of 4.99, 5.08, 5.31 and 5.47 MeV. Since in this excitation region a level density was very high, an identification among levels appeared in different reactions was difficult. In the (α,d) reaction by Lu et al.[22] at an alpha particle energy of 50 MeV, several strong peaks have been observed at 4.98, 5.44, 6.56 and 8.92 MeV excitations. They have assigned the 8.92 MeV only to be 9^+ with a $[\pi f_{7/2}^{-2}(0^+)\pi g_{9/2}\nu g_{9/2}]$ configuration . For other levels they have not discussed at all. Their 4.98 MeV state is identical with our 4.99 MeV state. As a peak width of their 5.44 MeV state seems to be somewhat broad compared with that of the 4.98 MeV, it may be composed with unresolved doublet levels which includes our 5.31 and 5.47 MeV states.

In the (^{3}He,p) reaction by Laget et al.[44] very strong two peaks have been seen at 5.337 and 5.471 MeV excitations but at 4.991 MeV only a weak peak has been observed. Cross section ratios of the 5.337 and 5.471 MeV states to the 4.991 MeV state were 5 and 12 in the (^{3}He,p) and were 1 and 2 in the present (α,d) reaction. An enhancement of transition strengthes to the 5.33 and 5.47 MeV states (or a hindrance of the 4.991 MeV transition) in the (^{3}He,p) reaction comparing with that in (α,d) reaction suggests that these two levels (5.337 and 5.471 MeV) should have relatively low-spins, while the 4.99 MeV state a high spin. These facts were supported by shapes of the experimental angular distributions of the (α,d) reaction. The angular distributions of the 5.31 and 5.47 MeV states showed oscillatory patterns , while that of the 4.99 MeV state decreased monotonically with angle which is a nature of a large angular momentum transfer. We could not obtain any good fit to both 5.31 and 5.47 MeV angular distributions by DWBA calculations, probably because of the large angular momentum mismatch discussed in chapter 5. To the contrary, the angular distribution of the 4.99 MeV state was well fitted with an L=7 transfer. Detailed discussions on the 4.99 MeV state will be stated in chapter 7.

§ 7. Highest spin states with configurations of $[\pi f_{7/2}^{n} \nu(\ell j)]$

7-1) General considerations

One of the important properties of the (α,d) reaction is that high spin states are excited preferentially. Experimental evidence of this property was first observed by Harvey et al.[20] in their (α,d) reactions on s-d shell nuclei at 50 MeV alpha particle energy. We will here discuss some theoretical considerations on the preferential excitation of the high spin states in the (α,d) reaction. The selective transition to the high spin states is understood from some considerations on kinematics of the reaction and geometrical conditions of angular momentum couplings of the transferred two nucleons.

At first we will consider an orbital angular momentum matching in the reaction, which is favorable to increase cross sections. A Q-value of the (α,d) reaction on even-even nuclei in the 1f-2p shell is typically -10 MeV. This large negative Q-value together with a mass ratio of the projectile alpha particle and the ejectile deuteron make a large angular momentum difference between the entrance and the exit channels. So the transition to bring a large angular momentum to the target nucleus occurs favorably. If we assume the reaction takes place at a nuclear surface in a semiclassical sense, the matching condition of the transferred orbital angular momentum L can be written as,

$$L = R_i k_i - R_f k_f \quad ,$$

where the R_i and the R_f denote the nuclear radii of the target and the residual nuclei, and k_i and k_f are wave numbers of the entrance and exit channels , respectively. For the (α,d) reaction

at 24 MeV alpha particle energy on the 1f-2p shell nuclei, relations of excitation energies versus the matched angular momentum transfers are shown in Fig.7-1. The angular momentum transferred to the target nucleus by the captured n-p pair is calculated to be about $4\sim5\hbar$ for the ground state transition and becomes up to about $6\sim7\hbar$ for the transitions to the states around 5 MeV in excitation when the deuteron is emitted at zero degree. Consequently, the transitions where each nucleon of the transferred n-p pair enters into an f or a p orbit for low-lying states and into an f or a g orbit for highly excited states are considered to be likely. However, at the relatively low energy of the alpha beam as in the present study, a centrifugal force suppresses the incident partial waves with large angular momentum to enter into the nuclear surface. Thus such striking selectivity about the angular momentum transfers as been seen in the high energy alpha beam may not be expected in the present case. Another kinematical cause to enhance the transitions to the higher excited states with high spin comes from a binding energy dependence of a form factor of the reaction. The form factor, the wave function of a transferred pair in the residual nucleus, extends to the nuclear surface with decreasing the binding energy. Therefore, an overlapping of both incident and outgoing distorted waves and the form factor becomes large at the nuclear surface. Fig.7-2 shows Q-value dependences of the form factors for L=4 and L= 6 transfers of a $[\pi f_{7/2}{}^{\nu}f_{5/2}]$ pair, where solid lines and dashed lines show the form factors of E_X=4.5 MeV and E_X=0.5 MeV, respectively. Q-value dependences of the DWBA cross sections for different L transfers are shown in Fig.7-3. The cross sections of

various L transfers are conventionally normarized to 1 at zero excitation energy. As can be seen in the figure, the cross sections of the transition with a large orbital angular momentum decrease less slowly with increase of a negative Q-value than that with small angular momentum transfers.

The high spin state is enhanced in the (α,d) reaction by a statistical factor 2J+1 for the magnetic substate of the residual state and by a geometrical factor for the transferred two nucleons. This latter effect comes from an angular momentum coupling scheme of the transferred two nucleons. The form factor of the (α,d) reaction is already described in equations (5-6) and (5-7). In these equations the 9j symbol is the coefficient of the angular momentum transformation from the j-j to L-S coupling of the proton and neutron transferred to $(\ell_p j_p)$ and $(\ell_n j_n)$ orbits, respectively. The resultant spins of the final state are allowed to be one of values limitted by $|j_p-j_n| \leq J \leq j_p+j_n$. When the J is a stretched coupling which means that the J takes the largest possible value in the angular momentum coupling, namely $j_p=s_p+\ell_p$, $j_n=s_n+\ell_n$ and $J=j_p+j_n$, the transformation coefficient becomes unity. While in the case of other coupling schemes a square of the 9j coefficient amounts to only 10~50% of the stretched one. This type of enhancement is inherent in the two-nucleon transfer reactions.

Putting all the effects above discussed together, we can expect that the highest spin states are strongly excited by the (α,d) reaction.

7-2) Excitation energies of high spin states

Energy spectra of deuterons from the (α,d) reactions on three N=28 targets (^{50}Ti, ^{52}Cr and ^{54}Fe) and on a neighboring N=30 target (^{56}Fe) are shown in Fig.4-3. In each spectrum two peaks marked with asterisks were strongly seen in the present work and were assigned to be 5^+ and 8^- states for the lower and the higher excitation energies, respectively. The peaks with hatched lines were caused form $^{12}C(\alpha,d)^{14}N$ reaction. The levels assigned to be 5^+ were all located up to 0.6 MeV excitation energy. Precisely the excitation energies were 0.020±0.020 MeV in ^{52}V, 0.363±0.010 MeV in ^{54}Mn, 0.575±0.010 MeV in ^{56}Co and 0.020±0.020 MeV in ^{58}Co nucleus. The prominent levels in the higher excitation energies which were assigned to be 8^- in the present work were located at 4.32 ±0.03 MeV in ^{52}V, 4.72 ±0.02 MeV in ^{54}Mn, 4.99 ±0.02 MeV in ^{56}Co and 3.75 ±0.03 MeV in ^{58}Co nucleus. Details of these spin-parity assignments will be discussed in the following sections. Here, we point out a distinct stractural difference among the deuteron energy spectra from those targets. In the $^{50}Ti(\alpha,d)^{52}V$ spectrum the peaks of 5^+ and 8^- were remarkably prominent compared with many peaks between them, while in the $^{54}Fe(\alpha,d)^{56}Co$ spectrum the strengthes of the two peaks were comparable to those of other several peaks located at around 2~6 MeV in excitation. Therefore, it is very interesting to compare the experimental energy spectra with those expected from the DWBA calculations based on a simple shell model. In the calculations the levels were assumed to lie at excitation energies determined from proton and neutron single particle energies of the neighboring odd mass nuclei. Thus the levels with the same configuration have the same excitation energy. The cross sections were estimated by the DWBA calculations assuming pure configurations which can be excited by

a direct (α,d) reaction. Fig.7-4 shows the expected (α,d) energy spectra thus obtained on the three N=28 targets. Comparing with the experimental ones in the Fig.4-3 we can see that gross structures of the energy spectra were well reproduced by these calculations. Below 5 MeV in excitation only two strongly excited levels were seen in the calculated ^{52}V spectrum, their configurations were $[\pi f_{7/2}^{3}\nu p_{3/2}]_{5}^{+}$ and $[\pi f_{7/2}^{3}\nu g_{9/2}]_{8}^{-}$. In the ^{56}Co spectrum, besides the two levels of 5^{+} and 8^{-} spins, other strong levels with $[\pi f_{7/2}^{-2}\pi p\ \nu p\ ]$ and $[\pi f_{7/2}^{-2}\pi p\ \nu f_{5/2}]$ configurations appeared at around 5 MeV excitation energy. Since both $2p_{3/2}$ and $2p_{1/2}$ proton shell orbits are entirely empty and the $1f_{7/2}$ proton orbit is occupied by six protons in the ^{54}Fe target nucleus, transition strengthes to the states with $[\pi f_{7/2}^{-1}\nu\ell j]$ configurations decrease to be comparable to those of the $[\pi f_{7/2}^{-2}\pi p\nu p$ or $f_{5/2}]$ configurations. Therefore in the ^{56}Co spectrum the $[\pi f_{7/2}^{-1}\nu p_{3/2}]_{5}^{+}$ and $[\pi f_{7/2}^{-1}\nu g_{9/2}]_{8}^{-}$ states are not so prominent compared with the two peaks in the ^{52}V spectrum.

Fig.7-5 shows experimental reaction Q-values corresponding to the lower and higher excitation members of the residual nuclei as a function of the atomic number of the residual nuclei. We represent former with an open circle and latter with a closed circle. As ^{48}Ca(α,d)^{50}Sc reaction was not performed in the present work, the data points of the ^{50}Sc nucleus was taken from the results of the ^{48}Ca (α,d)^{50}Sc reaction at 31 MeV alpha particle energy by Moazed et al.[18] The angular distribution to the state, however, has not been presented and no spin assignments have been carried out. In the ^{48}Ca(^{3}He,p)^{50}Sc reaction at 18 MeV ^{3}He energy by Fleming et al.[16] This state has only weakly been excited compared with low spin states. This is probably due to the high spin of the 4.42 MeV state. So the 4.42 MeV state is considered to be one of possible candidates for

the $[\pi f_{7/2}^{-1} \nu g_{9/2}]_{8^-}$ members. A monotonous increase of -Q-value of the (α,d) reaction with an atomic number of the residual nucleus was observed in the N=28 targets as can be seen in Fig.7-5. Quite similar atomic number dependences of the reaction Q-values for assumed 5^+ and 8^- states inferred a resemblance of configurations in the two members. Lu et al.[22] have first observed a linear relation between the mass number of the product nucleus and the (α,d) Q-value for formation of $[d_{5/2}^2]_{5^+}$, $[f_{7/2}^2]_{7^+}$ and $[g_{9/2}^2]_{9^+}$ states. Del Vecchio et al.[23] have extended this relation for the $[f_{7/2}^2]_{7^+}$ states to wider range of masses. For the $[j^2]_{Jmax}$ configurations investigated by them, the -Q-value decreased with mass number and it had an opposite gradient to our result. The decrease of -Q-value with mass number in the $[J^2]_{Jmax}$ configurations has been explained by Sherr et al.[68] in terms of the Barsal-French-Zamick weak coupling model. In our case we assumed the $[\pi f_{7/2}^n \nu \ell j]$ configuration for the final states. Here n denotes the number of protons in the $1f_{7/2}$ orbit of the residual nucleus. The last nth proton which enters into the $1f_{7/2}$ orbit by the (α,d) reaction cannot couple to 0^+ with one of other protons in the $1f_{7/2}$ orbit but to 2^+, 4^+ or 6^+. Then a resultant two particle interaction energy becomes repulsive and is proportional to (n-1), so an effective binding energy of the $1f_{7/2}$ proton decreases with increasing n. This is a qualitative explanation of the results. A more strict treatment will be given in section 7-4).

7-3) Angular distribution and cross section

In this section we discuss on the angular distributions and the total cross sections of the strongly excited two levels in each (α, d) reaction. Hereafter, we define a cross section integrated over an angular range from 14° to 82° by multipling $2\pi \cdot \sin(\theta_{CM})$ as a "total cross section". The DWBA cross section appearing below was already multiplied by the (α, d) normarization factor which has been determined to be 100 from our previous work on $^{51}V(\alpha, d)^{53}Cr$ reaction[24]. So the predicted cross section can be directly compared with the experimental one.

(i) 5^+ states

The angular distibutions of the lower excitation members assigned to be 5^+ are shown in Fig.4-4 together with the zero-range DWBA predictions. As can be seen in the figure the shapes of the angular distibutions were all similar to each other. They were characterized by a forward peaking at 15°, a rather flat shape in the anglar range from 25° to 50° and a rapid decrease at angles beyond 60°. The L=4 DWBA predictions assuming a $[\pi f_{7/2} \nu p_{3/2}]$ p-n pair transfer could reproduce the experimental angular distributions well. The L=4 assignment led to a spin-parity of a final state to be 3^+, 4^+ or 5^+. These levels have previously been established or tentatively assigned to be 5^+ by various reactions. Here, we will show that these levels have dominant $[\pi f_{7/2}^{n} \ \nu p_{3/2}]$ configurations and will demonstrate the validity of the DWBA calculation for the high spin states.

^{52}V

Near the ground state of the ^{52}V nucleus, two closely spaced levels have previously been observed by means of (n, γ) reactions[32]. They are 3^+ at 0.0 MeV, 2^+ at 0.018 MeV and 5^+ at 0.023 MeV in excitation energies. The 5^+ assignment of the 0.023 MeV state has been done by a conversion coefficient measurment. The low-lying levels of the ^{52}V nucleus have also been studied by ^{51}V(d, p)^{52}V reactions[30,31]. The ground and the 0.02 MeV states have been excited with strong ℓ_n=1 transitions by the (d, p) reactions. From the (d, p) results, main configurations of all these states are considered to be $[\pi f_{7/2}^{3} \quad \nu p_{3/2}]$. The ground state of the ^{52}V has been excited by ^{50}Ti(^{3}He, p)^{52}V reaction[34] with an orbital angular momentum transfer L=2 and the 0.018 MeV state with an L=2 with a small L=4 admixture at 15 MeV ^{3}He energy. In the present (α, d) study. The 0.017 and the 0.023 MeV states could not be resolved from the ground state because of the poor energy resolution (FWHM=90 keV). Though the cross section of the 0.023 MeV state included a contribution from the ground and the 0.018 MeV states, their contibution was estimated to be small from following two reasons. One is that the excitation energy of the strong peak was 0.023±0.020 MeV and the other is that the shape of the angular distribution was practically explained by an L=4 transfer. If the yield of the peak belongs to the ground 3^+ and the 0.018 MeV 2^+ states, the angular distribution should have a dominant L=2 shape. Actually the DWBA calculations for the 3^+ and the 2^+ states assuming a capture of a $[\pi f_{7/2}\nu p_{3/2}]$ p-n pair showed a pure L=2 shape and yielded only about 30% of the experimental cross section.

^{54}Mn

The 0.363 MeV state of the ^{54}Mn nucleus was the strongest one populated by the present (α, d) reaction. This level has been investigated by ^{53}Cr(^{3}He, d) reaction[35] and has been excited with an ℓ_p=3 transfer. Hjoth[13] has suggested a spin of 5^+ to this state from his ^{56}Fe(d, α) reaction in which the state has been excited strongly with an L=4 transfer. On the contrary a weak transition to the 0.363 MeV state through (^{3}He, p) reactions was observed by Lynn et al.[35] and Betts et al.[17] with 11 MeV and 15 and 16.5 MeV bombarding energies, respectively. This favors the high spin assignment to this state.

In connection with the (^{3}He, d) results[35], we can expect that a possible wave function of the 0.363 MeV state which was excited commonly and strongly by both (α, d) stripping and (d, α) pick-up reactions should be a $[\pi f_{7/2}^{5}\ \nu p_{3/2}]_J$. The L=4 assignment of the (α, d) angular distribution supported 3^+, 4^+ and 5^+ assignments to the 0.363 MeV state. The total cross section predicted by the DWBA calculation assuming a pure $[\pi f_{7/2}\nu p_{3/2}]_{5^+}$ transfer of a p-n pair amounted to 550 μb, which was very close to the experimental one of 540 μb. The 4^+ assumption to the level yielded only 21 μb in the DWBA calculation which is only 1/25 of the experimental total cross section. Then it was quite unreasonable to adopt the 4^+ assignment to the 0.363 MeV state. Though both L=2 and L=4 transfers are permitted in the (α, d) reaction to the 3^+ state with the $[\pi f_{7/2}^{5}\ \nu p_{3/2}]$ configuration, the DWBA angular distribution was dominated by the L=2 pattern

and the contribution from the L=4 component was negligibly small. So the 3^+ assignment was also abandoned.

Horie et al.[54] have predicted a 5^+ state with a dominant configuration of a $[\pi f_{7/2}^5 \nu p_{3/2}]$ at 0.37 MeV excitation energy in ^{54}Mn which was very close to the observed one.

^{56}Co

The 0.576 MeV state of the ^{56}Co nucleus was one of the strongest seen in the present (α,d) reaction and also in the (d,α) reaction by Schneider et al.[14] However it has weakly been excited by ^{54}Fe(^{3}He,p)[8,9] and ^{56}Fe(^{3}He,t)[69] reactions. Unfortunately the ^{56}Co nucleus cannot be reached by one nucleon stripping or pick-up reactions because of an absence of proper targets. Therefore, all informations about the ^{56}Co structure primarily came from the works on two-nucleon transfer or charge exchange reactions besides β-decay works.

If the (^{3}He,t) reaction goes primarily with charge exchange process, states composed with a $[\pi f_{7/2}^{-1}\nu f_{7/2}^{-1}p_{3/2}^{2}]$ or a $[\pi f_{7/2}^{-2}\pi p_{3/2}\ \nu p_{3/2}]$ configuration should be excited strongly. The former states cannot directly be excited by (α,d) and (^{3}He,p) reactions, while the latter cannot be excited by a (d,α) reaction. Both (α,d) and (^{3}He,p) reactions may have larger cross sections to excite levels of $[\pi f_{7/2}^{-1}\nu p_{3/2}]_J$, $[\pi f_{7/2}^{-1}\nu p_{1/2}]_J$ and $[\pi f_{7/2}^{-1}\nu f_{5/2}]_J$ configurations compared with a (^{3}He,t) reaction. However, in the two reactions the (α,d) reaction populates preferentially high spin states and the (^{3}He,p) reaction low spin states due to a well known angular momentum matching condition of the reactions. On the other hand, states with configurations of a $[\pi f_{7/2}^{-1}\ \nu p_{3/2}]$ and a $[\pi f_{7/2}^{-1}\ \nu f_{7/2}^{-1}\ p_{3/2}^{2}]$ can be populated strongly by (d,α) reactions. If a considerable amount of configuration mixing exists in a ^{58}Ni target nucleus, states with $[\pi f_{7/2}^{-1}\ \nu p_{1/2}]$ and $[\pi f_{7/2}^{-1}\nu f_{5/2}]$ configurations will be excited moderately.

Naturally, unnegligible configuration mixings in the ^{56}Co nucleus and in the target nuclei are realized and it obscures the selection of transitions above mentioned in each reaction.

The angular distribution to the 0.576 MeV state was well fitted by L=4 and J=5 DWBA assumption. The cross section of the state was the largest among levels excited with an L=4 and amounted to 210 μb. In the (d,α) reactions by Schneider et al.[14] and Laget et al.[44] the 0.576 MeV state was measured to have a second strongest cross section next to the 7^+ state with a $[\pi f_{7/2}^{-1}\ \nu f_{7/2}^{-1}\ p_{3/2}^{2}]$ configuration. The (d,α) cross section has been 440 μb[44]. On the contrary a (^{3}He, p) cross section to this level at ^{3}He energy of 18 MeV has been only 26 μb.[44] From these considerations we may conclude the 0.576 MeV to have a $[\pi f_{7/2}^{-1}\ \nu p_{3/2}]$ configuration coupled the proton and neutron angular momenta to the highest manner. With the assumption of the $[\pi f_{7/2}^{-1}\ \nu p_{3/2}]$ configuration, the (α,d) cross sections of the L=4 transfers predicted by the DWBA amounted to 5 μb, 13 μb and 230 μb for 3^+, 4^+ and 5^+, respectively. A remarkable agreement of the DWBA cross section with the experiment was obtained for the 5^+ assignment.

For the ^{56}Co nucleus, Horie and Ogawa[54] have predicted a 5^+ state to be located at 0.511 MeV which have a $[\pi f_{7/2}^{-1}\ \nu p_{3/2}]$ as a main configuration and a small admixture of a $[\pi f_{7/2}^{-1}\ \nu f_{5/2}]$ component. The DWBA calculation employing this wave function reduced the total cross section by 25 % due to a cancellation in transition amplitudes of the $[\pi f_{7/2}^{-1}\ \nu p_{3/2}]$ and $[\pi f_{7/2}^{-1}\ \nu f_{5/2}]$ components.

As a whole of the above considerations, we conclude that the spin-parity of the levels at around 0.5 MeV preferentially excited by the present (α,d) reactions through the L=4 transfer is 5^+ and have a dominant $[\pi f_{7/2}^{n}\nu p_{3/2}]$ configuration. In Table 7-1 the experimental and theoretical total cross sections of these 5^+ states are summarized. Fig.7-6 shows the experimental total cross sections with a closed circle and the predicted ones by the zero-range DWBA assuming a $[\pi f_{7/2}\nu p_{3/2}]_{L=4,J=5}$ transfer with an open circle. Values indicated with a triangle are the theoretical cross sections which include a contribution from the unresolved multiplets. Cross section errors in the figure arose primarily from an ambiguity of the target thicknesses besides a usual statistical errors.

A surprisingly good agreement between the experiments and the DWBA predictions were obtained both in the systematical decreasing trend with increasing the mass number of the target nucleus and in the absolute cross sections.

(ii) 8^- states

In the preceding subsection we showed that the angular distributions of the highest spin state with the $[\pi f_{7/2}^{n}\nu p_{3/2}]_{J=5}^{+}$ configuration could be fairly well reproduced by the zero-range DWBA calculations. The absolute cross sections were also explained by the assumption of the $[\pi f_{7/2}\nu p_{3/2}]_{L=4,J=5}$ transfer.

In this subsection the angular distributions and the cross sections for the levels excited at around 4~5 MeV excitation by the (α,d) reactions are discussed. For the levels spins and parities have not been assigned so far. Fig.7-7 shows the cross sections of the (α,d) reactions as a function of a mass number of the residual nucleus A_{res}. First of all, we point out that a mass depensence of the cross section was closely similar to that of the low-lying 5^+ states shown in Fig.7-6 except for the $^{56}Fe(\alpha,d)^{58}Co$ reaction. The cross sections rapidly decrease with increasing the mass number. The mass dependence of the 5^+ cross sections was essentially caused from the number of the $1f_{7/2}$ proton holes in the target nucleus. From the systematics of the cross sections and of the reaction Q-values (see Fig.7-5), the formation of the levels at Ex=4~5 MeV should be closely connected with the transfer of a proton into the $1f_{7/2}$ shell orbit. In the cross section systematics an appreciable discrepancy between the 5^+ and the higher excitation members was found in the $^{56}Fe(\alpha,d)^{58}Co$ reaction. For the ^{56}Fe nucleus which is not N=28 but N=30, the $2p_{3/2}$ neutron shell orbit is already occupied by two neutrons and hence the transition strength of a neutron transfer to the $2p_{3/2}$ shell orbit is one half of the strength for the N=28 target. On the other hand, since the higher neutron shell orbits ($2p_{1/2}$, $1f_{5/2}$ and $1g_{9/2}$) are entirely empty for both the N=28 and the N=30 targets,

transitions to the (ℓj) orbits other than the $2p_{3/2}$ should give same yields for both the ^{54}Fe and the ^{56}Fe targets.

The angular distributions of the higher excitation members are shown in Fig.4-5 for the present four reactions. The experimental angular distributions showed structurless patterns. Hence, it is not so easy to assign a transferred orbital angular momentum L to the states definitly. In the figure the zero-range DWBA calculations assuming an L=7 transfer of a [$\pi f_{7/2}\nu g_{9/2}$] pair and an L=6 transfer of a [$\pi f_{5/2}\nu f_{5/2}$] pair are presented by solid and dashed lines, respectively. For all reactions better fits were obtained with the results of the L=7 transfer than with the L=6 transfer. The DWBA predictions of other possible orbital angular momentum transfers for the ^{52}Cr(α, d)^{54}Mn reaction are shown in Fig.7-8 for comparison. The cross sections of the odd L transfers were calculated assuming a [$\pi f_{7/2}\nu g_{9/2}$] transfer of the n-p pair and those of the even L's were obtained assuming a [$\pi f_{5/2}\nu f_{5/2}$] transfer. The patterns of the experimental angular distributions slightly varied over the target nuclei from ^{50}Ti to ^{56}Fe. However, characteristic shapes of the angualr distributions were not changed for all reactions. They were characterized by a flat top in an angular range from 15° to 45° followed by a gentle decrease of the cross section with angles. The L=7 DWBA predictions well reproduced the target dependence of the angular distribution shape. The L=6 DWBA angular distributions fell off steeply from 30° for all targets. This tendency was not altered by the DWBA calculations with the A2-D2 set. The DWBA curves of the L=4 and L=5 shown in Fig.7-8 had some structured patterns and did not reproduce the experimental shapes. For comparison, experimentally observed

L=6 angular distributions of the ^{56}Co and ^{54}Mn are presented in Fig.7-9 toegther with the DWBA predictions of an L=6 transfer. These states have been assigned to be 6^+ at 2.372 MeV of ^{56}Co and at 2.274 MeV of ^{54}Mn by the (α,pn γ)[67] and the (d,α)[13] reactions, respectively. Good agreements between the experiments and the DWBA predictions for the large L transfers is due to a good matching condition of orbital angular momenta among the incident and the exit channels and the transferred particles as already discussed in chapter 5.

The 4.32 MeV state of ^{52}V, the 4.715 MeV state of ^{54}Mn and the 4.99 MeV state of ^{56}Co which were all assigned to be 8^- in the present work are discussed individually below.

^{52}V 4.32 MeV

The level scheme of ^{52}V has been determined mainly by means of $^{51}V(d,p)$ and $^{51}V(n,\gamma)$ reactions.[31,29] Except for several levels, the (d,p) reaction to the levels below 3.6 MeV excitation have proceeded through ℓ_n=1 transfers. Then the levels identified have been considered to have dominant $[\pi f_{7/2}^3\ \nu p_{3/2}]$ and $[\pi f_{7/2}^3\ \nu p_{1/2}]$ configurations. Negative parity states observed in the (d,p) reaction have been populated through ℓ_n=2 transfers. No ℓ_n=4 transfers have been observed yet. This is not so strange, since such a large ℓ_n transfer can hardly occur in the (d,p) reaction at a low incident deuteron energy of 10 MeV. The 4.32 MeV state excited most strongly in the present (α,d) reaction has not clearly seen in any other reactions. In $^{50}Ti(^3He,p)$ reactions at 15.11 MeV by Caldwell et al.[34] and at 17 MeV by Hardie et al.[33], the 4.32 MeV state has only weakly been excited or has not been seen. In general a $(^3He,p)$ reaction is known to excite low spin states favorably. Actually, the $(^3He,p)$ reaction has been used as a tool to search 0^+ and 1^+ states in doubly-odd nuclei. On the contrary the (α,d) reaction is favored to excite high spin states. Therefore, we can expect from the characteristic difference in the transition strengthes between the (α,d) and the $(^3He,p)$ reactions that the 4.32 MeV state have a spin larger than 4 ħ.

According to an unperturbed shell model calculation, states with configurations of a $[\pi f_{7/2}^3\ \nu g_{9/2}]$ and a $[\pi f_{7/2}^3\ \nu f_{5/2}]$ are expected to lie at around 4 MeV and 5 MeV in excitation energies, respectively. In due consideration of a residual interaction,

it is better to include states with a configuration $[\pi f_{7/2}^{2}\ \pi f_{5/2}\nu f_{5/2}]$ which are expected to lie at higher than 6 MeV excitation.

The DWBA total cross sections with transfers of a $[\pi f_{7/2}\nu g_{9/2}]$ p-n pair coupled to 8^-, 7^- and 6^- were 580 μb, 1.2 μb and 200 μb, respectively. In the calculations the transitions to the 8^- and the 7^- states proceeded through an L=7 and the 6^- state through mainly an L=5 transfer . The total cross sections of both L=6 transitions assuming a $[\pi f_{7/2}\nu f_{5/2}]_{6^+}$ and a $[\pi f_{5/2}\nu f_{5/2}]_{5^+}$ amounted to 59 μb and 350 μb, respectively , in the DWBA estimation. These values should be compared with the experimental total cross section of 790 ±120 μb. With respect to the angular distribution and the total cross section, an agreement with the experiment was superior in the L=7 , J=8 transfer of the $[\pi f_{7/2}\nu g_{9/2}]$ p-n pair compared with other transitions.

^{54}Mn 4.715 MeV

The 4.715 MeV state of the ^{54}Mn nucleus has first been observed in the ^{52}Cr(α,d)^{54}Mn reaction by Lu et al[22]. In their deuteron energy spectrum at 20°, the 4.70 MeV state has been excited most strongly. However, they have not argued on the 4.70 MeV state at all, since the angular distributions have not been measured in their work. On the other hand, in the (^{3}He,p) reaction at 15 MeV ^{3}He energy by Betts et al.[17] this level has been excited weakly compared with the neighboring states. Although the (^{3}He,p) angular distribution to the level has not been analyzed by the DWBA calculation, its monotonically decreasing shape inferred a large orbital angular momentum transfer in the reaction. Other (d,α)[13], (^{3}He,d)[35] and (p,n)[37] reactions have not excited the 4.715 MeV state at all, so a possibility of $[\pi f_{7/2}^{4}\pi(\ell j)\nu p_{3/2}]$ and $[\pi(\ell j)\nu(\ell' j')^{-1}(p_{3/2})^{2}]$ configurations for the state could be excluded. Therefore, remaining candidates to form the 4.715 MeV state were possibly $[\pi f_{7/2}^{5}\nu g_{9/2}]_{6^-,8^-}$ and a $[\pi f_{5/2}\nu f_{5/2}]_{5^+}$. As can be seen in Fig.4-5, an L=7 DWBA prediction reproduced the experimental angular distribution fairly well. While an L=5 DWBA curve which is a main component to excite the $[\pi f_{7/2}^{5}\nu g_{9/2}]_{6^-}$ configuration, gave a quite out of phase shape against the experiment (see Fig.7-8). The cross section assuming the $[\pi f_{7/2}\nu g_{9/2}]_{L=7,J=8}$ transfer was calculated to be 280 μb and that of the $[\pi f_{5/2}\nu f_{5/2}]_{L=6,J=5}$ to be 270 μb. These values were comparable to the experimental cross section of 360$\pm$50 μb. Although the two predicted cross sections were too close to determine the best configuration, the good agreement of the predicted L=7 angular distribution with the experiment supported the $[\pi f_{7/2}^{5}\nu g_{9/2}]_{8^-}$ assignment.

^{56}Co 4.99 MeV

The 4.99 MeV state of the ^{56}Co nucleus has first been seen in the ^{54}Fe(α,d)^{56}Co reaction by Lu et al.[22] In the present (α,d) reaction three strongly populated levels were observed at an excitation energy higher than 4.9 MeV. They lay at 4.99, 5.34 and 5.50 MeV. The angular distribution of the 4.99 MeV state showed a structurless pattern, while those of the 5.34 and 5.50 MeV states showed somewhat oscillatory patterns. So it is hard to regard the upper two levels as the one of the members of the high spin states. In fact in the (^{3}He,p) reaction by Laget et al.[26] at 18 MeV ^{3}He energy these two levels have been strongly populated at 5.347 and 5.495 MeV excitation energies, while the 4.993 MeV state has only weakly been seen. Cross section ratios $d\sigma(\alpha,d)/d\sigma(^3He,d)$ at $\Theta = 35°$ were 2.4, 0.27 and 0.26 for the 4.99, the 5.34 and the 5.50 MeV states, respectively. From the ratios it is clear that the 4.99 MeV state remains as a candidate for the $[\pi f_{7/2}^{7} \nu g_{9/2}]_{8^-}$ state and the 5.34 and the 5.50 MeV states are expected to have a [πpν(p or f)] configuration coupled to relatively low spin.

The experimental total cross section amounted to 130μb. The predicted total cross sections to the 4.99 MeV state were 105μb and 190μb for the transfers of the $[\pi f_{7/2} \nu g_{9/2}]_{L=7\ J=8}$ and the $[\pi f_{5/2} \nu f_{5/2}]_{L=6\ J=5}$, respectively. Then the former configuration is favorable to the state.

Comparison of the total cross sections deduced from the experiments and the DWBA calculations are summarized in Table 7-II. Fig.7-7 also shows the total cross sections predicted by the DWBA calculations assuming a $[\pi f_{7/2}{}^{\nu}g_{9/2}]_{L=7,\ J=8}$ and a $[\pi f_{5/2}{}^{\nu}f_{5/2}]_{L=6,J=5}$ transfers by an open circle and a triangle, respectively. Here the DWBA cross sections were already multiplied by the (α,d) normarization factor of 100 which has been determined in our previous experiment of $^{51}V(\alpha,d)^{53}Cr$ reaction.[24] The resemblance of the angular distributions among the higher excited members implied that they should have a common configuration in the residual nuclei. This assumption was supported by the systematical mass dependence of the reaction Q-values (see Fig.7-5). In the discussions on the individual levles we could limit a configuration as the common wave function for the higher excitation members to either a $[\pi f_{7/2}{}^{\nu}g_{9/2}]_{8^-}$ or a $[\pi f_{5/2}{}^{\nu}f_{5/2}]_{5^+}$. As seen in Fig.7-7 the cross section systematics was well reproduced by the DWBA predictions with the $[\pi f^{n}_{7/2}{}^{\nu}g_{9/2}]$ assumption, while the $[\pi f_{5/2}{}^{\nu}f_{5/2}]$ assumption failed to explain the experimental tendency.

Now we summarize criteria for identification of these states to have a common $[\pi f^{n}_{7/2}{}^{\nu}g_{9/2}]$ configuration coupled to the 8^- highest spin.

(i) The cross sections to the levels were very large in the (α,d) reactions while in the $(^3He,p)$ reactions these states have weakly been excited or not.

(ii) All these levels were located at around E_x=4~5 MeV excitation

energies and the (α,d) Q-values varied linearly with the atomic number of the residual nucleus. This relationship was similar to that seen in the low-lying $[\pi f_{7/2}^{n}\nu p_{3/2}]_{5}^{+}$ states. (Fig. 7-5)

(iii) The angular distributions of the states showed structurless patterns and could be well reproduced by the L=7 DWBA predictions. The L=7 transfer allows spins of 6^{-}, 7^{-} and 8^{-}. (Fig. 4-5)

(iv) The integrated cross sections decreased with increasing the atomic number of the target nucleus. This was also very similar to the target dependence of the low-lying 5^{+} cross sections except for the $^{56}Fe(\alpha,d)^{58}Co$ reaction. The systematical change in the 5^{+} cross sections was due to the number of the $1f_{7/2}$ protons occupied in the target nucleus. (Figs. 7-6 and 7-7)

(v) The absolute (α,d) cross sections could be explained by the $[\pi f_{7/2}\nu g_{9/2}]_{L=7,J=8}$ p-n pair transfers including the ^{58}Co irregularity. While the DWBA calculations with the $[\pi f_{7/2}\nu g_{9/2}]_{L=7,J=7}$ and the $[\pi f_{7/2}\nu g_{9/2}]_{L=7,J=6}$ transfers gave only 1/550 and 1/150 of the experimental cross sections, respectively.

7-4) Residual interaction energy of the $[\pi f_{7/2}{}^{n}\nu g_{9/2}]_{8^-}$

In the preceding sections the states preferentially excited by the (α,d) reactions at around Ex ~4.5 MeV were assigned to have the highest spin 8^- in the $[\pi f_{7/2}{}^{n}\nu g_{9/2}]$ configuration. The angular momenta of the proton and neutron coupled to maximum in the stretched manner. In this section we will further consider the relation between the Q-value and the atomic number of the target nucleus. Then it follows to be clear that these levels have a common configuration $[\pi f_{7/2}{}^{n}\nu(\ell j)]_J$. Finally we will extract a two-body residual interaction energy between the proton and the neutron in the configuration $[\pi f_{7/2}\nu g_{9/2}]_{8^-}$.

From the excitation energies of the high spin states together with single particle excitation energies of the neighboring odd-mass nuclei, empirical residual interaction energies $V'^{pn}(j_1 j_2 J)$ can be calculated. The $V'^{pn}(j_1 j_2 J)$ means a two-particle interaction energy in a [(target) X $\pi(\ell_1 j_1)\nu(\ell_2 j_2)]_J$ configuration, which includes two-particle interactions between the target nucleons and the transferred j_1, j_2 nucleons besides the j_1-j_2 interaction. In terms of binding energies of the neighboring odd-mass nuclei ($\varepsilon'(\ell j)$) and the $V'^{pn}(j_1 j_2 J)$, a mass of the residual nucleus of the (α,d) reaction can be written as,

$$ {}^{Z=20+n}_{N=29}A(J_0) + Ex(J) = {}^{Z=20+n-1}_{N=28}A(0^+) + m_p + m_n + \varepsilon'_\pi(\ell_1 j_1) + \varepsilon'_\nu(\ell_2 j_2) + V'^{pn}(j_1 j_2 J) \ . \qquad (7\text{-}1) $$

In the relation ${}^{Z}_{N}A(J_0)$ denotes the ground state mass of the nucleus

with Z protons and N neutrons, n means a number of protons outside the ^{48}Ca inert core and m_p and m_n are masses of a proton and a neutron ,respectively. The Ex(J) is an observed excitation energy of a spin J state in the residual doubly-odd nucleus with a configuration $[(\text{Target}(0^+)) \times (\pi(\ell_1 j_1)\nu(\ell_2 j_2))_J]_J$. The $\varepsilon'_\pi(\ell_1 j_1)$ and the $\varepsilon'_\nu(\ell_2 j_2)$ are proton and neutron binding energies in an $(\ell_1 j_1)$ and an $(\ell_2 j_2)$ single particle states of a $^{Z=20+n}_{N=28}A$ and a $^{Z=20+n-1}_{N=29}A$ nuclei, respectively. The single particle binding energies ε'_π and ε'_ν can be expressed as,

$$\varepsilon'_\pi(\ell_1 j_1) = {}^{Z=20+n}_{N=28}A(j_0) + \overline{Ex}(j_1) - ({}^{Z=20+n-1}_{N=28}A(0^+) + m_p) \qquad (7\text{-}2)$$

and

$$\varepsilon'_\nu(\ell_2 j_2) = {}^{Z=20+n-1}_{N=29}A(j'_0) + \overline{Ex}(j_2) - ({}^{Z=20+n-1}_{N=28}A(0^+) + m_n) \ , \qquad (7\text{-}3)$$

where $\overline{Ex}(j)$ is an energy centroid of the single particle states in the (ℓj) shell orbit. In the eqs.(7-1),(7-2) and (7-3) the ε'_π , ε'_ν and $V'^{pn}(j_1 j_2 J)$ are thought to be a proton and a neutron single particle energies and a two-body matrix element between the j_1 and j_2 nucleons, respectively, when the target nucleus can be regarded as a rigid core. The binding energy $\varepsilon'(\ell j)$ was estimated from the single particle states in the neighboring nuclei by using eqs. (7-2) and (7-3). Then we can extract the $V'^{pn}(j_1 j_2 J)$ from eq.(7-1).

The extracted results for the nuclei ^{50}Sc, ^{52}V, ^{54}Mn, ^{56}Co and ^{58}Co are tabulated in Table 7-III. The neighboring single particle

states used in the calculations are listed in Table 7-IV .
In the calculations the states excited at around Ex ~4.5 MeV are assumed to be formed by a $[\pi f_{7/2}^{n} \ \nu g_{9/2}]_{8^-}$ or a $[\pi f_{7/2}^{n-1}(0^+) \times \pi f_{5/2} \ \nu f_{5/2}]_{5^+}$ configuration. The excitation energies of the single particle states of the odd-mass nuclei are taken from the results of $(^3He,d)$[73,74,75,76,77] and (d,p)[71,72] reactions. For the $1f_{5/2}$ proton shell orbit, the binding energies were deduced by summing energy centroids for the isospin lower and higher states which were weighted with squares of isospin Clebsh-Gordan coefficients. The weight factor in the $T_>$ state is $1/(2T_0+1)$ and that in the $T_<$ state is $2T_0/(2T_0+1)$, where the T_0 is an isospin quantum number of the target nucleus. The binding energies are shown in Figs.7-10 and 7-11 for the proton and the neutron orbits, respectively, as a function of the proton number in the $1f_{7/2}$ shell orbit of the target nucleus (n-1). As can be seen in the figures, the binding energy is linearly proportional to the number of the $1f_{7/2}$ proton in the target. It must be noted that these binding energies are not identical with the single particle energies of the shell model but include average energies of the two-particle interactions between the $1f_{7/2}$ proton and the active nucleon outside the target nucleus(transferred nucleon). Therefore, if the average interaction energy between the active nucleon and the $1f_{7/2}$ proton is attractive, the binding energy increases linearly in going from A=49 to A=55 nucleus, while the binding energy decreases with increasing the $1f_{7/2}$ proton number if the average interaction energy is repulsive. The proton-proton interaction acts between the two-protons coupled to T=1 only, while the proton-neutron interaction acts for both T=0 and T=1 pairs. Horie and Ogawa[54] have deduced

the average interaction energy between the $1f_{7/2}$ protons in T=1 to be repulsive. In Fig. 7-11 a gradient of the $1f_{5/2}$ neutron line is about twice steeper than that of other lines. It can be explained by a large overlap of the wave functions between the $1f_{7/2}$ proton and the $1f_{5/2}$ neutron. The wave function of the $1f_{5/2}$ orbit has the quite same radial dependence as that of the $1f_{7/2}$ proton orbit, if we neglect a small difference caused from a spin-orbit and a Coulomb forces. Therefore, a value of the radial overlap integral between the $1f_{7/2}$ proton and the $1f_{5/2}$ neutron is larger than those between the $1f_{7/2}$ proton and the $2p_{3/2}$, $2p_{1/2}$ or $1g_{9/2}$ orbit .

Fig. 7-12 shows the residual interaction energy $V'^{pn}(j_1 j_2 J)$ as a function of the number of the $1f_{7/2}$ proton in the target nucleus. The values presented by open circles are obtained by assuming the residual state to have a $[\pi f_{7/2}^{n} \ \nu g_{9/2}]_{8^-}$ configuration and the values indicated by closed circles are obtained from a $[\pi f_{7/2}^{n-1}(0^+) \times \pi f_{5/2} \nu f_{5/2}]_{5^+}$ assumption. In both cases the values are not constant but show linearly increasing trends with the proton number in the $1f_{7/2}$ orbit. As will be shown in the following discussion, these results lead to exclude a possibility of the $[\pi f_{7/2}^{n-1}(0^+) \times \pi f_{5/2} \nu f_{5/2}]_{5^+}$ configurations to the Ex ~4.5 MeV states.

An effective two-body matrix element can be deduced from a calculation based on the shell model, in which a ^{48}Ca nucleus is assumed as an inert core. In the present calculation ,however, we excluded an effect come from a configuration mixing among states with the same J^{π}. This assumption is not so unreasonable, since the states treated in this work have the highest spins with a

stretched coupling of the angular momentum in the 1f-2p shell nuclei and the excitation energies, so the wave functions are expected to be pure. Detailes of the calculations are presented in Appendix.

From eqs.(A-3)~(A-8) , the masses of the ground state of the even-even nucleus with N= 28, the proton odd nucleus with N=28, the neutron odd nucleus with N=29 and the doubly-odd nucleus with N=29 can be written as follows.

$$ {}^{Z=20+n-1}_{N=28}A(0^+) = {}^{48}Ca + (n-1)m_p + (n-1)\varepsilon_\pi(f_{7/2}) + \frac{(n-1)(9-n)}{2(2j_1-1)} V_0^{pp} + \frac{(n-1)(n-3)}{2(2j_1-1)} E_0^{pp} , \qquad (7-4) $$

for the N=28 even mass nuclei.

$$ {}^{Z=20+n}_{N=28}A(\ell_1 j_1 = f_{7/2}) = {}^{48}Ca + nm_p + n\varepsilon_\pi(f_{7/2}) - \overline{Ex}(j_1) + \frac{(n-1)(7-n)}{2(2j_1-1)} V_0^{pp} + \frac{(n-1)^2}{2(2j_1-1)} E_0^{pp} , \qquad (7-5) $$

for proton odd nuclei in which the configuration is $[\pi(f_{7/2})^n_{7/2} \times {}^{48}Ca(0^+)]$.

$$ {}^{Z=20+n}_{N=28}A(\ell_1' j_1') = {}^{48}Ca + nm_p + (n-1)\varepsilon_\pi(f_{7/2}) + \varepsilon_\pi(\ell_1' j_1') - \overline{Ex}(j_1') + \frac{(n-1)(9-n)}{2(2j_1-1)} V_0^{pp} + \frac{(n-1)(n-3)}{2(2j_1-1)} E_0^{pp} + (n-1)\frac{\sum_{J'=even} (2J'+1) V^{pp}(j_1 j_1' J')}{\sum_{J'=even} (2J'+1)} , \qquad (7-5') $$

for proton odd nuclei in which the configuration is $[\pi(f_{7/2})_{0^+}^{n-1} \pi(\ell_1' j_1') \times {}^{48}Ca(0^+)]$.

$$
\begin{matrix} Z=20+n-1 \\ A(\ell_2 j_2) \\ N=28+j_2 \end{matrix} = {}^{48}Ca + (n-1)m_p + m_n + (n-1)\varepsilon_\pi(f_{7/2}) + \varepsilon_\nu(\ell_2 j_2)
$$

$$
- \overline{Ex}(j_2) + \frac{(n-1)}{(2j_1+1)(2j_2+1)} \sum_{J'} (2J'+1)\, V^{pn}(j_1 j_2 J') \quad , \tag{7-6}
$$

for neutron odd nuclei.

Finally, for doubly-odd nuclei the equations are written as

$$
\begin{matrix} Z=20+n \\ A(J) \\ N=29 \end{matrix} = {}^{48}Ca + n m_p + m_n + n\varepsilon_\pi(f_{7/2}) + \varepsilon_\nu(\ell_2 j_2) - Ex(J)
$$

$$
+ \frac{(9-n)}{2j_1+1} V^{pn}(j_1 j_2 J)
$$

$$
+ \frac{2(n-1)}{2j_1+1} \sum_{J_{11}} (2J_{11}+1) \sum_{J'} (2J'+1)\, V^{pn}(j_1 j_2 J') \begin{Bmatrix} J_{11} & j_1 & j_1 \\ j_2 & J & J' \end{Bmatrix}^2 \quad , \tag{7-7}
$$

for the nuclei with $[\pi f_{7/2}^{\,n} \quad \nu(\ell_2 j_2) \times {}^{48}Ca(0^+)]_J$ configuration and

$$
\begin{matrix} Z=20+n \\ A(J) \\ N=29 \end{matrix} = {}^{48}Ca + n m_p + m_n + (n-1)\varepsilon_\pi(f_{7/2}) + \varepsilon_\pi(\ell_1' j_1') + \varepsilon_\nu(\ell_2 j_2)
$$

$$
- Ex(J) + V^{pn}(j_1' j_2 J) + \frac{(n-1)}{(2j_1+1)(2j_2+1)} \sum_{J'} (2J'+1) V^{pn}(j_1 j_2 J')
$$

$$
+ \frac{(n-1)(9-n)}{2(2j_1-1)} V_0^{pp} + \frac{(n-1)(3-n)}{2(2j_1-1)} E_0^{pp}
$$

$$
+ (n-1) \sum_{J'=\text{even}} (2J'+1) V^{pp}(j_1 j_1' J') \Big/ \sum_{J'=\text{even}} (2J'+1) \quad , \tag{7-7'}
$$

for the nuclei with a $[\pi(f_{7/2})^{n-1}_{0^+}(\pi(\ell'_1 j'_1)\nu(\ell_2 j_2))_J \times {}^{48}Ca(0^+)]_J$ configuration.

In the above equations the $\varepsilon_\pi(\ell j)$ and the $\varepsilon_\nu(\ell j)$ are proton and neutron single particle energies in a one-body potential. Other notations appeared here are explained in the Appendix.

The ε'_π ε'_ν and the $V'^{pn}(j_1 j_2 J)$ which were deduced empirically in the present work are easily related to the $\varepsilon_\pi(\ell j)$, $\varepsilon_\nu(\ell j)$ and the two-body matrix elements seen in the eqs.(7-4)~(7-7').
The relations among these values are deduced as

$$\varepsilon'_\pi(\ell_1 j_1) = \varepsilon_\pi(\ell_1 j_1) + \frac{n-1}{2j_1-1}(E_0^{pp} - V_0^{pp}) \qquad (7\text{-}8)$$

$$\varepsilon'_\pi(\ell'_1 j'_1) = \varepsilon_\pi(\ell'_1 j'_1) + (n-1)\bar{v}^{pp}(j_1 j'_1) \qquad (\ell'_1 j'_1 \neq 1f_{7/2}) \qquad (7\text{-}8')$$

$$\varepsilon'_\nu(\ell_2 j_2) = \varepsilon_\nu(\ell_2 j_2) + (n-1)\bar{V}^{pn}(j_1 j_2) \qquad (7\text{-}9)$$

$$V'^{pn}(j_1 j_2 J) = n\{ \bar{V}^{pn}(g_J j_1 j_2) - \bar{V}^{pn}(j_1 j_2) - \frac{1}{2j_1+1} V^{pn}(j_1 j_2 J) \}$$
$$+ \frac{2j_1+2}{2j_1+1} V^{pn}(j_1 j_2 J) + \bar{V}^{pn}(j_1 j_2) - \bar{V}^{pn}(g_J j_1 j_2) \qquad (7\text{-}10)$$

$$V'^{pn}(j'_1 j_2 J) = V^{pn}(j'_1 j_2 J) \qquad (\ell'_1 j'_1 \neq 1f_{7/2}) \qquad (7\text{-}10')$$

It is apparent from eqs. (7-8) ~ (7-9) that the $\varepsilon'_\pi(\ell j)$ and $\varepsilon'_\nu(\ell j)$ are linearly proportional to the number of the $1f_{7/2}$ protons in the target nucleus (n-1). From these equations and the values shown in Figs. 7 -10, 7 -11 , the $\varepsilon_\pi(\ell j)$, $\varepsilon_\nu(\ell j)$, $(E_0^{pp} - V_0^{pp})$ and

the $\bar{V}^{pn}(j_1 j_2)$ can be obtained for the single particle levels of the $1f_{7/2}$ and the $1f_{5/2}$ proton orbits and of the $2p_{3/2}$, $2p_{1/2}$, $1f_{5/2}$ and the $1g_{9/2}$ neutron orbits. These values are listed in Table 7-V comparing with the values deduced by Horie and Ogawa.[54] In their calculations effects of configuration mixings are taken into account. In our derivation of these values , since the experimentally observed energies were used for the binding energies of the odd-mass nuclei, some core excitation has already been taken into account. Our simple treatment to extract the two-body matrix element may still be accurate even when the target configuration is not so pure.

Eqs.(7-10) and(7-10') are the relations to combine the two-body matrix elements deduced from empirically and from the shell model. When the proton transferred by the (α,d) reaction enters into the $1f_{7/2}$ shell orbit, the V'^{pn} is proportional to the number of the $1f_{7/2}$proton in the residual nucleus n, on the other hand when the proton is transferred into the higher shell orbit other than the $1f_{7/2}$, the $V'^{pn}(j_1' j_2 J)$ is identical with the two-body matrix element of the shell model $V^{pn}(j_1' j_2 J)$. Then the $V'^{pn}(j_1' j_2 J)$ must be constant independently of the atomic numbers of the target. Actually, the $V'^{pn}(f_{7/2} g_{9/2})$ is linearly increased with n. This trend supports that the 4.32 MeV state in ^{52}V, 4.175 MeV state in ^{54}Mn and the 4.99 MeV state in ^{56}Co have a common $[\pi f_{7/2}^{\ n}\ \nu(\ell j)]_J$ configuration as was assigned from the cross section systematics in section 7-3). On the other hand the empirical residual interactions $V'^{pn}(f_{5/2} f_{5/2} 5^+)$ extracted by assuming the $[\pi f_{7/2}^{n-1} \pi f_{5/2} \nu f_{5/2}]$ configuration did not stay constant but changed largely with n.(see Fig.7-12) This result is inconsistent with the shell model prediction given by eq.(7-10') and excludes the possibility of the $[\pi f_{7/2}^{n-1} \pi f_{5/2} \nu f_{5/2}]$

configuration for the higher excitation members completely. Then it can be concluded that the linearly decreasing trend of the reaction Q-values shown in Fig.7-5 is essentially due to the proton transfer into the $1f_{7/2}$ orbit for both the lower 5^+ and higher 8^- states.

The residual interaction energy $V^{pn}(f_{7/2}g_{9/2}\ 8^-)$ and the average interaction energy $\bar{V}(f_{7/2}g_{9/2})$ are deduced to be -0.76 ± 0.09 and 0.73 ± 0.08 MeV, respectively. To compare the extracted residual interaction energies with theoretical calculations a simple δ-force between proton and a neutron is introduced. It contains a usual spin-exchange term and is written as[78]

$$V_{pn} \propto \delta(\vec{r}_p-\vec{r}_n)[(1-\alpha) + \alpha P(\vec{\sigma}_p\vec{\sigma}_n)], \qquad (7\text{-}11)$$

where α is a strength factor of the spin-exchange term and P is a spin-exchange operator. The calculated residual interaction energies $V^{pn}(f_{7/2}g_{9/2}J)$ were -2.02,-1.04,-0.44,-0.76,-0.22,-0.80,-0.11 and -1.42 MeV for $J=1^-,2^-,3^-,\cdots$, and 8^-, respectively, and the average interaction energy was -0.69 MeV. The experimental residual interaction of the J=8 state was considerably small compared with the calculated value. Kuo and Brown[79] have calculated proton-neutron interaction energies by using the Hamada-Johnston potential for the mass region A~40. In table 7-V the average interaction $\bar{V}^{pn}(j_1j_2)$ and the residual interaction energies of the stretched configurations $V^{pn}(j_1j_2J_{max})$ are listed for the interactions between the $1f_{7/2}$ proton and the $2p_{3/2}$,$2p_{1/2}$,$1f_{5/2}$, $2s_{1/2}$,$1d_{5/2}$ and $1d_{3/2}$ neutron states. The $V^{pn}(j_1j_2J_{max})$ are -0.65~ -1.04 for negative parity states. The somewhat small experimental value of -0.76 may be due to unaccurate $1g_{9/2}$ single neutron excitation energies in the N=29 odd mass nuclei,where the spectroscopic factors of the $1g_{9/2}$ states have been found only 50~70 % of the total strength (see Table 7-IV). Further (d,p) reactions may change the experimental value slightly.

§ 8. Summary and conclusions

The present work showed that the direct (α,d) reaction has a number of useful features to investigate a nuclear structure of doubly-odd nuclei. Particularly, the reaction is adequate to study high spin states. The (α,d) reaction on the 1f-2p shell nuclei at 23.9 MeV incident energy is favor to transfer an orbital angular momentum 4~7ħ, which is carried by the transferred p-n pair. At the same time, however, this large angular momentum mismatch between the entrance and the exit channels brought a disadvantage in the DWBA analysis for small orbital angular momentum transfer (L) reactions. The angular distributions of small L transfers (L= 0 and 2) were poorly fitted by the zero-range DWBA calculations if the conventional optical potential parameters which reproduce the elastic scattering angular distributions were employed. On the other hand, the experimental angular distributions of large L transfers could be well fitted by the conventional DWBA calculations. Only a few partial waves of both the entrance and exit channels, which are defined near the nuclear surface, contribute to the overlap integrals in the DWBA calculations for the large L transfers, while for the small L transfers almost all partial waves contribute to the overlap integrals with nearly the same weight. The large contribution from the lower partial waves which are not well defined by the elastic scattering angular distribution fitting procedure (optical potential parameters search) causes the poor DWBA fit for the small L transfers.

The experimental (α,d) normarization constant determined previously in the $^{51}V(\alpha,d)^{53}Cr$ analysis by Kawa et al.[24,60] was still valid for the analyses of the present (α,d) reactions on ^{50}Ti, ^{52}Cr,

^{54}Fe and ^{56}Fe target nuclei, especially for the low-lying 5^+ states the DWBA predictions with the $[f_{7/2}\ p_{3/2}]_{L=4,J=5}$ transfer gave N=111, 100, 92 and 113 for the four reactions. They are much close to the normal value N_0=100.

In the (α,d) reactions at 23.9 MeV alpha particle energy, cross sections via two-step processes of successive nucleon transfer (α-t-d) and (α-^{3}He-d) channels were factors of 8~10 weaker than the direct one-step process even when the (α-t-d) and the (α-^{3}He-d) channels worked cohelently. Constructive and destructive interferences between the one- and two-step amplitudes modified the predicted cross sections by factors of 0.7~1.3 but the shapes of the angular distributions were not affected.

All the (α,d) reactions on N=28 single closed nuclei (^{50}Ti, ^{52}Cr and ^{54}Fe) and a neighboring N=30 nucleus (^{56}Fe) at 23.9 MeV incident energy , two levels were found to be strongly populated (see Fig. 4-3). They were classified into two group in accordance with the excitation energies and the shapes of the angular distributions. The lower excitation members were all located at around 0.5 MeV excitation. They were 0.02 MeV in ^{52}V, 0.363 MeV in ^{54}Mn , 0.576 MeV in ^{56}Co and 0.020 MeV in ^{58}Co. The higher excitation members were distributed at around 4~5 MeV in excitation energies and they were located at 4.32 MeV in ^{52}V, 4.72 MeV in ^{54}Mn , 4.99 MeV in ^{56}Co and 3.75 MeV in ^{58}Co. For the lower excitation members the spin and parity have been determined or tentatively assigned previously but for the higher excitation members no spin and parity assignments have been done so far. We analyzed the angular distributions of these levels individually by means of the DWBA analysis. Some systematical trends observed in reaction Q-values and in the total cross sections were

analyzed precisely in terms of an interaction model method based on a shell model calculation and the DWBA calculation.

From these analyses the following could be concluded:

(i) The angular distributions of the lower excitation members have very similar patterns with each other, and were well reproduced by the DWBA predictions of an L=4 transfer.

(ii) The total cross sections of the lower excitation members decrease rapidly with increasing the number of protons in the $1f_{7/2}$ shell orbit in the target nuclei. This systematical trend was fairly well explained by the zero-range DWBA calculations when $[\pi f_{7/2}^{n}\ \nu(\ell j)]$ configurations were adopted as final state wave functions. The predicted absolute cross sections agreed with the experimental ones only if we assume the $[\pi f_{7/2}^{n}\ \nu p_{3/2}]_{5^+}$ configurations. Then spin and parity of the lower excitation members were confirmed to be 5^+ with a dominant $[\pi f_{7/2}^{n}\ \nu p_{3/2}]$ configuration.

(iii) The angular distributions of the higher excitation members have also very similar patterns with each other. They were reproduced by the DWBA predictions with an L=7 transfer.

(iv) A quite similar systematical trend as observed in the lower excitation 5^+ members (see (ii)) was also seen in the higher excitation members except for the 3.75 MeV in ^{58}Co data. This was also explained by the $[\pi f_{7/2}\ \nu(\ell j)]$ transfer. A irregularity seen in the cross sections of ^{58}Co could be interpreted as follows. Since the $2p_{3/2}$ neutron shell is one half closed while other higher neutron orbits are fully open like as the N=28 nuclei for the ^{56}Fe nucleus, the cross section of the neutron transfer into the $2p_{3/2}$ shell shows the irregular value.

The absolute cross sections were reproduced by assuming a $[\pi f_{7/2}\nu g_{9/2}]_{L=7,J=8}$ p-n pair transfer, though the predicted ones were smaller than the experiments by about 20 % systematically in all reactions. We assigned these levels to be 8^- with $[\pi f_{7/2}^{n}\ \nu g_{9/2}]$ configurations.

(v) The preferential excitations of the high spin states in the (α,d) reaction could be explained by following reasons. A large angular momentum difference between the entrance and the exit channels has to be carried by the transferred two nucleons. In the present case it was about 4~7 $\hbar$ varying with an excitation energy. Cross sections of large angular momentum transfers do not decrease so rapidly with an excitation energy as those of small angular momentum transfers. A usual statistical (2J+1) factor in stripping reactions enhances a transition strength to high spin states. The most significant factor is the geometrical factor for the (α,d) reaction (transformation coefficient from j-j to L-S coupling scheme). A transition amplitude became maximum when intrinsic spins of the transferred nucleons were parallel with each other and their total angular momenta (j_p and j_n) coupled in a stretched manner to make a resultant spin to be maximum. This situation is realized in $[\pi f_{7/2}\nu p_{3/2}]_{J=5}$, $[\pi f_{7/2}\nu g_{9/2}]_{J=8}$, $[\pi f_{5/2}\nu f_{5/2}]_{J=5}$ and $[\pi p_{3/2}\nu p_{3/2}]_{J=3}$ transfers.

(vi) In both the transitions to the 5^+ and the 8^- states it was found that the -Q-value linearly increased with increasing the atomic number of the target nuclei. This linear tendency was also explained by assuming the final state wave function to be $[\pi f_{7/2}^{n}\ \nu(\ell j)]$.

(vii) The residual interaction energy between proton and neutron in the configuration $[\pi f_{7/2}{}^{\nu}g_{9/2}]_{J=8}$ was deduced to be -0.76 MeV. The average interaction energy in this configuration was also extracted and was -0.73 MeV. The magnitude of the residual interaction was considerably small compared with the calculated value -1.42 MeV, while the average energy was very close to the calculated value -0.69 MeV. The large discrepancy in the residual interaction may be due to an unrealistic form of the δ-force interaction used in the calculation and somewhat unaccurate single particle energies of the $1g_{9/2}$ neutron shell orbit for whom the spectroscopic factors found so far were 50~70 % of the total strength in the odd-mass nuclei.

Acknowledgements

The author would like to acknowledge Professor T. Wakatsuki and Professor H. Ejiri for the continuing guidance, encouragement and useful discussions. Throughout the progress of the work, the author had many discussions with his colleagues Dr. J. Kawa and Mr. T. Yamagata. Their contributions to this work have been very great and it is his great pleasure to acknowledge for the valuable discussions and helpful co-operations. The author wishes to express his thanks to Dr. K. Suzuki and Dr. Y. Aoki for the valuable suggestions on the DWBA and form factor calculations. Thanks are also due to Professor S. Kato for the useful suggestions. The author is indebted to the operating crews of the Osaka University Cyclotron for providing the beam used in the work.

References

1) W.Tobocman, Theory of Direct Nuclear Reactions (Oxford University Press, New York, 1961).

2) C.L.Lin and S.Yoshida, Progress Theor. Phys. 32 (1964) 885.

3) N.K.Glendenning, Phys. Rev. 137 (1965) B102.

4) B.F.Bayman and A.Kallio, Phys. Rev. 156 (1970) 1121.

5) K.Yagi, Y.Aoki, J.Kawa and K.Sato, Phys. Letters 29B (1969) 647.

6) J.B.Ball, R.L.Auble, J.Rapaport and C.B.Fulmer, Phys.Letters 30B (1969)533.

7) O.Hansen, O.Nathan, R.Chapman and S.Hinds, Nucl. Phys. A127 (1969) 71.

8) T.A.Belote,W.E.Dorenbusch and J.Rapaport, Nucl. Phys. A109 (1968) 666.

9) T.Caldwell, O.Nathan, O.Hansen and H.Bork, Nucl. Phys. A202 (1973) 225.

10) G.Bruge and R.F.Reonard, Phys. Rev. C2 (1970) 2200.

11) Y.Dupont, P.Martin and M.Chable, Phys. Rev. C7 (1973)637.

12) J.Kawa, K.Okada and T.Yamagata, J.Phys.Soc.Japan 37 (1974) 789.

13) S.A.Hjorth, Arkiv Fysik 33 (1966) 147.

14) M.J.Schneider and W.W.Daehnick, Phys. Rev. C4 (1971) 1649.

15) K.Suzuki, J.Kawa and K.Okada, Nucl. Phys. A228 (1974) 513.

16) D.G.Fleming, R.A.Brogria, K.Abdo, O.Nathan, D.J.Pullen, B.Rosner and O.Hansen, Phys.Rev. C5 (1972) 1356.

17) R.R.Betts, O.Hansen and D.J.Pullen, Nucl. Phys. A182 (1972) 69.

18) C.Moazed, K.Nagatani and A.M.Bernstein, Nucl. Phys. A139 (1969) 1.

19) D.G.Fleming, O.Nathan, H.B.Jensen and O.Hansen, Phys. Rev. C5 (1972) 1365.

20) B.G.Harvey, J.Cerny , R.H.Pehl and E.Rivet, Nucl. Phys. 39 (1962) 160.

21) E.Rivet, R.H.Pehl, J.Cerny and B.G.Harvey, Phys.Rev. 141 (1966) 1021.

22) C.C.Lu, M.S.Zisman and B.G.Harvey, Phys. Rev. 186 (1969) 1086.

23) R.M.DelVecchio, R.T.Kouzes and R.Sherr, Nucl. Phys. A265 (1976) 220.

24) J.Kawa, K.Okada and T.Yamagata, J. Phys. Soc. Japan 36 (1974) 929.

25) H.Ohnuma, J.R.Erskine, J.A.Nolen, J.P.Schiffer and P.G.Roos, Phys. Rev. 177 (1969) 1695.

26) J.M.Laget, J.Vervier, G.Bruge, J.M.Loiseaux and L.Valentin, Nucl. Phys. A125 (1969) 481.

27) T.Engeland and E.Osnes, Nucl. Phys. A226 (1974) 45.

28) F.A.El Bedewi and S.Tadros, Nucl. Phys. 8 (1958) 71.

29) A.W.Dalton, A.Kirk, G.Parry and H.D.Scott, Proc. Phys. Soc.(London) 75 (1960) 95.

30) J.H.Bjerregaard, P.F.Dahl, O.Hansen and G.Sidenius, Nucl. Phys. 51 (1964) 641.

31) J.Catala, A.Garcia, J.M.Bolta, S.Hinds, H.Marchant and A.E.Forest, Nucl. Phys. 74 (1965) 1.

32) N.C.Rasmussen, Y.Hukai, T.Inouye and V.J.Orphan, AFCRL-69-0071 (MITNE-85) (1969).

33) G.Hardie, D.Gloeckner, L.Meyer-Schützmeister and T.H.Braid, Phys. Rev. C10 (1974) 1829.

34) T.Caldwell, D.J.Pullen and O.Hansen, Nucl. Phys. A242 (1975) 221.

35) L.L.Lynn, W.E.Dorenbusch, T.A.Belote and J.Rapaport, Nucl. Phys. A135 (1969) 97.

36) J.K.Dickens, Phys. Rev. C5 (1972) 1977.

37) R.Hill and S.G.Buccino, Bull. Am. Phys. Soc. 15 (1970) 1345.

38) D.O.Wells, S.L.Blatt and W.E.Meyerhof, Phys. Rev. 130 (1963) 1961.

39) R.C.Jenkins and W.E.Meyerhof, Nucl. Phys. 58 (1964) 417.

40) H.Ohnuma, Y.Hashimoto and I.Tomita, Nucl. Phys. 66 (1965) 337.

41) C.J.Piluso, D.O.Wells and D.K.McDaniels, Nucl. Phys. 77 (1966) 193.

42) L.E.Samuelson, W.H.Kelly, R.R.Todd, R.A.Warner, W.C.McHarris, F.M.Bernthal, E.M.Bernstein and R.Shamu, Phys. Rev. C7 (1973) 2379.

43) P.Goode and L.Zamick, Phys. Rev. Letters 22 (1969) 958.

44) J.M.Laget and J.Gastebois, Nucl. Phys. A122 (1968) 431.

45) C.Shin, B.Povh, K.Schadewaldt and J.P.Wurm, Phys. Rev. Letters 22 (1969) 1124.

46) N.Frascaria, J.P.Didelez, J.P.Garron, E.Gerlic and J.C.Roynette, Phys. Rev. C10 (1974) 1422.

47) F.S.Goulding, D.A.Landis, J.Cerny and R.H.Pehl, Nucl. Inst. Meth. 31 (1964) 1.

48) E.Newman and J.C.Hiebert, Nucl. Phys. A110 (1968) 366.

49) G.D.Gunn, J.D.Fox and G.J.Kekelis, Phys. Rev. C13 (1976) 595.

50) B.J.O'Brien, W.E.Dorenbusch, T.A.Belote and J.Rapaport, Nucl. Phys. A104 (1967) 609.

51) S.Fortier, J.M.Maison, S.Galès, H.Laurent and J.P.Schapira, Nucl. Phys. A288 (1977) 82.

52) A.Trier, L.Gonzalez, J.Rapaport, T.A.Belote and W.E.Dorenbusch, Nucl. Phys. A111 (1968) 241.

53) Nuclear Data Sheets, B-3-5,6 (1970).

54) H.Horie and K.Ogawa, Prog. Theor.Phys. 46 (1971) 439 and private communication.

55) P.D.Kunz, Computer code "DWUCK", University of Colorado.

56) K.Suzuki, Ph. Dr. Thesis, University of Osaka, (1973).

57) L.McFadden and G.R.Satchler, Nucl. Phys. 84 (1966) 177.

58) M.B.Lewis, Phys. Rev. 184 (1969) 1081.

59) W.W.Daehnick, Y.S.Park, Phys. Rev. 180 (1969) 1062.

60) J.Kawa, Ph. Dr. Thesis, University of Osaka, (1974).

61) R.Stock, R.Bock, P.David, H.H.Duhm and T.Tamura, Nucl. Phys. A104 (1967) 136.

62) M.Toyama and M.Igarashi, Computer code "TWOSTP".

63) M.Toyama, Nucl. Phys. A211 (1973) 254.

64) M.Toyama, Phys. Letters, 49B (1974) 311.

65) J.Kawa, K.Okada and T. yamagata, OULNS Annual Report 72-1(1971)4.

66) R.H.Bassel, Phys. Rev. 149 (1966) 791.

67) D.G.Sarantities, J.Urbon and L.L.Rutledge,Jr, Phys. Rev. C14 (1976) 1412.

68) R.Sherr, R.T.Kouzes and R.M.DelVecchio, Phys. Letters, 52B (1974) 401.

69) L.D.Rickertsen, M.J.Schneider, J.J.Kraushaar, W.R.Zimmerman and H.Rudolph, Phys. Letters 60B (1975) 19.

70) M.J.Schneider and W.W.Daehnick, Phys. Rev. C5 (1972) 1330.

71) D.C.Kocher and W.Haeberli, Nucl. Phys. A196 (1972) 225.

72) J.A.Thomson, Nucl. Phys. A227 (1974) 485.

73) D.J.Pullen, B.Rosner and O.Hansen, Phys. Rev. 177 (1969) 1568.

74) S.Galès, S.Fortier, H.Laurent, J.M.Maison and J.P.Schapira, Nucl. Phys. A259 (1976) 189.

75) D.D.Armstrong and A.G.Blair, Phys. Rev. 140 (1965) B1226 .

76) S.Galès, S.Fortier, H.Laurent, J.M.Maison and J.P.Schapira, Phys. Rev. C14 (1976) 131.

77) A. de-Shalit and I.Talmi, Nuclear Shell Theory (Academic Press, New York and London) (1963).

78) M.Moienster, J.P.Schiffer and W.P.Alford, Phys. Rev. 179 (1969) 984.

79) T.T.S.Kuo and G.E.Brown, Nucl. Phys. A114 (1968) 241.

Appendix Two-particle interaction energy of the shell model

The two-body interaction energy in the j^n configuration with identical particles can be expressed by[77]

$$\begin{aligned}
&\langle j^n v\alpha J|\sum_{i<h}^{n} V_{ih}|j^n v\alpha' J\rangle \\
&= \langle j^v v\alpha J|\sum_{i<h}^{v} V_{ih}|j^v v\alpha' J\rangle + \frac{n-v}{2} E_0 \delta_{\alpha\alpha'} \\
&+ \frac{(n-v)(2j+1-n-v)}{2(2j-1-2v)} \Big[\langle j^{v+2} v\alpha J|\sum_{i<h}^{v+2} V_{ih}|j^{v+2} v\alpha' J\rangle \\
&- \langle j^v v\alpha J|\sum_{i<h}^{v} V_{ih}|j^v v\alpha' J\rangle - E_0 \delta_{\alpha\alpha'} \Big] \quad , \qquad \text{(A-1)}
\end{aligned}$$

where E_0 means the average interaction energy of the j^2 configuration and is written in terms of the matrix element in the j^2 configuration $\langle j^2 J|V_{12}|j^2 J\rangle = V_J$ as

$$E_0 = \frac{2}{2j+1} \sum_{J=\text{even}} (2J+1) V_J \quad . \qquad \text{(A-2)}$$

The v and α represent a seniority and other quantum numbers in the j^n configuration. Equation (A-1) can be written explicitly in the cases of v=0 and v=1. For the J=0 state with v=0 eq.(A-1) is

$$\langle j^n v=0\ J=0|\sum_{i<h}^{n} V_{ih}|j^n v=0\ J=0\rangle = \frac{n(2j+1-n)}{2(2j-1)} V_0 + \frac{n(n-2)}{2(2j-1)} E_0 . \qquad \text{(A-3)}$$

And for the J=j state with v=1,

$$\langle j^n v=1\ J=j|\sum_{i<h}^{n} V_{ih}|j^n v=1\ J=j\rangle = \frac{(n-1)(2j-n)}{2(2j-1)} V_0 + \frac{(n-1)^2}{2(2j-1)} E_0 . \qquad \text{(A-4)}$$

Next, the interaction energy in the configuration $j_1^n j_2$ coupled to spin J can be written as[77]

$$\langle j_1^n(\alpha_1 J_1) j_2 J | \sum_{i=1}^{n} V_{i,n+1} | j_1^n(\alpha_1' J_1') j_2 J \rangle \qquad \text{(A-5)}$$

$$= n \sum_{\alpha_{11} J_{11}} [j_1^n \alpha_1 J_1 \{| j_1^{n-1}(\alpha_{11} J_{11}) j_1 J_1] [j_1^{n-1}(\alpha_{11} J_{11}) j_1 J_1' \}| j_1^n \alpha_1' J_1']$$

$$\times [(2J_1+1)(2J_1'+1)]^{1/2} \sum_{J'} (2J'+1) V(j_1 j_2 J') \begin{Bmatrix} J_{11} & j_1 & J_1 \\ j_2 & J & J' \end{Bmatrix} \begin{Bmatrix} J_{11} & j_1 & J_1' \\ j_2 & J & J' \end{Bmatrix} ,$$

where [....{|...] denotes the coefficient of fractional parentage and {...} denotes the 6-j symbol. In the equation we assumed that the j^n particles are coupled to have the minimum seniority. This assumption is quite true for the ^{56}Co nucleus because there is only one proton holes in the $1f_{7/2}$ orbit. For other nuclei this assumption means that excited states are formed by a coupling of single particle with the target nucleus. For an n=odd nucleus the equation (A-5) is written as

$$\langle j_1^n(v=1, J_1=j_1) j_2 J | \sum_{i=1}^{n} V_{i,n+1} | j_1^n(v=1, J_1=j_1) j_2 J \rangle$$

$$= \frac{2j_1+2-n}{(2j_1+1)} V(j_1 j_2 J)$$

$$+ \sum_{\substack{J_{11}>0 \\ \text{even}}} \frac{2(n-1)(2J_{11}+1)}{(2j_1-1)} \sum_{J'} (2J'+1)\, V(j_1 j_2 J') \begin{Bmatrix} J_{11} & j_1 & j_1 \\ j_2 & J & J' \end{Bmatrix}^2 . \qquad \text{(A-6)}$$

For an even n nucleus the (A-5) is

$$\langle j_1^n(v=0, J_1=0) j_2 J | \sum_{i=1}^{n} V_{i,n+1} | j_1^n(v=0, J_1=0) j_2 J \rangle$$

$$= \frac{n}{(2j_1+1)(2j_2+1)} \sum_{J'} (2J'+1) V(j_1 j_2 J') \equiv n\, \bar{V}(j_1 j_2) . \qquad \text{(A-7)}$$

For a special case of n=1, the equation (A-6) represent a two-particle interaction energy $V(j_1 j_2 J)$.

For a nucleus with n protons in the $1f_{7/2}$ orbit and a neutron in the $(\ell_2 j_2)$ orbit outside the ^{48}Ca inert core, the resultant two-particle residual interactions are expressed as

$$<\pi(\ell_1 j_1)^n \nu(\ell_2 j_2) J \; | \sum_{i>h}^{n} V_{ih}^{pp} + \sum_{i=1}^{n} V_{i,n+1}^{pn} | \pi(\ell_1 j_1)^n \nu(\ell_2 j_2) J>. \quad \text{(A-8)}$$

where V^{pp} is a proton-proton interaction and V^{pn} is a proton-neutron interaction.

Figure captions

Fig.3-1 Layout of the beam transport line.

Fig.3-2 Typical particle identification spectrum of the ^{52}Cr + 23.9 MeV alpha particles.

Fig.3-3 Block diagram of the electronic circuit.

Fig.4-1 Typical energy spectrum of deuterons from the $^{54}Fe(\alpha,d)^{56}Co$ reaction at $\theta_{lab.}$ = 50 degrees. The numbers indicated above the peaks refer the peak numbers in table 4-I. The contaminants in the spectrum are shown hatched and are labelled by residual nucleus.

Fig.4-2-a Experimental deuteron angular distributions and DWBA predictions for an L=0 transfer of the $^{54}Fe(\alpha,d)^{56}Co$ reaction. Solid lines: DWBA predictions by using the optical potential set A1-D1. Dashed lines: DWBA predictions by using the optical potential set A2-D2.

Fig.4-2-b Angular distributions for an L=2 transfer. See caption of Fig.4-2-a for details.

Fig.4-2-c Angular distributions for L=4, 6 and 7 transfers. See caption of Fig.4-2-a for details.

Fig.4-2-d Angular distributions for an uncertain L transfer.

Fig.4-3 Deuteron energy spectra of the $^{50}Ti(\alpha,d)^{52}V$, $^{52}Cr(\alpha,d)^{54}Mn$ $^{54}Fe(\alpha,d)^{56}Co$ and $^{56}Fe(\alpha,d)^{58}Co$ reactions at E_α=23.9 MeV. The prominent peaks marked by single- and double-asterisks are identified to be high spin states with configurations of $[\pi f_{7/2}^{n}\nu p_{3/2}]_{5}^{+}$ and $[\pi f_{7/2}^{n}\nu g_{9/2}]_{8}^{-}$, respectively. The cross hatched peaks in the spectra are due to the $^{12}C(\alpha,d)^{14}N$(gnd. state) reaction.

Fig.4-4 Experimental angular distributions and DWBA predictions for the lower excitation members excited strongly by the (α,d) reactions. The solid lines are the DWBA curves obtained by assuming a $[\pi f_{7/2}\nu p_{3/2}]_{L=4,J=5}$ transfer with the A1-D1 potential set. Error bars are due to statistical and background subtraction errors. An absolute scale error is less than 15%.

Fig.4-5 Experimental and DWBA angular distributions for the higher excitation members excited strongly by the (α,d) reactions at Ex= 4~5 MeV. The solid and dashed lines are the DWBA curves obtained by assuming a $[\pi f_{7/2}\nu g_{9/2}]_{L=7,J=8}$ and a $[\pi f_{5/2}\nu f_{5/2}]_{L=6,J=5}$ transfers, respectively. Error bars are mainly due to background subtraction errors.

Fig.4-6 Elastic scattering angular distributions of the $^{52}Cr(\alpha,\alpha)$ and $^{54}Fe(\alpha,\alpha)$ at E_α=23.9 MeV. The solid and dashed lines are the optical-model fits using the parameter sets A1 and A2 of table 5-II, respectively.

Fig.4-7 Elastic scattering angular distribution of the $^{52}Cr(d,d)$ reaction at E_d= 11.3 MeV. The solid line is the optical model fit using the D1 parameters of table 5-II.

Fig.5-1 Reflection coefficients for the elastic alpha and deuteron scattering. For the 23.9 MeV alpha particles the $|\eta_\ell|$ are shown by a solid line. For the deuterons, the $|\eta_\ell|$ are shown for the excitation energies corresponding to Ex=0.0 and 5.0 MeV in the $^{54}Fe(\alpha,d)^{56}Co$ reaction by dotted and dashed lines, respectively. The lower part of the figure shows radial overlap integrals $F_{SLJ}(\ell_\alpha \ell_d)$ for L=0 and L=6 transfers by dashed and solid lines respectively.

The $F_{SLJ}(\ell_\alpha \ell_d)$ shown are restricted to the ones for L= $\ell_\alpha - \ell_d$, for simplicity.

Fig.5-2 Schematical reaction processes to excite a ^{56}Co level of J^π by the ^{54}Fe + 23.9 MeV alpha particles. Direct, two-step and compound processes are shown by solid, double and dashed lines, respectively. The two-step processes here considered are sequential nucleon transfer processes via (α-t-d) and (α-^{3}He-d) channels.

Fig.5-3 Experimental angular distributions of the ^{51}V(α,d)^{53}Cr reaction at E_α=22 MeV by Kawa et al.[24] The angular distributions measured from 15° to 130° show assymmetric patterns with respect to the 90° center of mass system. This suggests that contributions from the compound process to the (α,d) cross sections are small.

Fig.5-4 Experimental and calculated angular distributions of the ^{54}Fe(α,d)^{56}Co reaction. Solid lines labeled by 'D' are the one-step DWBA predictions. Two-step cross sections via (α-t-d) and (α-^{3}He-d) channels are shown by solid and dash-dotted lines, respectively. Cross sections of constructive and destructive interferences between these two-step channels are shown by dashed and dotted lines, respectively. Cohelent sums of the one- and two-step amplitudes are shown by dashed lines labeled by 'D+T' and dotted lines labeled by 'D-T' for the constructive and destructive interferences, respectively.

Fig.7-1 Matched angular momentum defined by $L_m = k_i R_i - k_f R_f$ is shown as a function of an excitation energy of the residual nucleus of the (α,d) reactions at E_α=24 MeV.

Fig.7-2 Q-value dependences of the (α,d) form factors for L=4 and L=6 transfers of the $[\pi f_{7/2}\nu f_{5/2}]$ n-p pair. For transitions to Ex=4.5 MeV the form factor extend to outer region compared with those of Ex=0.5 MeV. This causes a large overlap integral at the higher excitation energy.

Fig.7-3 Q-value dependences of the DWBA cross sections of the $^{54}Fe(\alpha,d)^{56}Co$ reaction for L=0, 2, 4 and 6 transfers. The optical potential parameters used are the A1-D1 set. The cross sections are obtained by integrating over an angular range from 14° to 105°. They are conventionally normarized to 1 at Q=-9.5 MeV.

Fig.7-4 Calculated energy spectra of the (α,d) reactions on N=28 target nuclei at E_α=23.9 MeV. In the calculations the excitation energies of the levels formed by $[\pi(\ell_p j_p)\nu(\ell_n j_n)]$ transfers are determined from the proton and neutron single particle excitation energies of the neighboring odd-mass nuclei. In all the spectra 5^+ states populated by the $[\pi f_{7/2}\nu p_{3/2}]_{L=4}$ transfer and 8^- states by the $[\pi f_{7/2}\nu g_{9/2}]_{L=7}$ transfer have large cross sections.

Fig.7-5 Reaction Q-values of the 5^+ and 8^- states as a function of the atomic number of the residual nuclei are shown by open and closed circles, respectively. The negative Q-values increase linearly with increasing the atomic number of the residual nuclei for both transitions. The ^{50}Sc data in the higher excitation members is taken from the $^{48}Ca(\alpha,d)^{50}Sc$ reaction by Moazed et al.[18] in which the 4.42 MeV state has been strongly excited.

Fig.7-6 Cross sections of the lower excitation members (5^+) as a function of the mass number of the residual nuclei. DWBA cross sections obtained by the $[\pi f_{7/2}\nu p_{3/2}]_{L=4,J=5}$ transfer are indicated by open circles. The cross sections are obtained by integrating the differential cross sections over an angular range from 14° to 82° ($\sigma_T=2\pi \int_{14°}^{82°}(d\sigma/d\omega)_{CM}\sin(\theta_{CM})\ d\theta_{CM}$). The values indicated by triangles include cross sections of unresolved multiplets for ^{52}V and ^{58}Co (see text).

Fig.7-7 Cross sections of the higher excitation members (8^-) as a function of the mass number of the residual nuclei. DWBA cross sections obtained by the $[\pi f_{7/2}\nu g_{9/2}]_{L=7,J=8}$ and $[\pi f_{5/2}\nu f_{5/2}]_{L=6,J=5}$ transfers are shown by open circles and triangles, respectively. The experiments are well reproduced by the $[\pi f_{7/2}\nu g_{9/2}]$ transfers. See caption of Fig.7-7 for the cross section definition.

Fig.7-8 The angular distributions of the DWBA predictions for large orbital angular momentum transfers. The $^{52}Cr(\alpha,d)$ ^{54}Mn reaction to Q=-15.3 MeV state is assumed. For odd L transfers the $[\pi f_{7/2}\nu g_{9/2}]_L$ pair is assumed and the $[\pi f_{5/2}\nu f_{5/2}]_L$ for even L transfers.

Fig.7-9 Comparison of the DWBA calculations of L=6 transfers with the experimental angular distributions of known 6^+ states in ^{54}Mn at 2.27 MeV and in ^{56}Co at 2.37 MeV excitation energies. The DWBA calculations are made using the optical potential set Al-Dl in table 5-II.

Fig.7-10 Binding energies of a proton in the N=28 proton odd nucleus as a function of the number of the protons in the $1f_{7/2}$ shell orbit in the N=28 even mass nucleus. The linearly decreasing trend of the binding energy ($\varepsilon'_{\pi}(\ell j)$) with increasing the number of the $1f_{7/2}$ protons means that sum of the residual two-particle interaction energies is repulsive (see equations (7-8) and (7-8')). In Table 7-IV spectroscopic informations of the $(\ell_p j_p)$ single particle states are summarized.

Fig.7-11 Binding energies of a neutron in the N=29 neutron odd nucleus as a function of the number of the protons in the $1f_{7/2}$ shell orbit. The linearly increasing trends of the binding energy ($\varepsilon'_{\nu}(\ell j)$) with increasing the number of the $1f_{7/2}$ protons means that sum of the residual two-particle interaction energies is attractive (see equations (7-9)). In Table 7-IV spectroscopic informations of the $(\ell_n j_n)$ single particle states are summarized.

Fig.7-12 Empirical residual interaction energies (V'^{pn}) of the higher excitation members as a function of the number of protons in the $1f_{7/2}$ shell orbit (n-1) in the target nucleus of the (α,d) reaction. The values indicated by open circles and closed circles are deduced by assuming that these levels have a common configuration of $[\pi f_{7/2}^{n} \nu g_{9/2}]_{8^-}$ and $[\pi f_{7/2}^{n-1} \pi f_{5/2} \nu f_{5/2}]_{5^+}$, respectively.

Fig. 3-1.

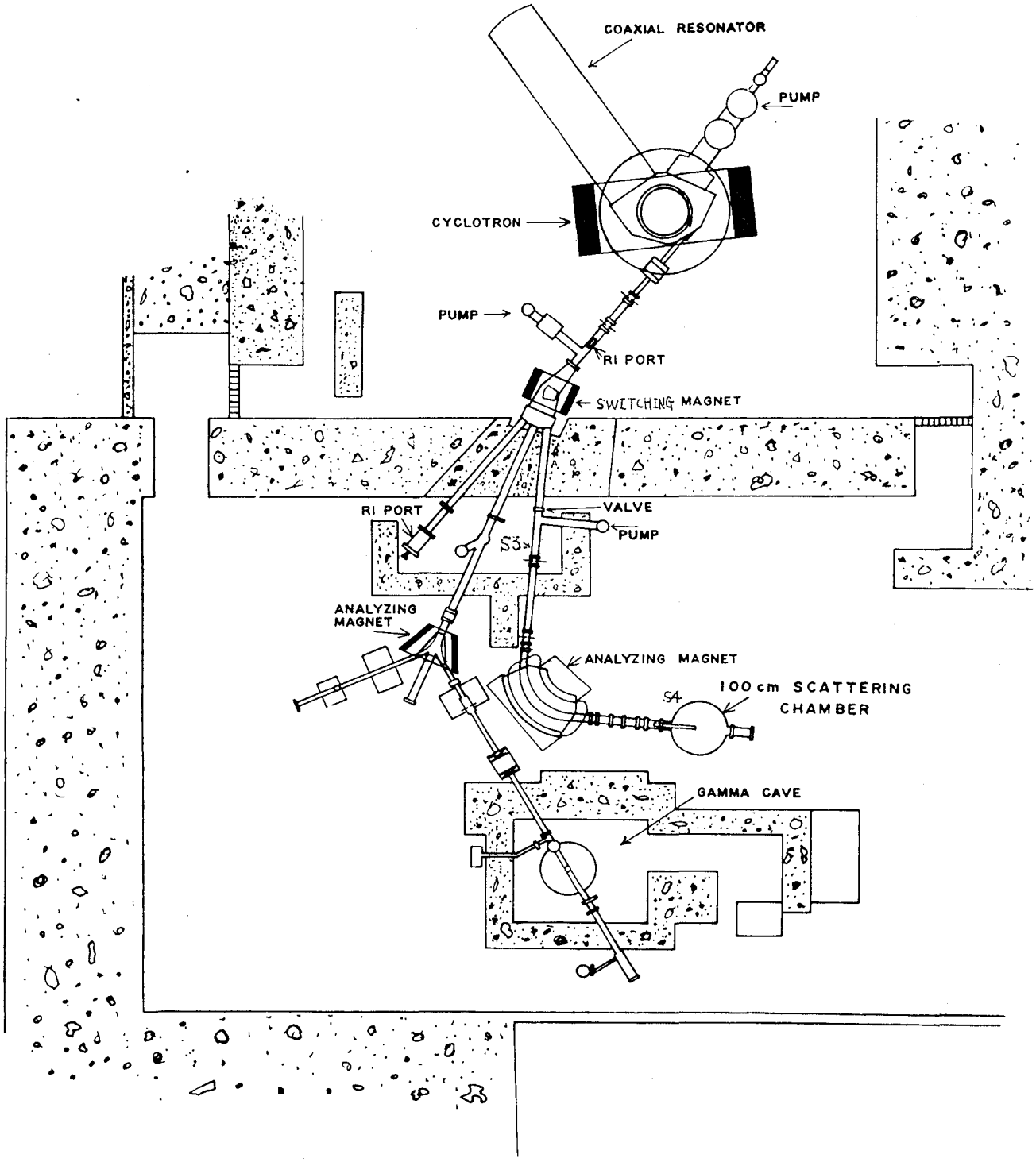
COAXIAL RESONATOR
PUMP
CYCLOTRON
PUMP
RI PORT
SWITCHING MAGNET
RI PORT
VALVE
PUMP
S3
ANALYZING MAGNET
ANALYZING MAGNET
S4
100 cm SCATTERING CHAMBER
GAMMA CAVE

Fig. 3-2.

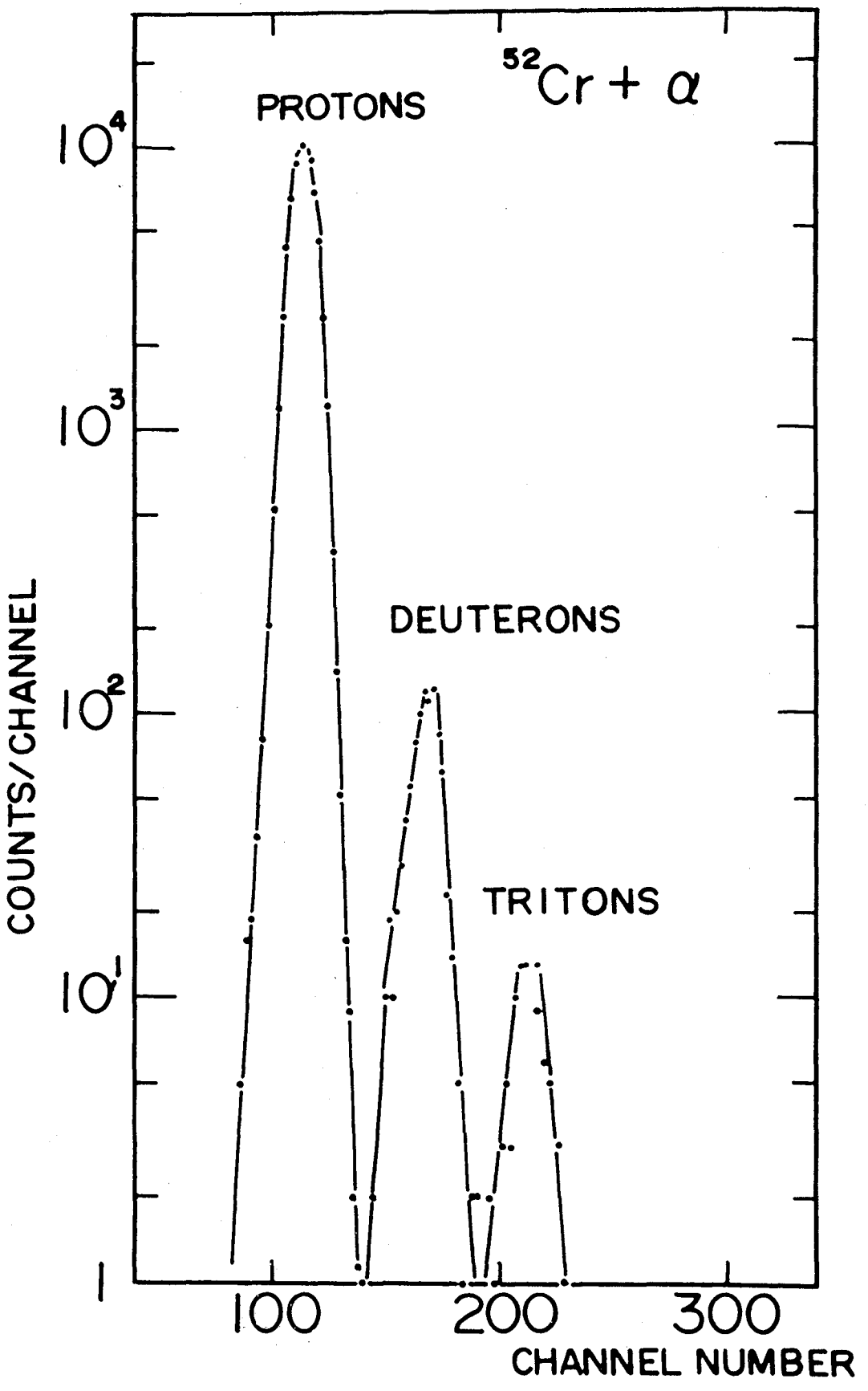
$^{52}Cr + \alpha$
PROTONS
DEUTERONS
TRITONS
10^4
10^3
10^2
10^1
1
COUNTS/CHANNEL
100
200
300
CHANNEL NUMBER

Fig. 3-3.

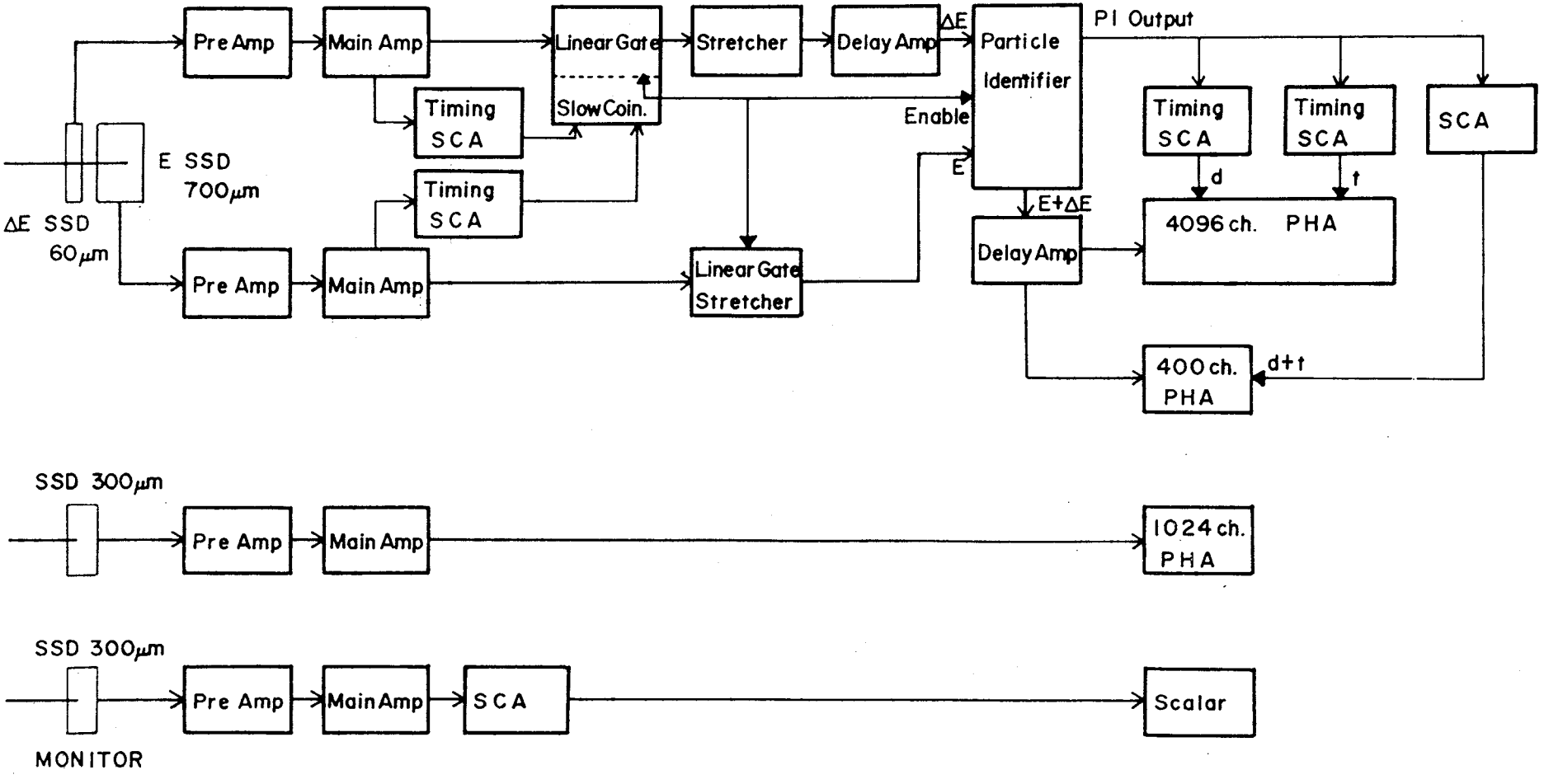
Pre Amp
Main Amp
Linear Gate
Stretcher
Delay Amp
ΔE
Particle Identifier
PI Output
Timing SCA
Slow Coin.
Enable
E
E SSD 700μm
ΔE SSD 60μm
Timing SCA
Timing SCA
SCA
d
t
E+ΔE
4096 ch. PHA
Pre Amp
Main Amp
Linear Gate Stretcher
Delay Amp
400 ch. PHA
d+t
SSD 300μm
Pre Amp
Main Amp
1024 ch. PHA
SSD 300μm
Pre Amp
Main Amp
SCA
Scalar
MONITOR

Fig. 4-1.

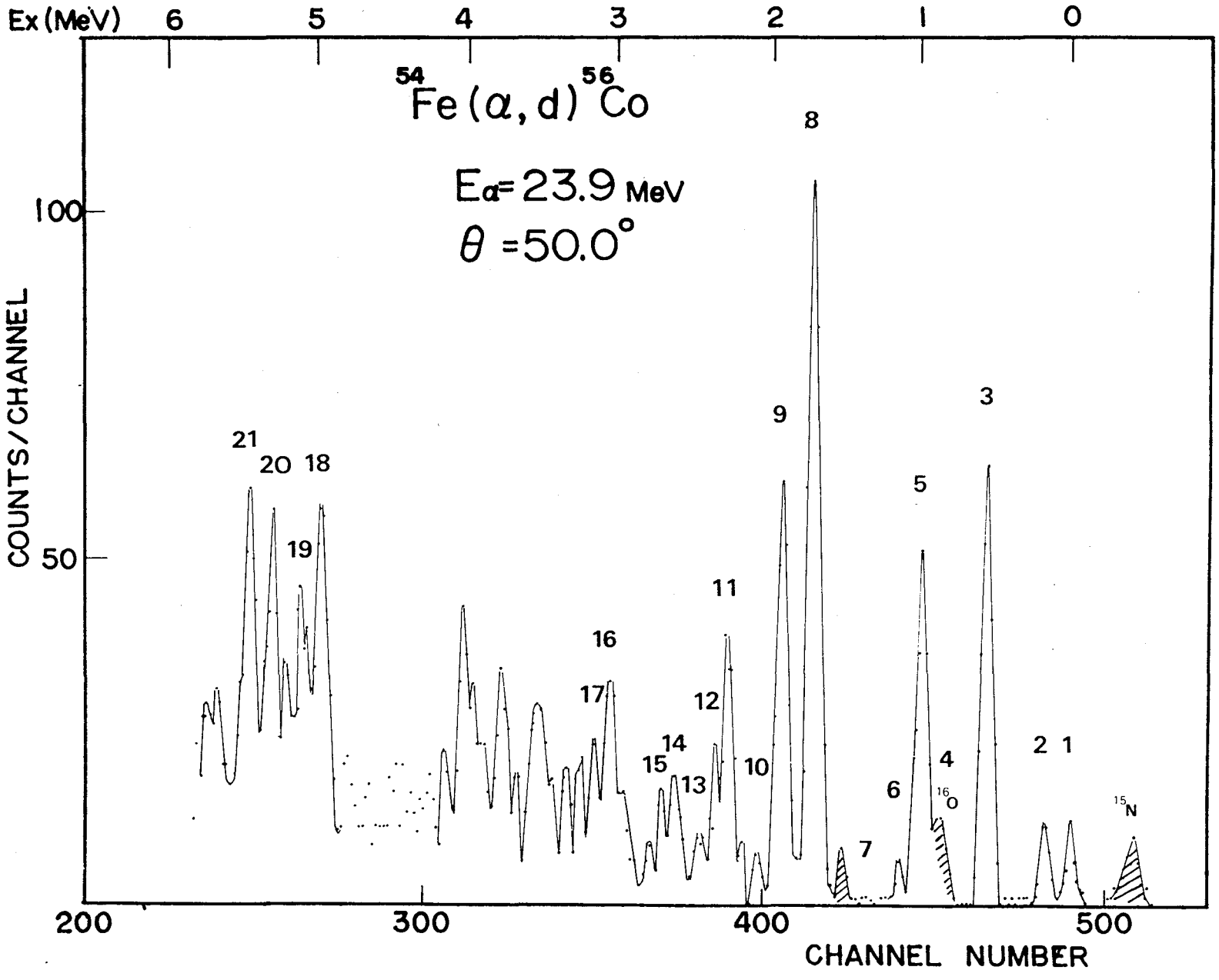
Ex (MeV)
6
5
4
3
2
1
0
54Fe(α, d)56Co
Eα= 23.9 MeV
θ =50.0°
COUNTS/CHANNEL
100
50
200
300
400
500
CHANNEL NUMBER
21
20
18
19
16
17
11
12
14
15
13
10
9
8
7
6
5
4
16O
3
2
1
15N

Fig. 4-2-a.

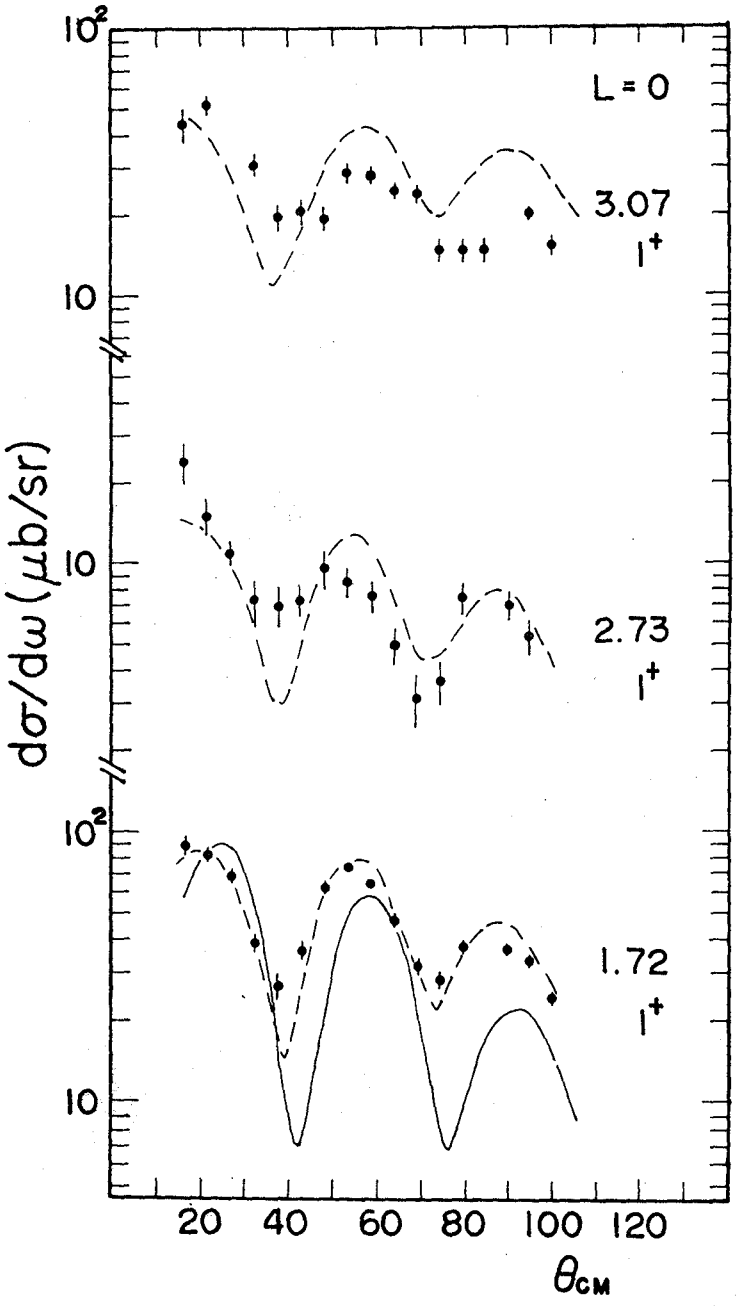

Fig. 4-2-b.

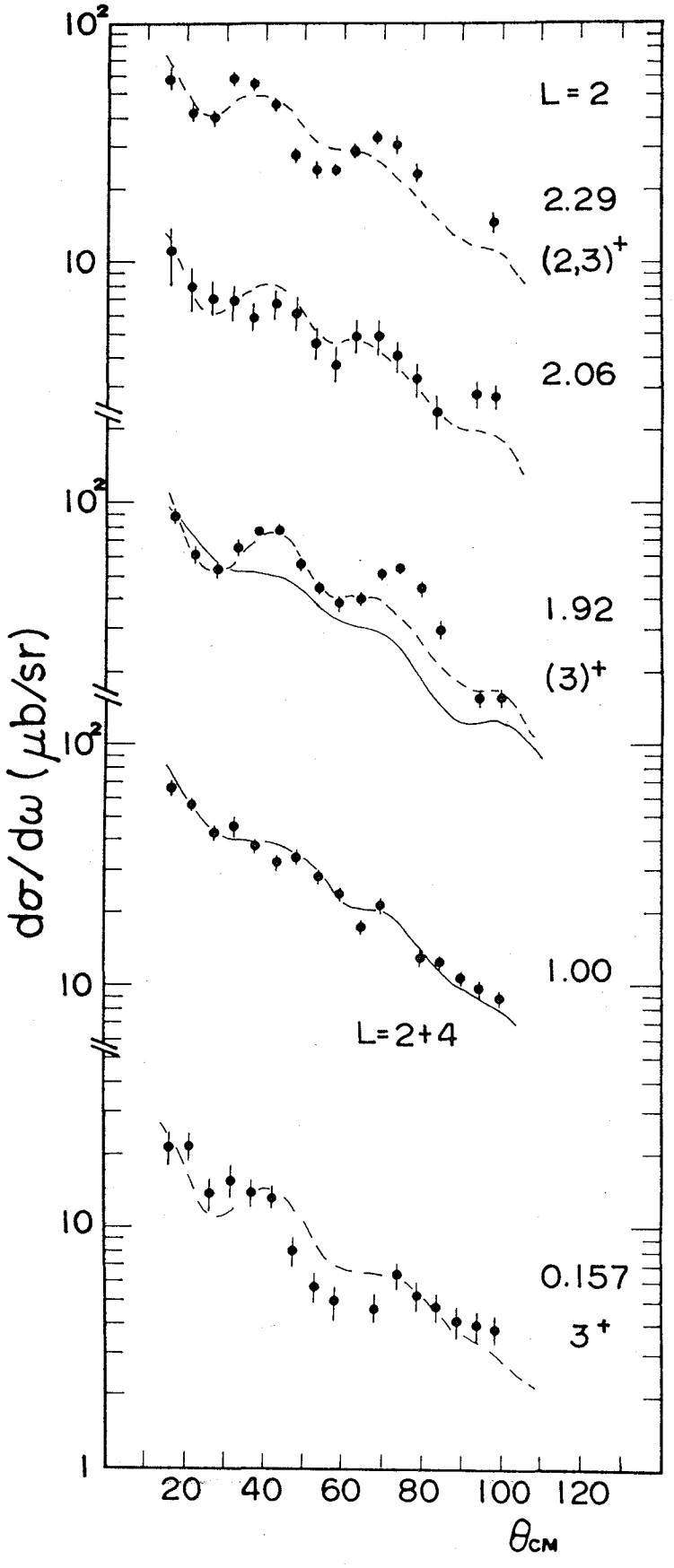
L = 2
2.29
(2,3)+
2.06
1.92
(3)+
1.00
L=2+4
0.157
3+
dσ/dω (μb/sr)
θcm
20
40
60
80
100
120

Fig. 4-2-c.

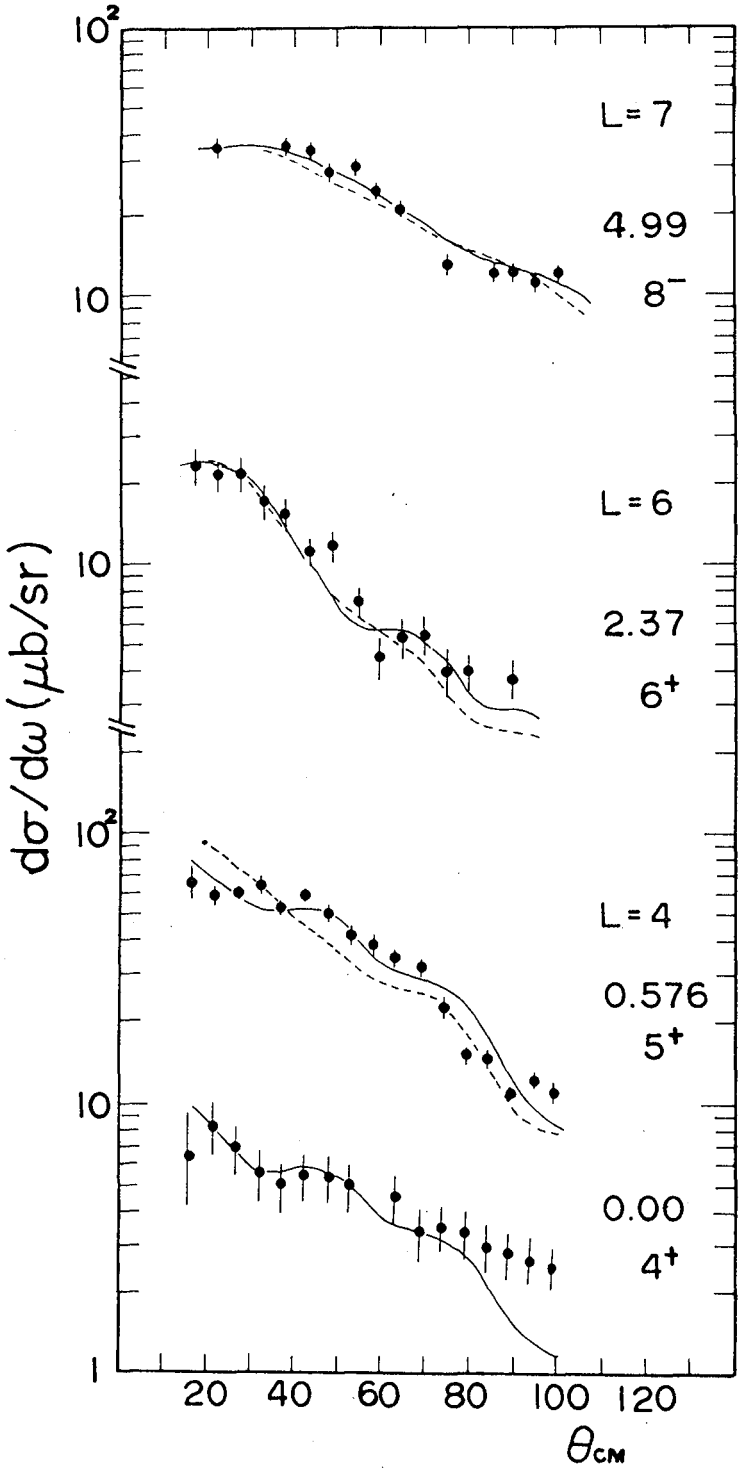
10^2
10
10^2
10
1
$d\sigma/d\omega$ (μb/sr)
L=7
4.99
8^-
L=6
2.37
6^+
L=4
0.576
5^+
0.00
4^+
20
40
60
80
100
120
θ_{CM}

Fig. 4-2-d.

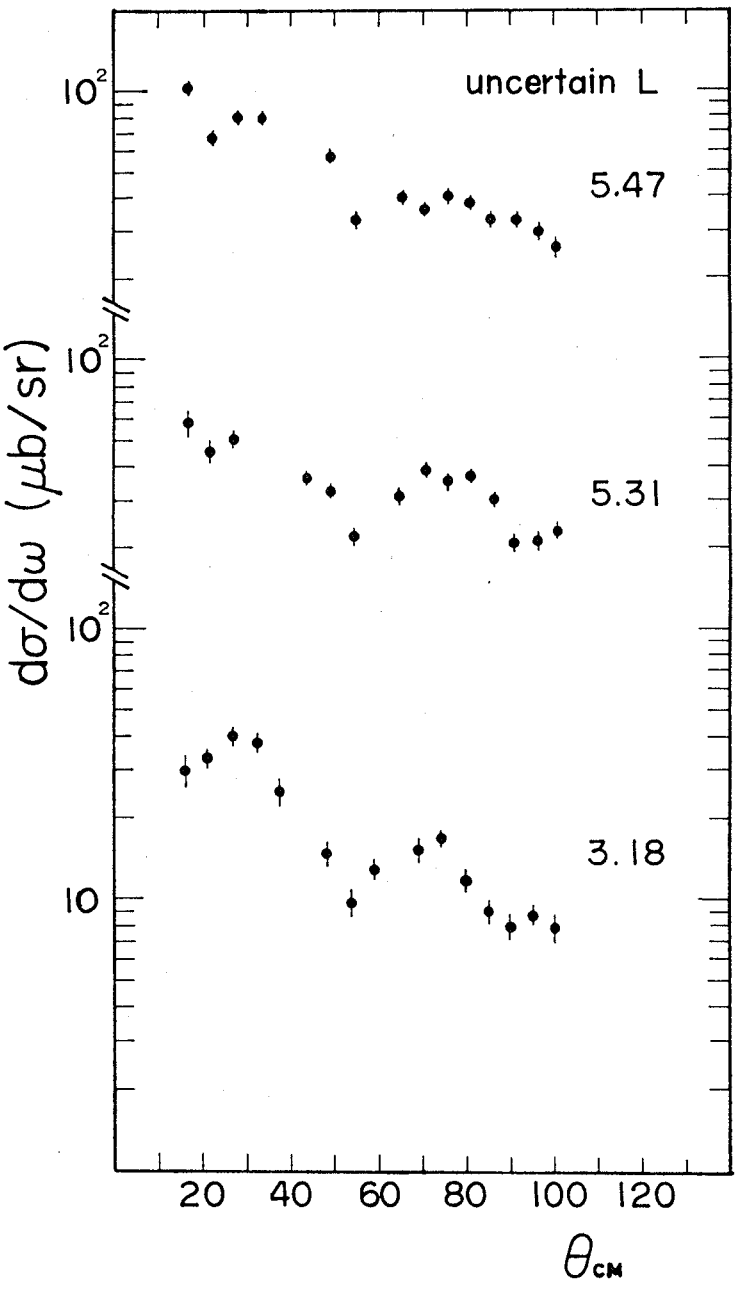
uncertain L
5.47
5.31
3.18
10^2
10^2
10^2
10
$d\sigma/d\omega$ (μb/sr)
20
40
60
80
100
120
θ_{CM}

Fig. 4-3.

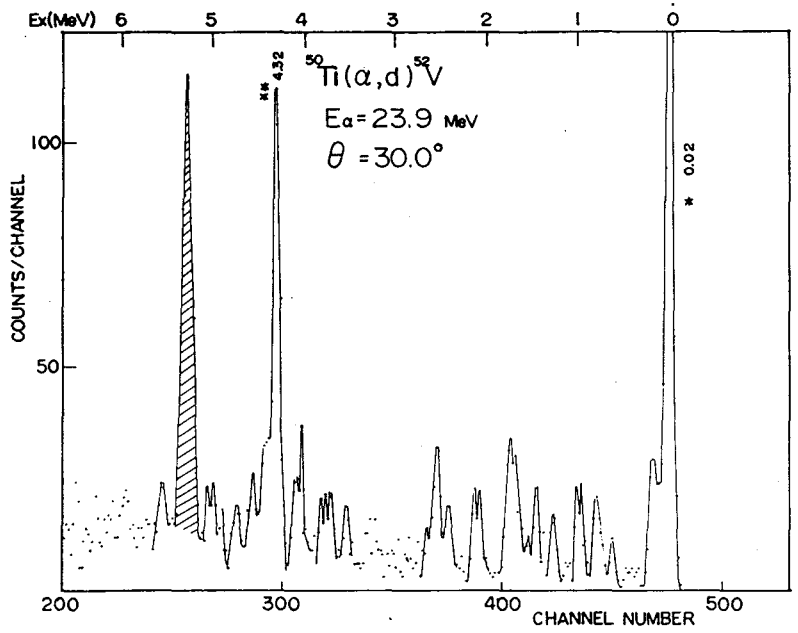
Ex(MeV) 6 5 4 3 2 1 0
^{50}Ti(α,d)^{52}V
Eα=23.9 MeV
θ =30.0°
** 4.32
* 0.02
COUNTS/CHANNEL
100
50
200 300 400 500
CHANNEL NUMBER

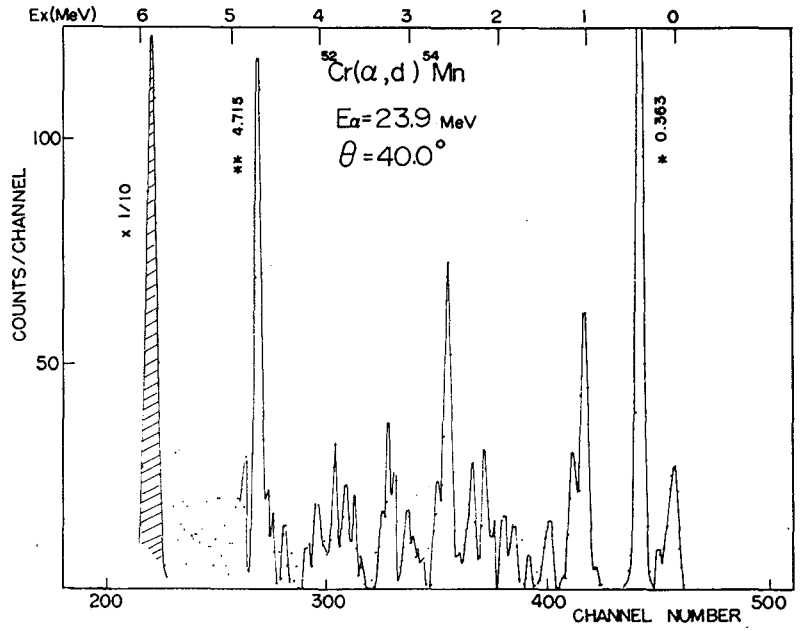
Ex(MeV) 6 5 4 3 2 1 0
^{52}Cr(α,d)^{54}Mn
Eα=23.9 MeV
θ =40.0°
x 1/10
** 4.715
* 0.363
COUNTS/CHANNEL
100
50
200 300 400 500
CHANNEL NUMBER

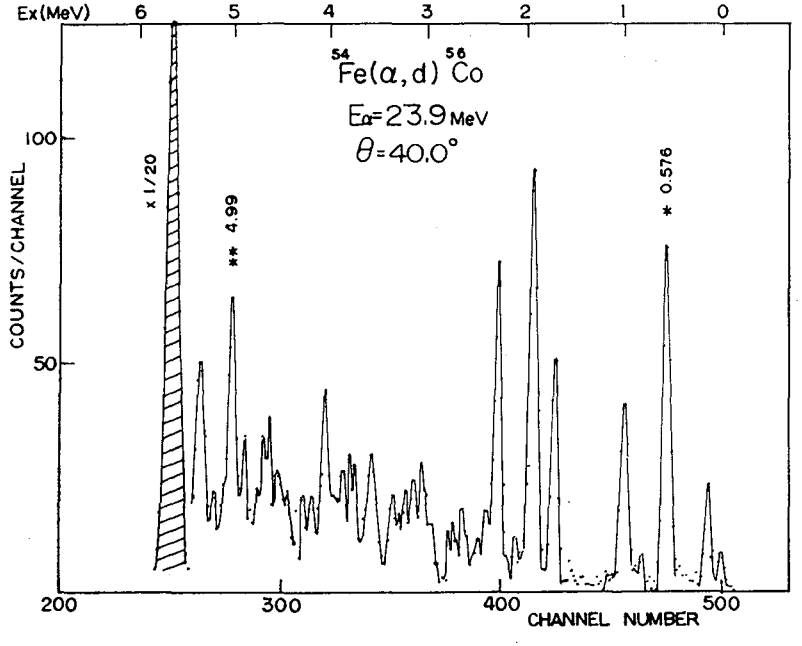
Ex(MeV) 6 5 4 3 2 1 0
^{54}Fe(α,d)^{56}Co
Eα=23.9 MeV
θ=40.0°
x 1/20
** 4.99
* 0.576
COUNTS/CHANNEL
100
50
200 300 400 500
CHANNEL NUMBER

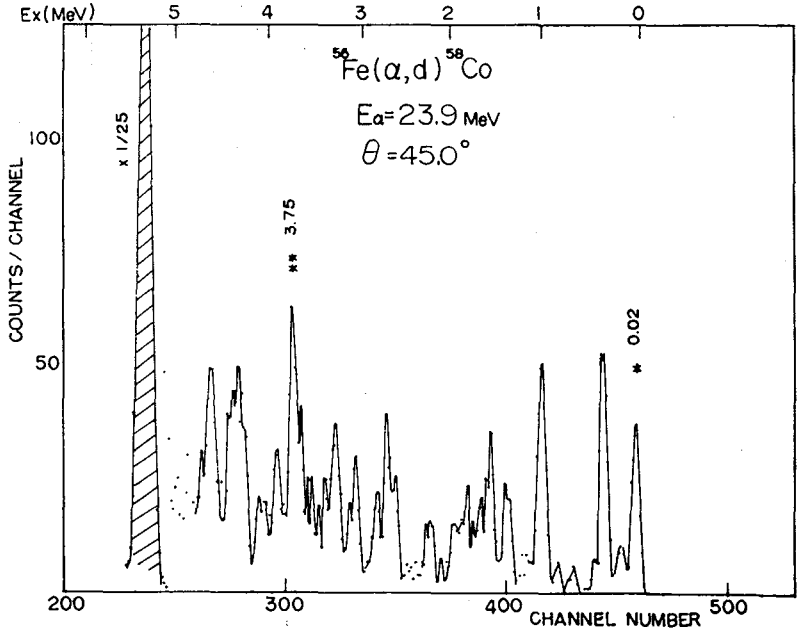
Ex(MeV) 5 4 3 2 1 0
^{56}Fe(α,d)^{58}Co
Eα=23.9 MeV
θ =45.0°
x 1/25
** 3.75
* 0.02
COUNTS/CHANNEL
100
50
200 300 400 500
CHANNEL NUMBER

Fig. 4-4.

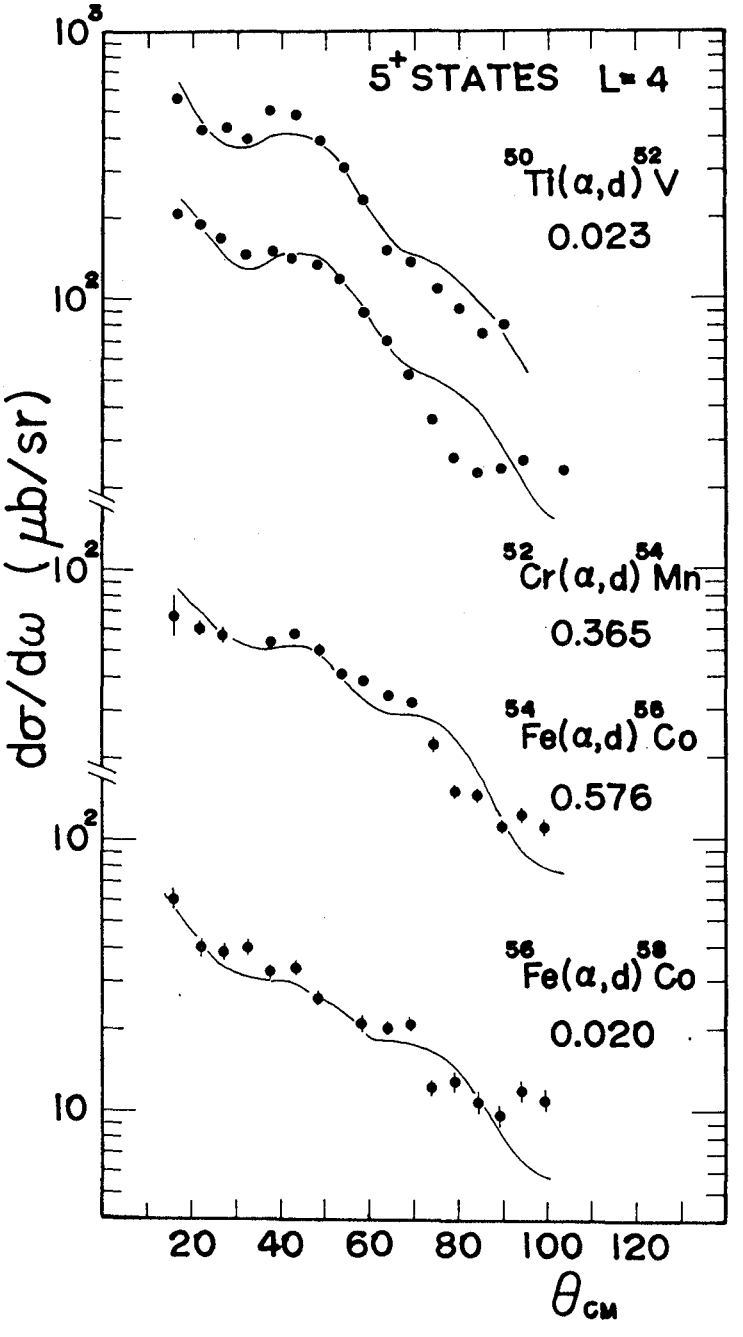
5+ STATES L= 4
50Ti(α,d)52V
0.023
52Cr(α,d)54Mn
0.365
54Fe(α,d)56Co
0.576
56Fe(α,d)58Co
0.020
dσ/dω (μb/sr)
θCM
20
40
60
80
100
120

Fig. 4-5.

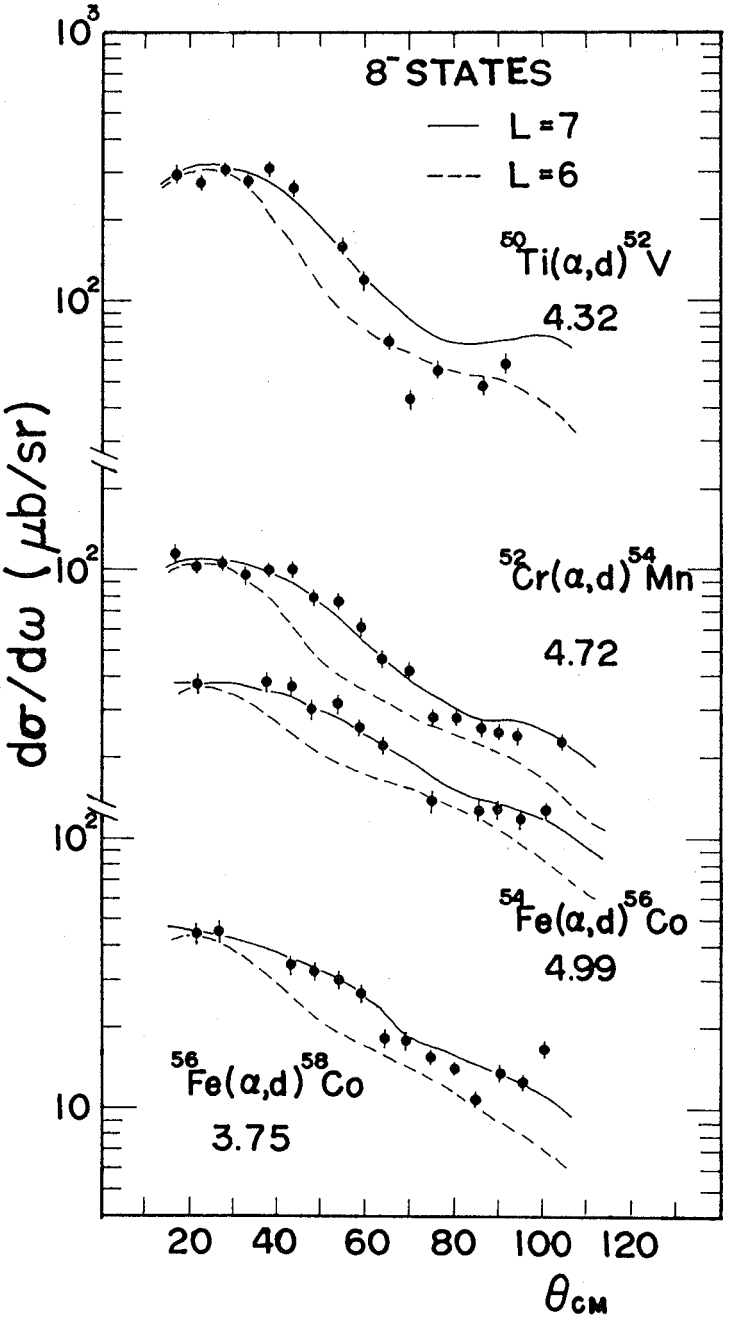
8⁻ STATES
L=7
L=6
^{50}Ti(α,d)^{52}V
4.32
^{52}Cr(α,d)^{54}Mn
4.72
^{54}Fe(α,d)^{56}Co
4.99
^{56}Fe(α,d)^{58}Co
3.75
dσ/dω (μb/sr)
10^3
10^2
10^2
10^2
10
20
40
60
80
100
120
θ_{CM}

Fig. 4-6.

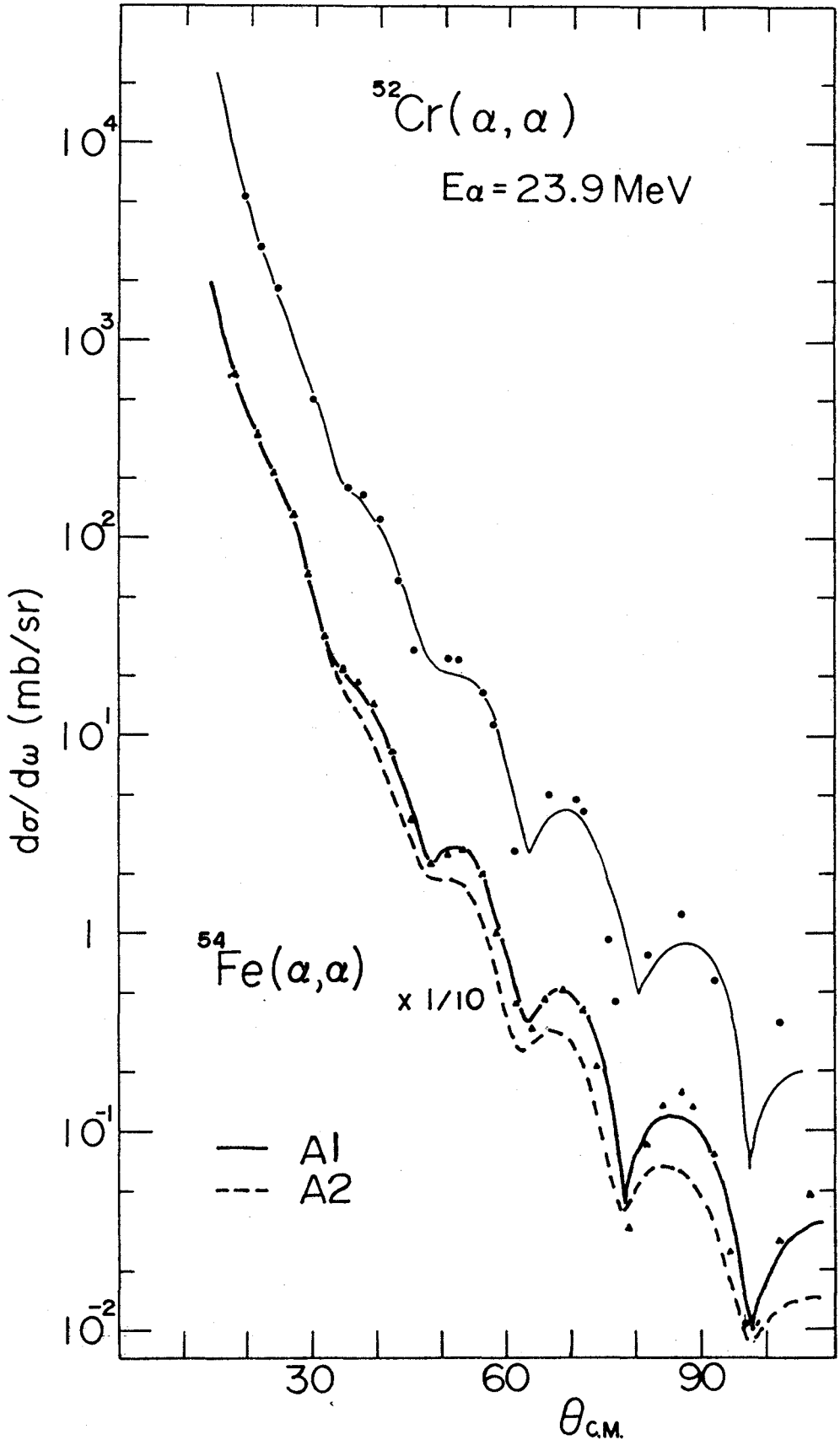
$^{52}Cr(\alpha,\alpha)$
$E\alpha = 23.9$ MeV
10^4
10^3
10^2
10^1
1
10^{-1}
10^{-2}
$d\sigma/d\omega$ (mb/sr)
$^{54}Fe(\alpha,\alpha)$
x 1/10
A1
A2
30
60
90
$\theta_{C.M.}$

Fig. 4-7.

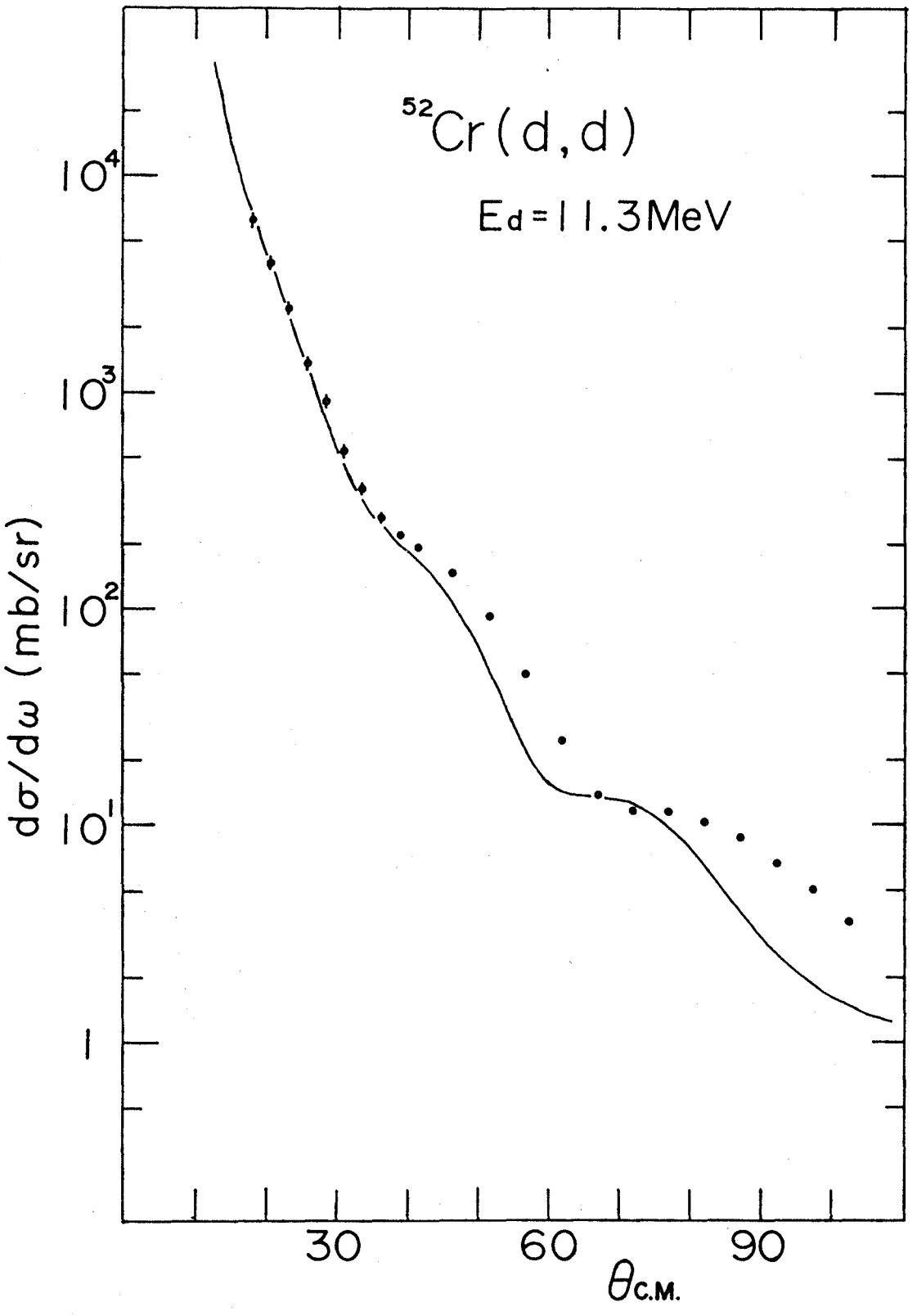

Fig. 5-1.

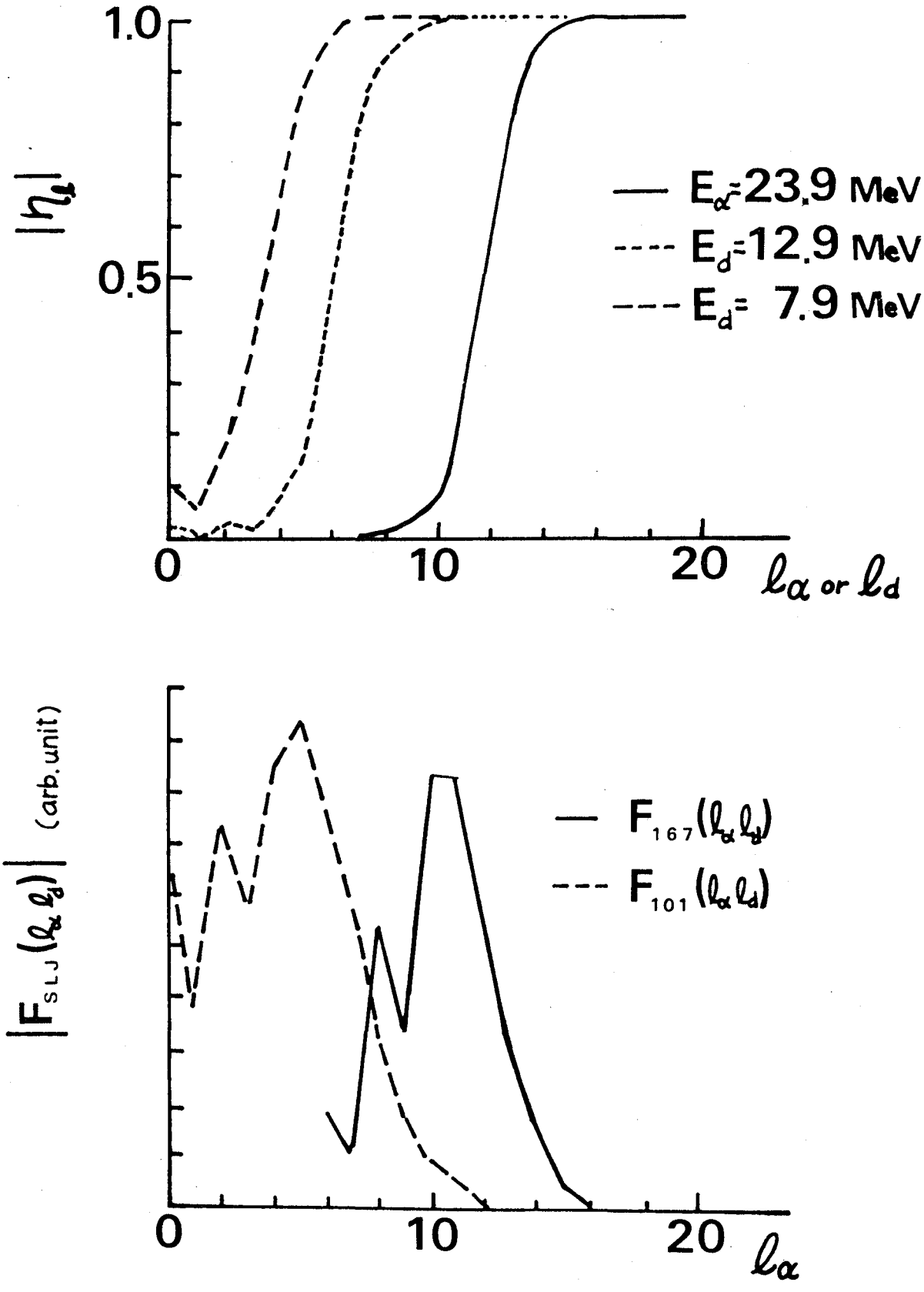
1.0
0.5
$|\eta_l|$
E_α=23.9 MeV
E_d=12.9 MeV
E_d= 7.9 MeV
0
10
20
l_α or l_d
$|F_{SLJ}(l_\alpha l_d)|$ (arb.unit)
$F_{167}(l_\alpha l_d)$
$F_{101}(l_\alpha l_d)$
0
10
20
l_α

Fig.5-2.

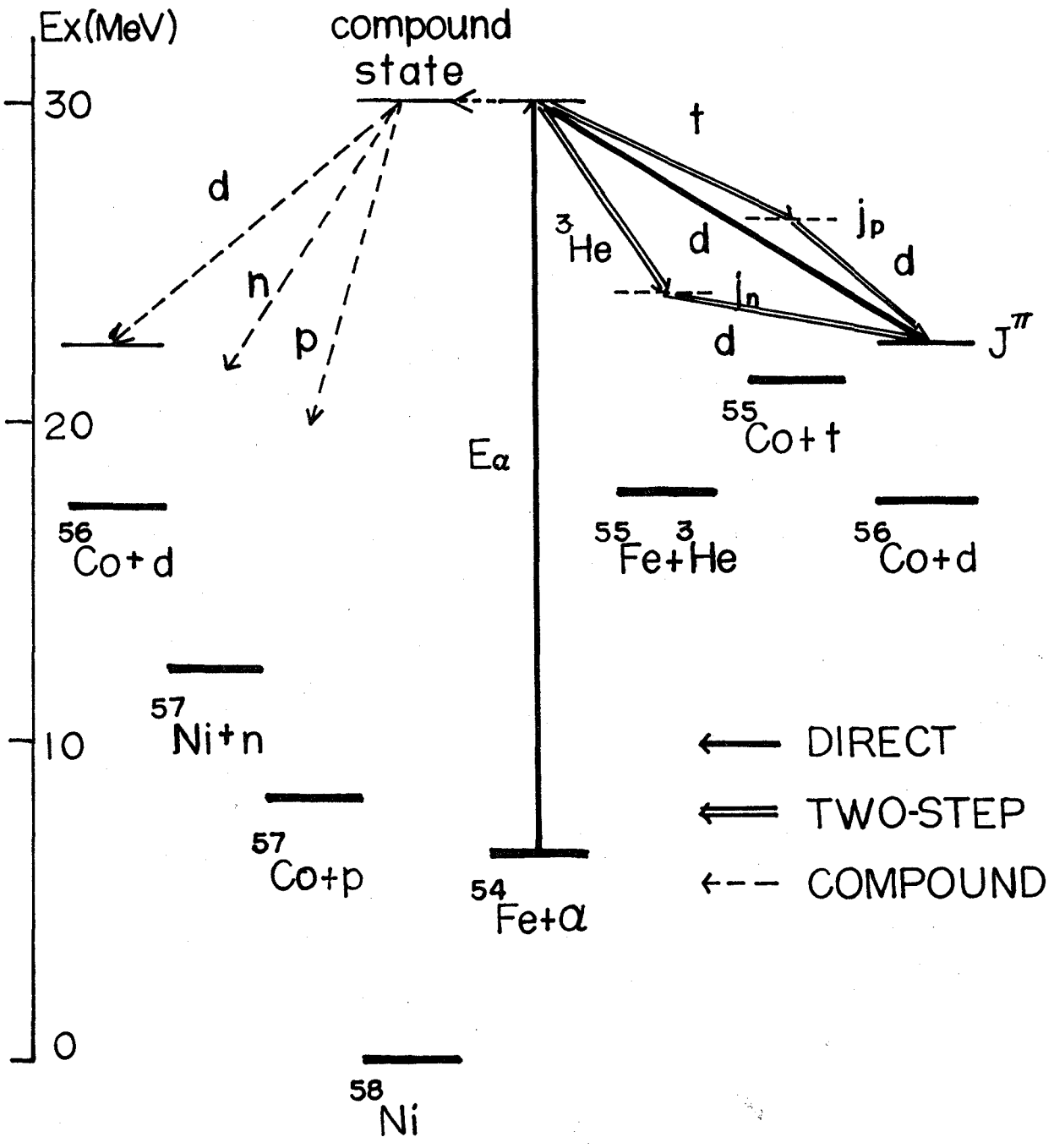
Ex(MeV)
compound state
30
20
10
0
d
n
p
t
^{3}He
d
j_p
d
j_n
d
J^π
^{55}Co+t
E_α
^{56}Co+d
^{55}Fe+^{3}He
^{56}Co+d
^{57}Ni+n
^{57}Co+p
^{54}Fe+α
^{58}Ni
DIRECT
TWO-STEP
COMPOUND

Fig. 5-3.

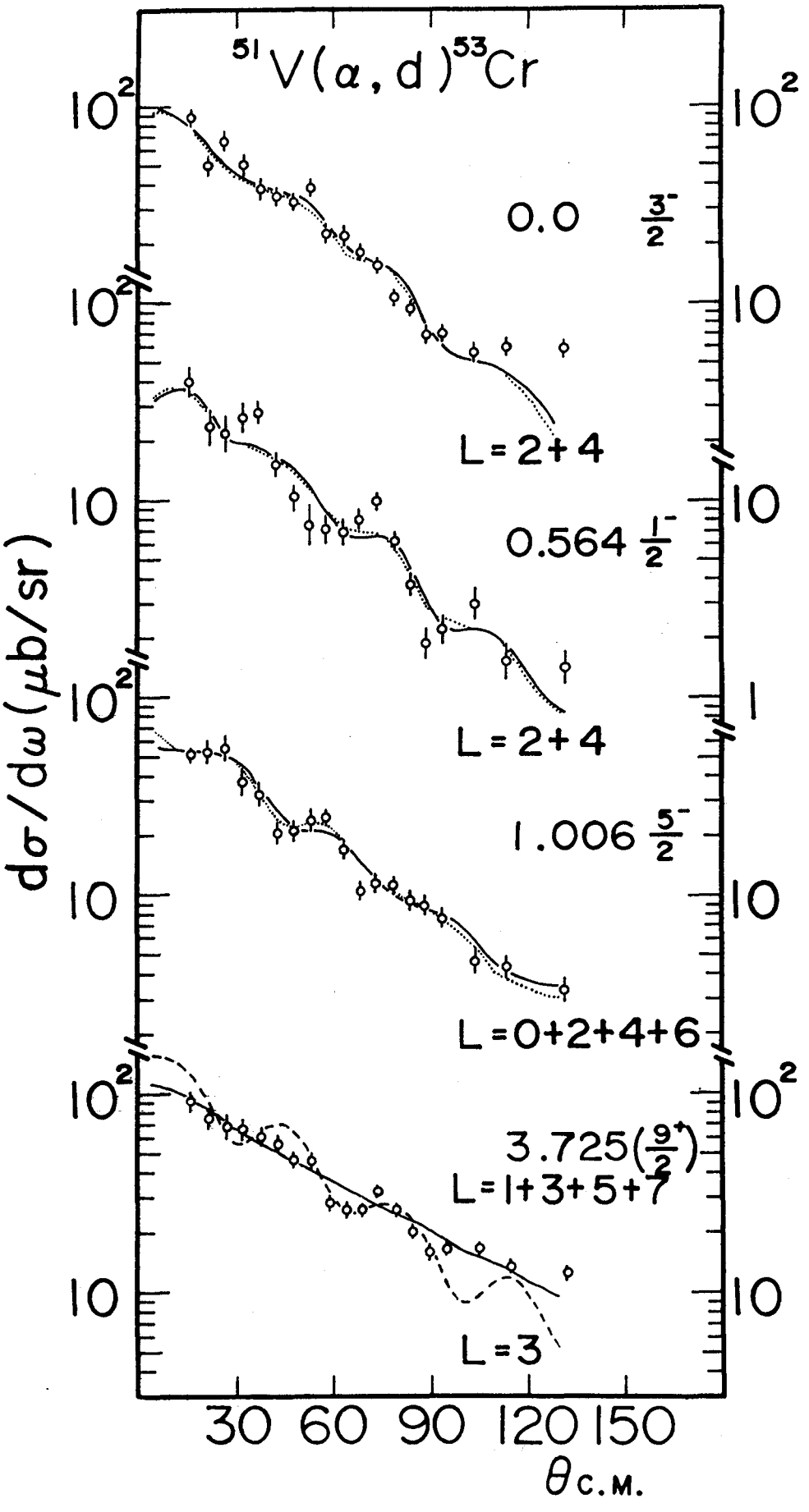
$^{51}V(\alpha,d)^{53}Cr$
0.0 $\frac{3^-}{2}$
L=2+4
0.564 $\frac{1^-}{2}$
L=2+4
1.006 $\frac{5^-}{2}$
L=0+2+4+6
3.725($\frac{9^+}{2}$)
L=1+3+5+7
L=3
$d\sigma/d\omega$ (μb/sr)
$\theta_{c.m.}$
30 60 90 120 150

Fig.5-4

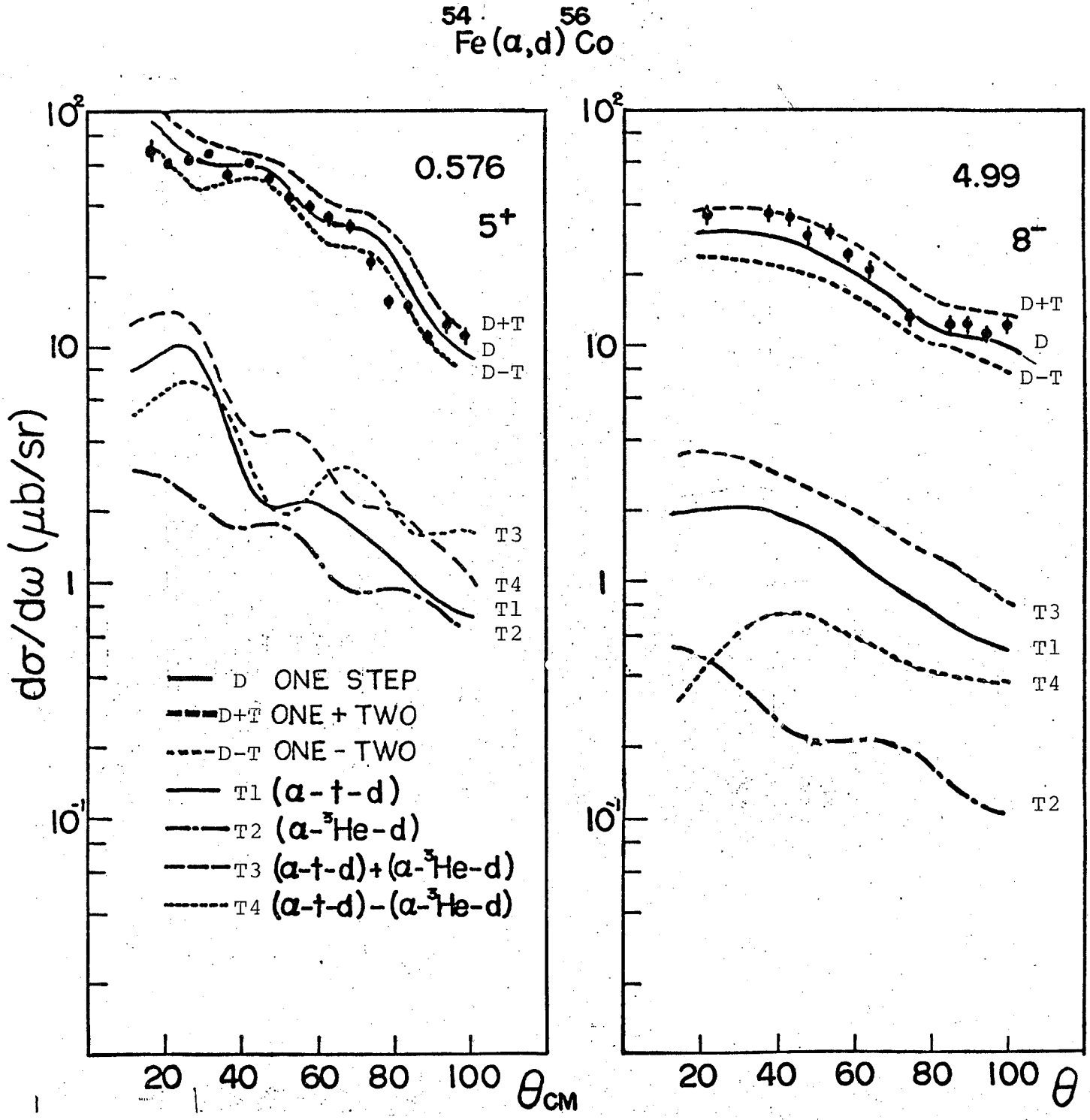
54 56
Fe(α,d) Co
0.576
5+
4.99
8−
D+T
D
D−T
T3
T4
T1
T2
D ONE STEP
D+T ONE + TWO
D−T ONE - TWO
T1 (α-t-d)
T2 (α-³He-d)
T3 (α-t-d)+(α-³He-d)
T4 (α-t-d)-(α-³He-d)
dσ/dω (μb/sr)
θCM
θ

Fig. 7-1.

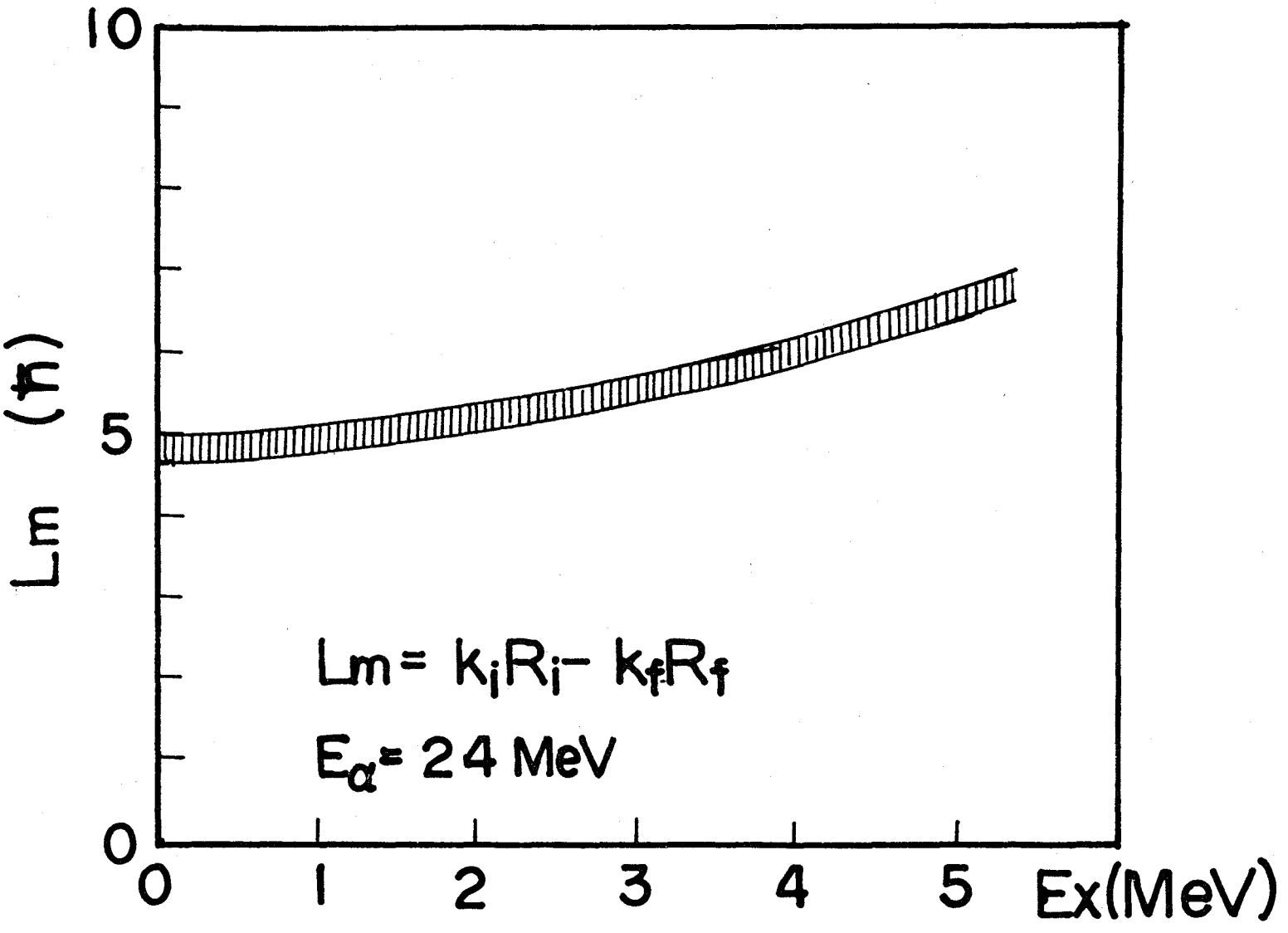

Fig. 7-2.

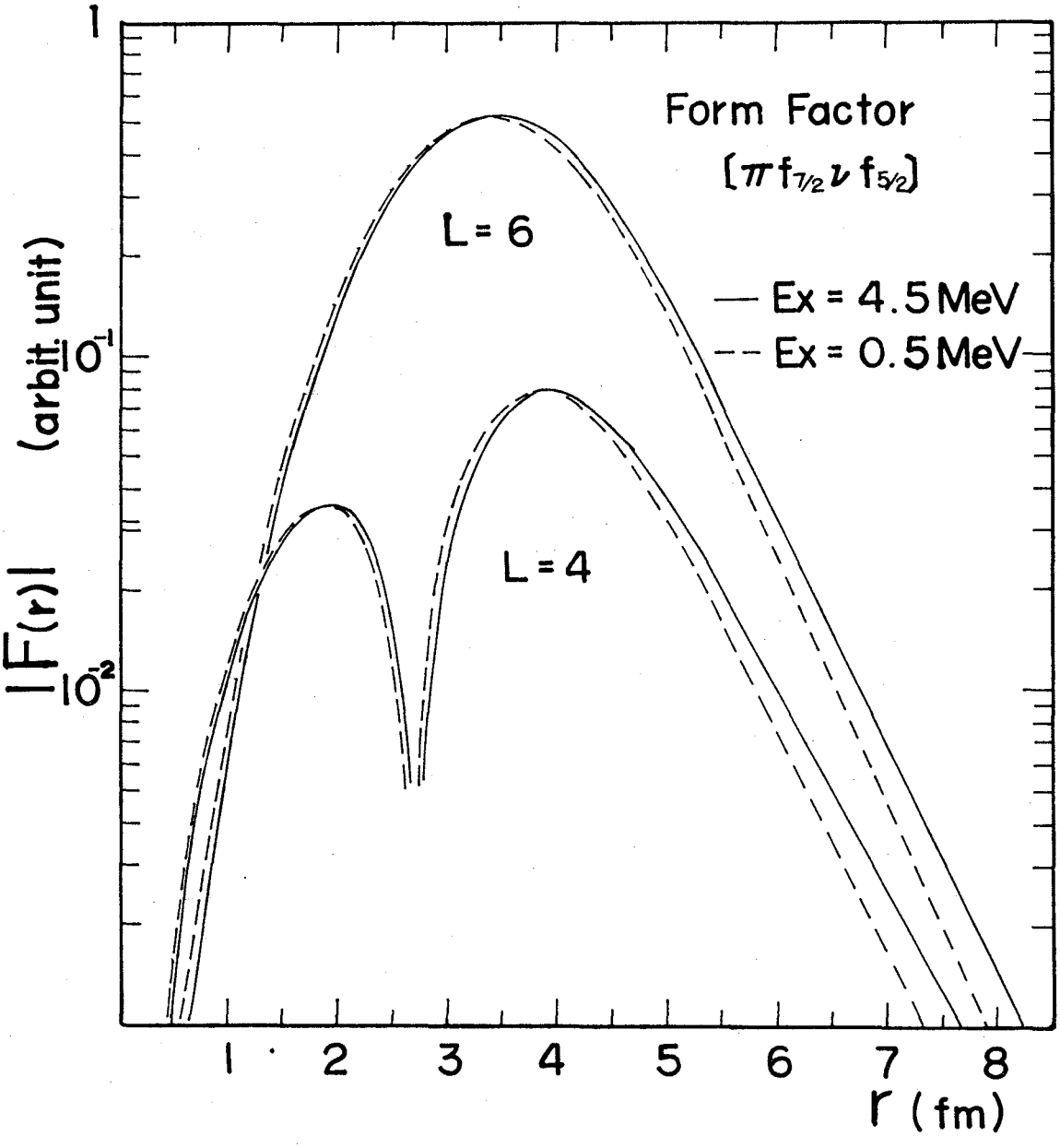
Form Factor
[π f7/2 ν f5/2]
L = 6
L = 4
— Ex = 4.5 MeV
-- Ex = 0.5 MeV
|F(r)| (arbit. unit)
1
10-1
10-2
1
2
3
4
5
6
7
8
r (fm)

Fig. 7-3.

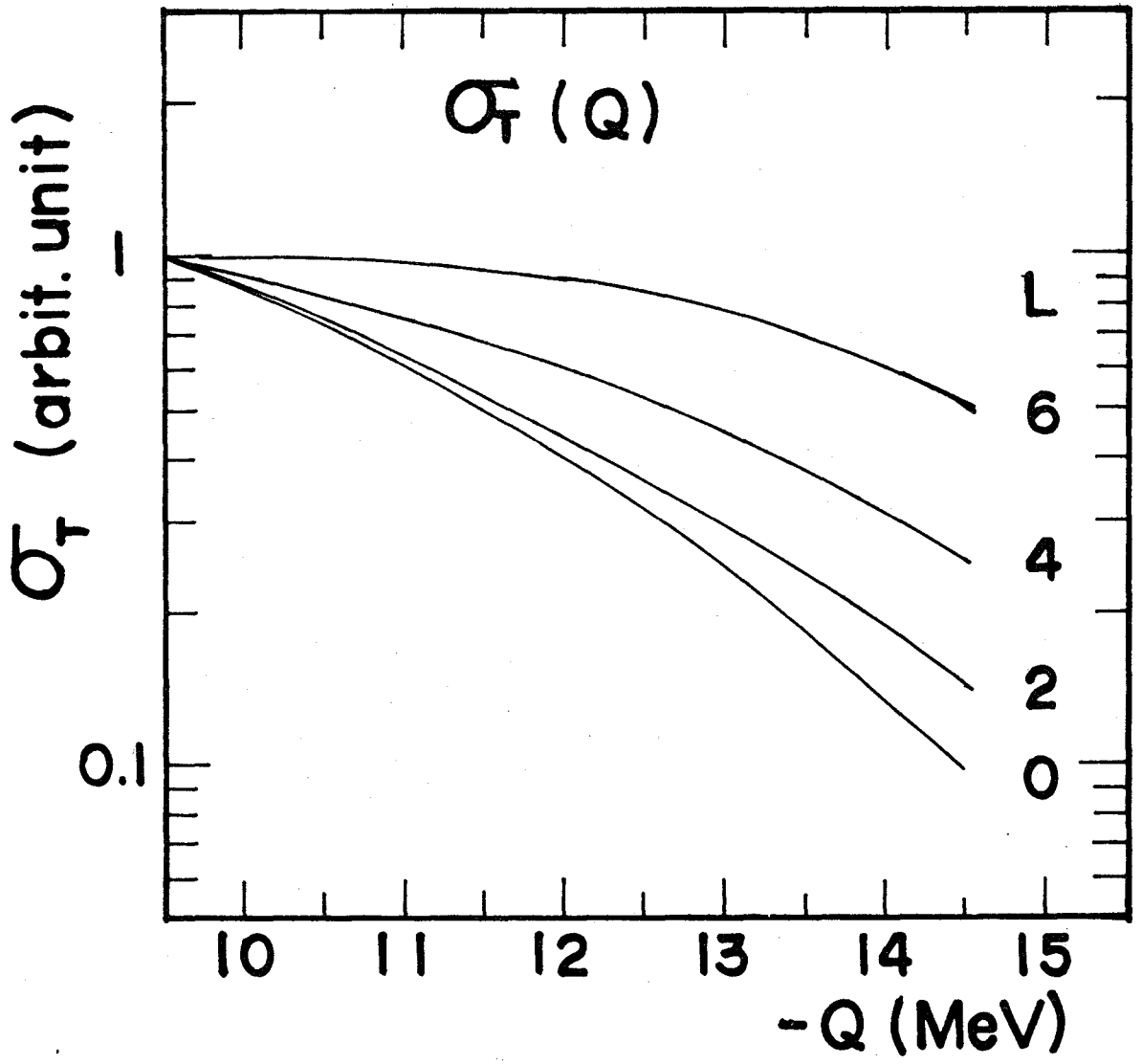

Fig. 7-4.

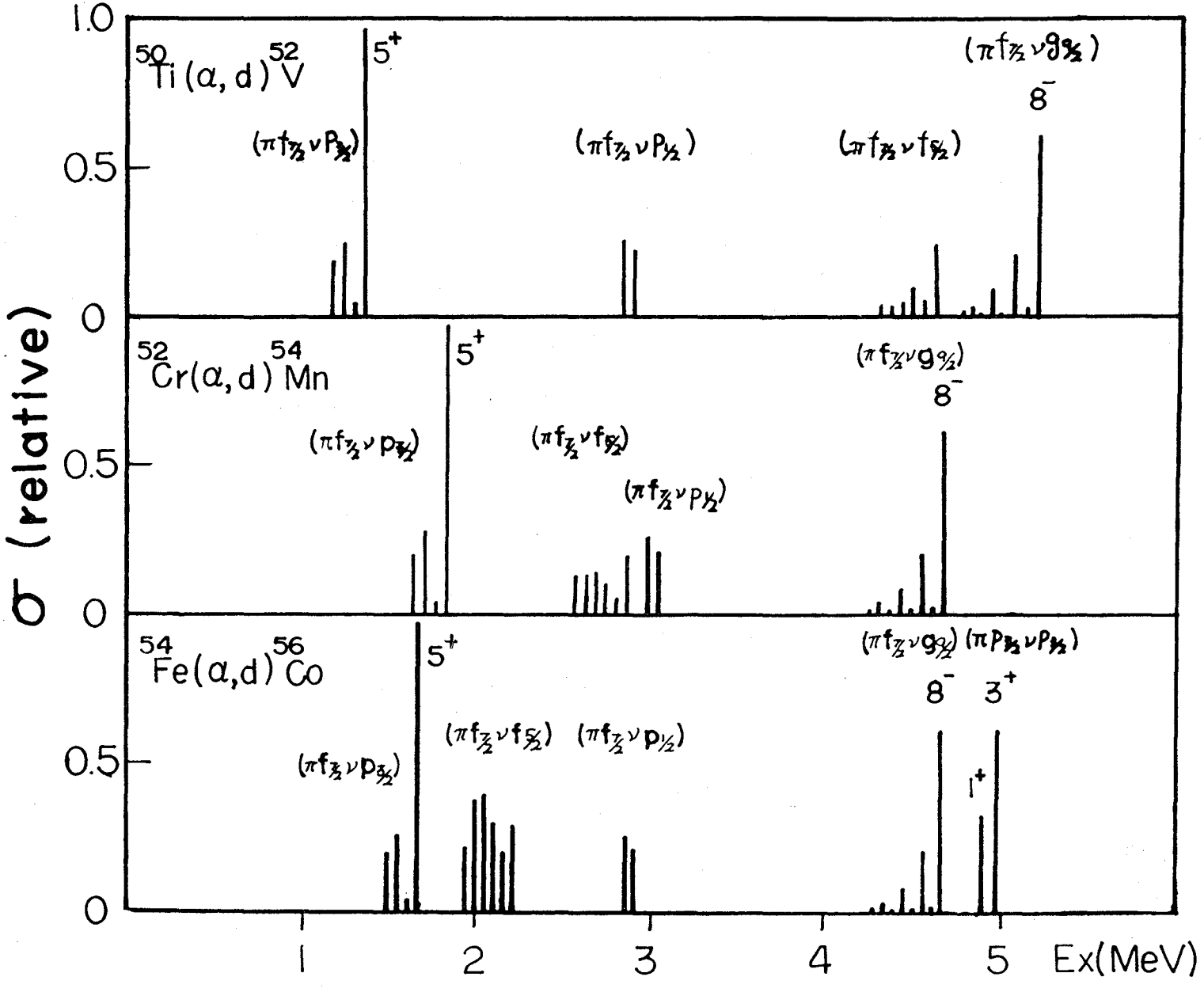
1.0
0.5
0
σ (relative)
^{50}Ti(α, d)^{52}V
5+
(πf7/2 νp3/2)
(πf7/2 νp1/2)
(πf7/2 νf5/2)
(πf7/2 νg9/2)
8−
^{52}Cr(α, d)^{54}Mn
5+
(πf7/2 νp3/2)
(πf7/2 νf5/2)
(πf7/2 νp1/2)
(πf7/2 νg9/2)
8−
^{54}Fe(α,d)^{56}Co
5+
(πf7/2 νp3/2)
(πf7/2 νf5/2)
(πf7/2 νp1/2)
(πf7/2 νg9/2)
8−
(πp3/2 νp3/2)
3+
1+
1
2
3
4
5
Ex(MeV)

Fig. 7-5.

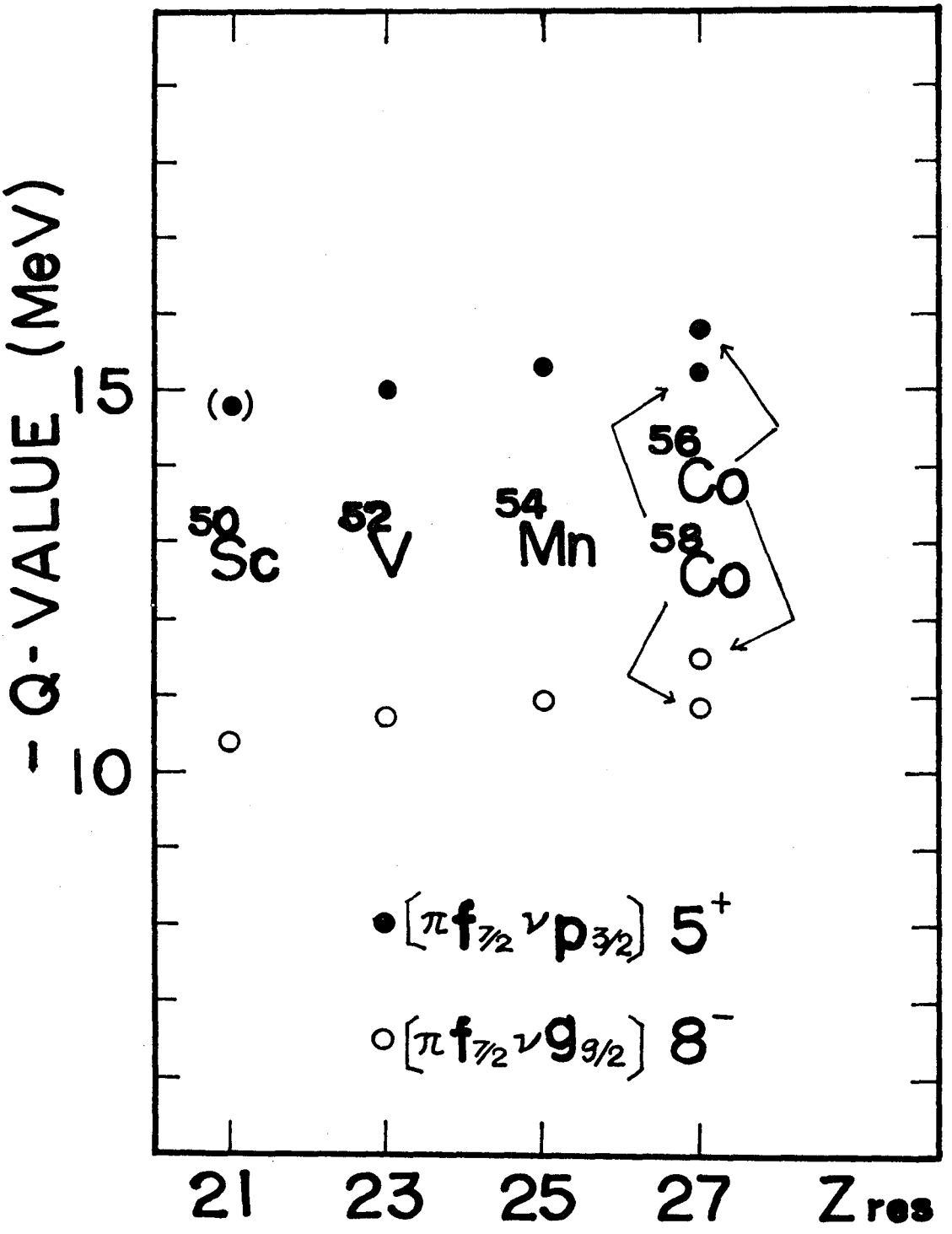
- Q-VALUE (MeV)
15
10
(●)
50 Sc
52 V
54 Mn
56 Co
58 Co
● [π f7/2 ν p3/2] 5+
○ [π f7/2 ν g9/2] 8−
21
23
25
27
Z res

Fig. 7-6.

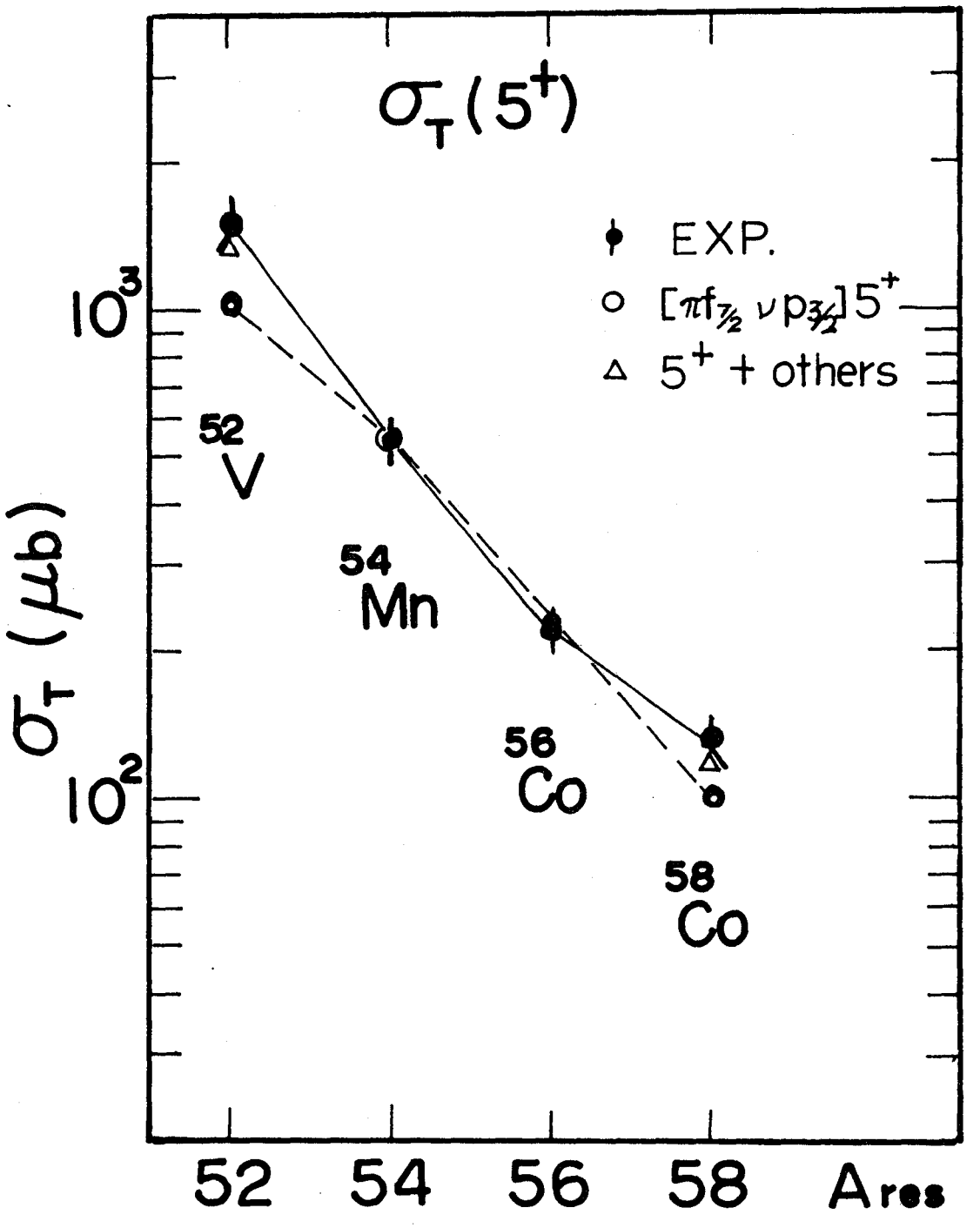
$\sigma_T(5^+)$
EXP.
$[\pi f_{7/2}\ \nu p_{3/2}]5^+$
5^+ + others
10^3
10^2
σ_T (μb)
52 V
54 Mn
56 Co
58 Co
52
54
56
58
Ares

Fig. 7-7.

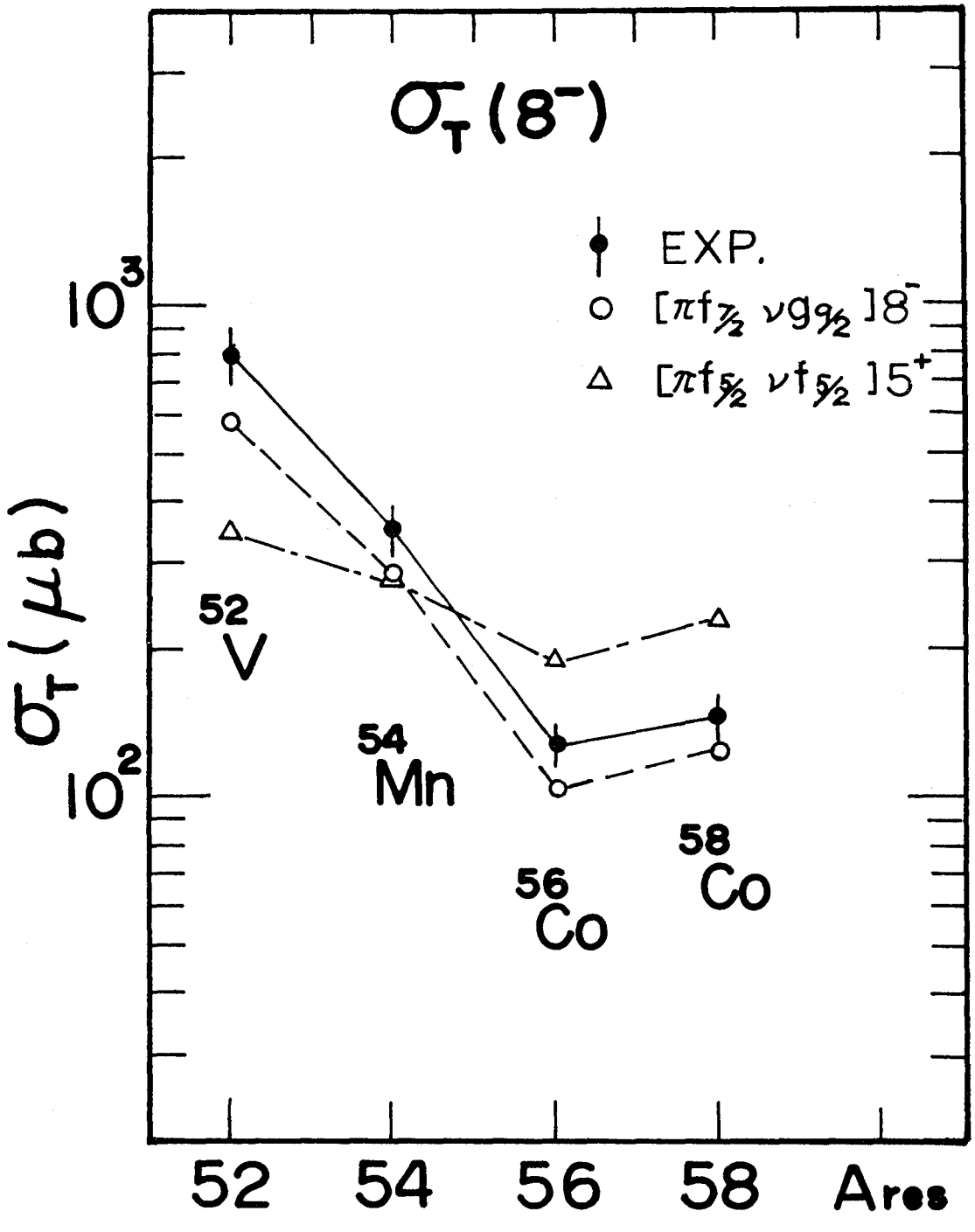
$\sigma_T(8^-)$
EXP.
$[\pi f_{7/2}\ \nu g_{9/2}]8^-$
$[\pi f_{5/2}\ \nu f_{5/2}]15^+$
10^3
10^2
σ_T (μb)
^{52}V
^{54}Mn
^{56}Co
^{58}Co
52
54
56
58
Ares

Fig. 7-8.

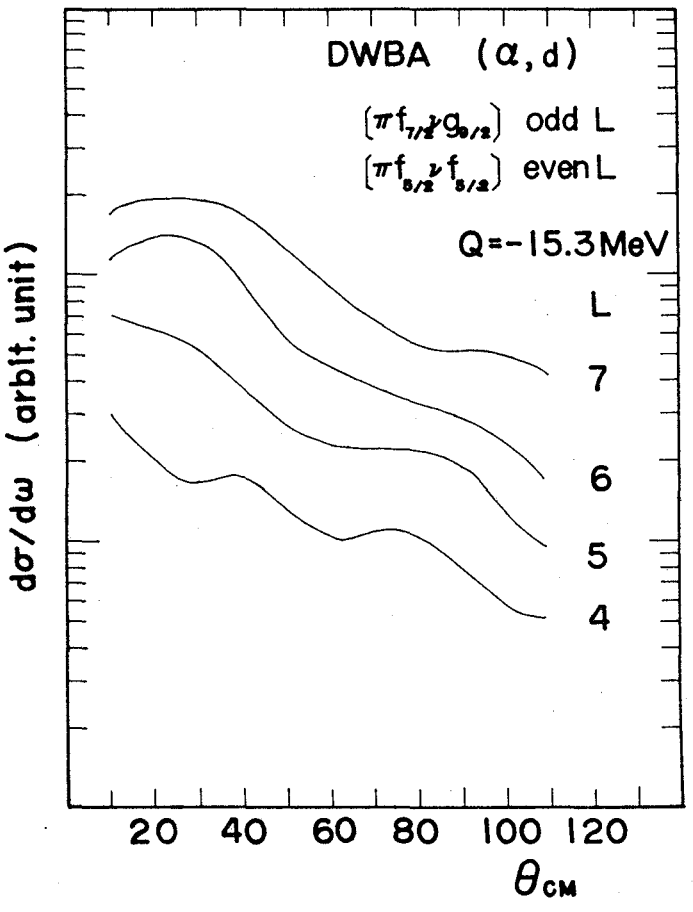
DWBA (α, d)
[πf7/2 νg9/2] odd L
[πf5/2 νf5/2] even L
Q=-15.3MeV
L
7
6
5
4
dσ/dω (arbit. unit)
20 40 60 80 100 120
θCM

Fig. 7-9.

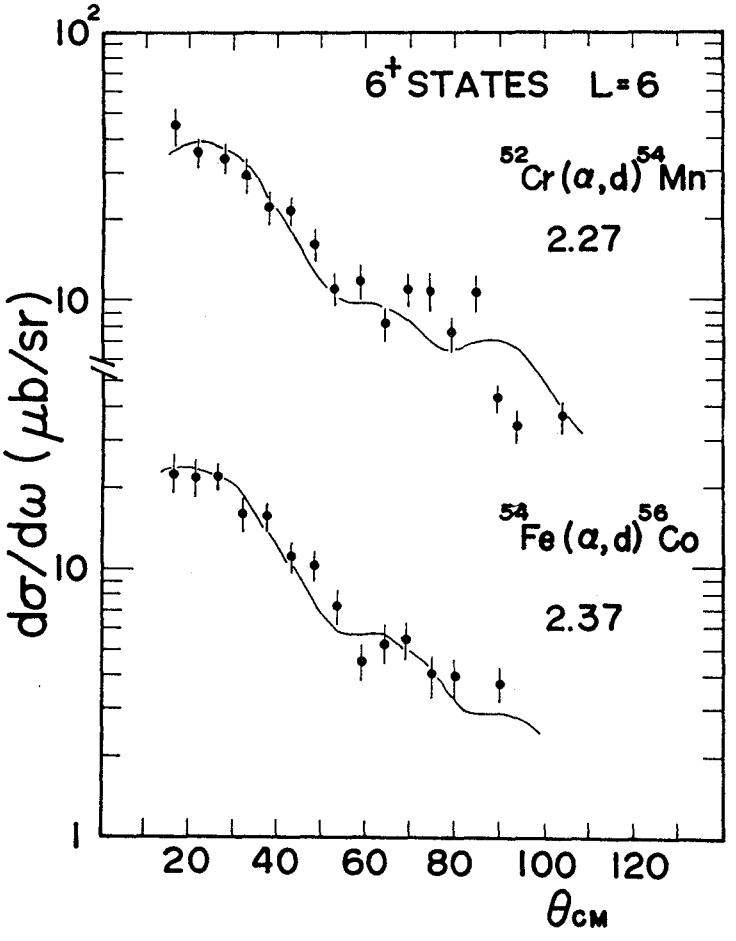
6+ STATES L=6
52Cr(α,d)54Mn
2.27
54Fe(α,d)56Co
2.37
dσ/dω (μb/sr)
10²
10
10
1
20
40
60
80
100
120
θcm

Fig. 7-10.

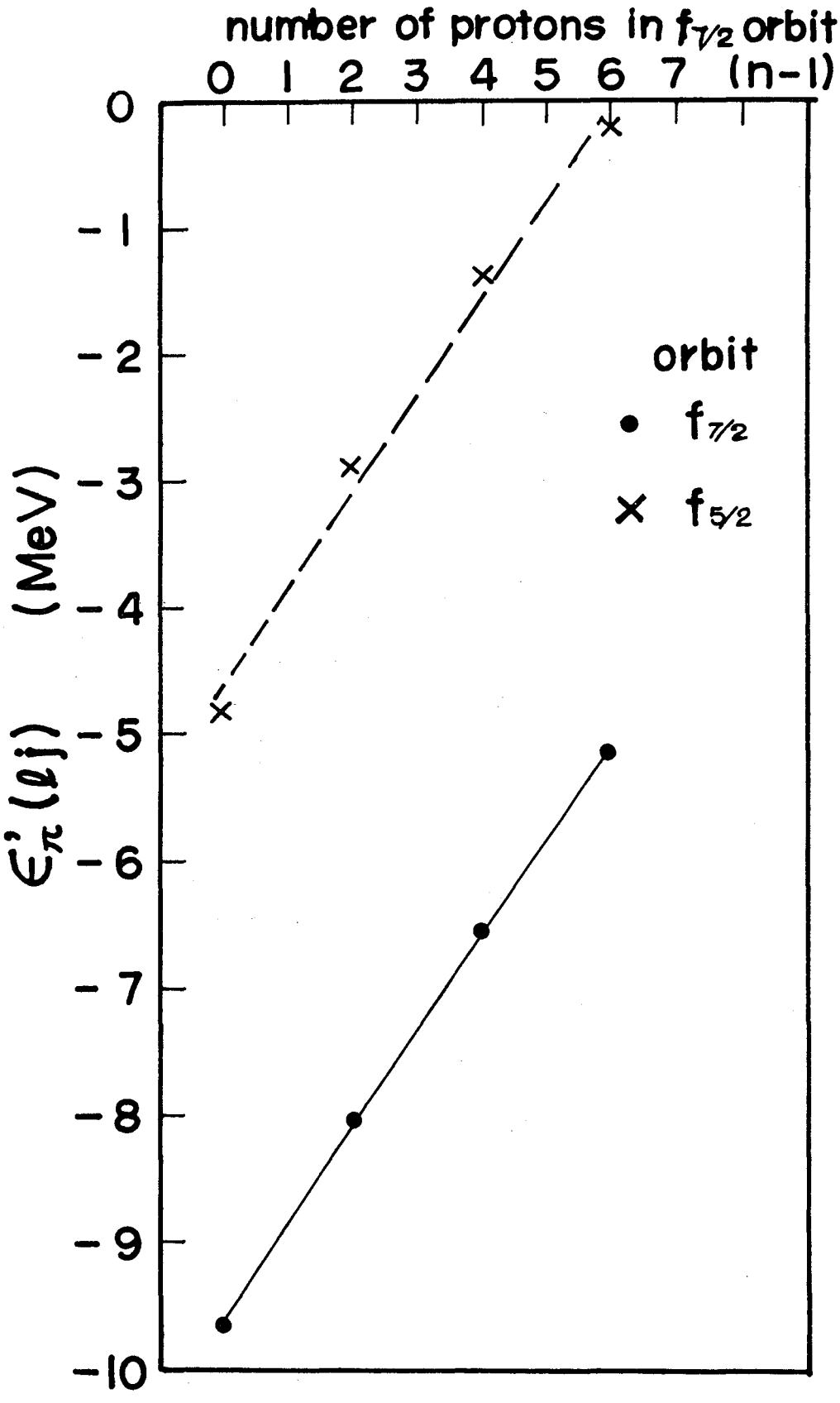
number of protons in $f_{7/2}$ orbit
0 1 2 3 4 5 6 7 (n-l)
0
-1
-2
-3
-4
-5
-6
-7
-8
-9
-10
ϵ'_π (lj) (MeV)
orbit
$f_{7/2}$
$f_{5/2}$

Fig. 7-11.

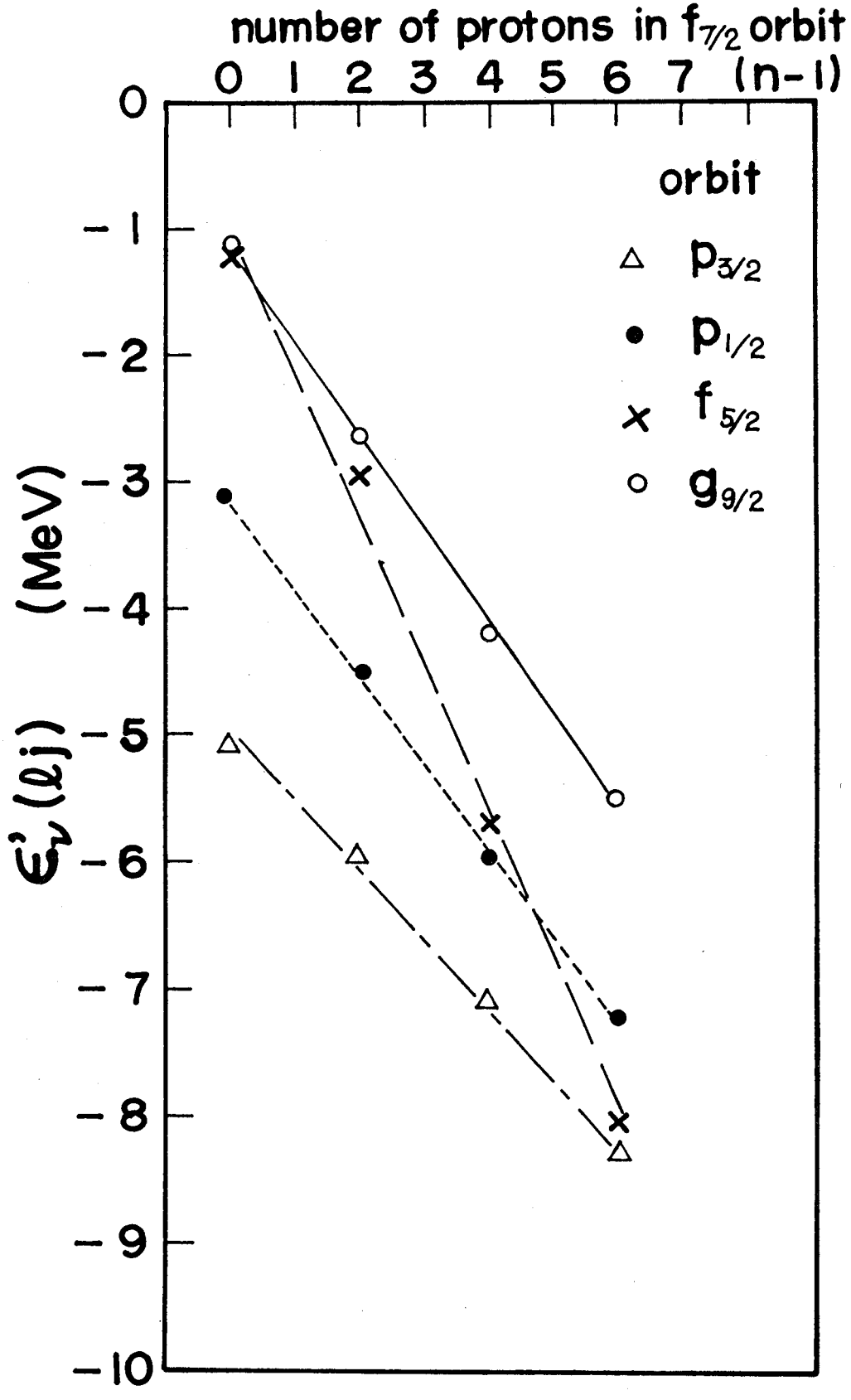
number of protons in $f_{7/2}$ orbit
0 1 2 3 4 5 6 7 (n-1)
0
-1
-2
-3
-4
-5
-6
-7
-8
-9
-10
$\epsilon'_\nu(lj)$ (MeV)
orbit
$p_{3/2}$
$p_{1/2}$
$f_{5/2}$
$g_{9/2}$

Fig. 7-12.

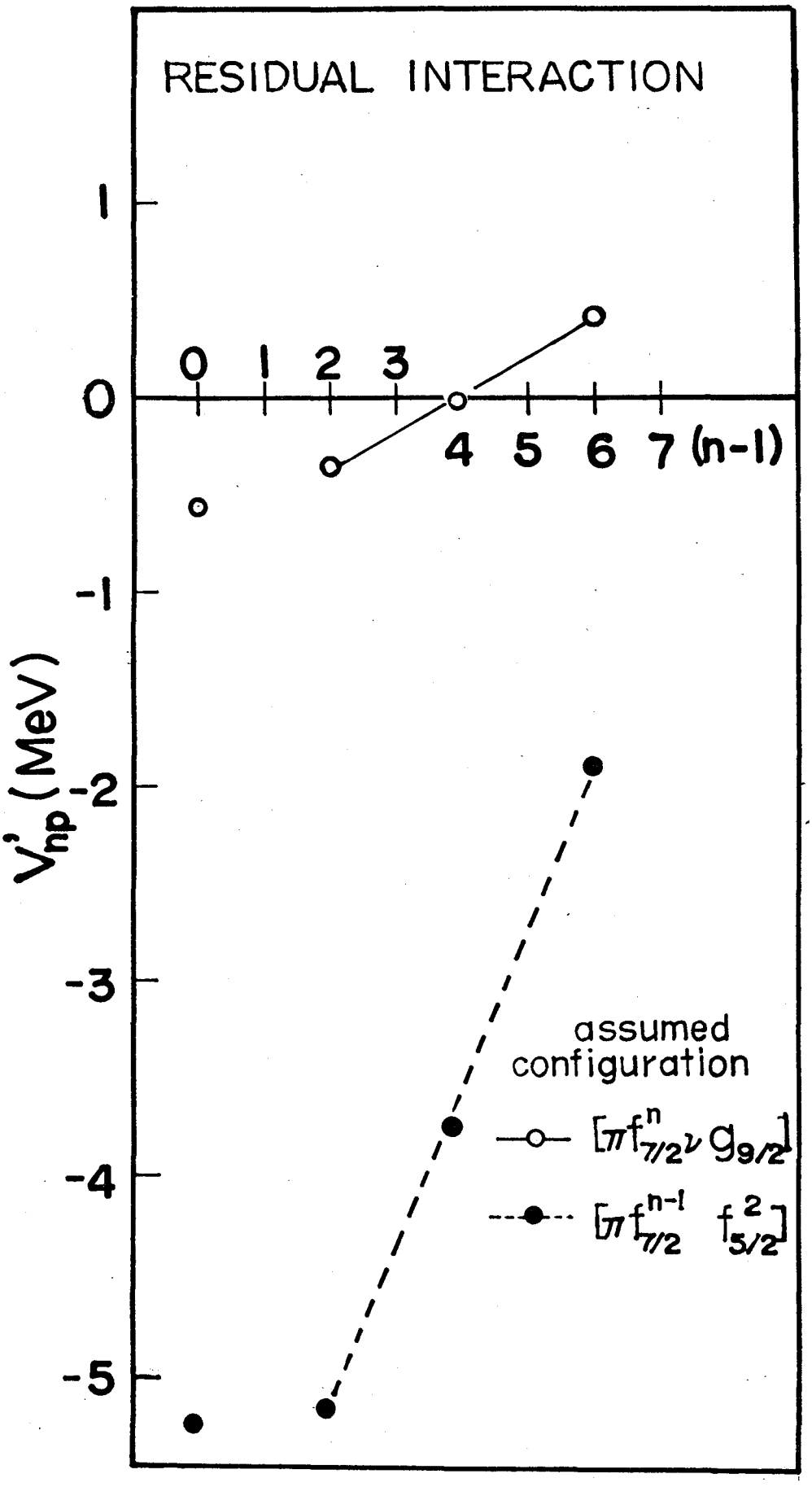
RESIDUAL INTERACTION
1
0
-1
-2
-3
-4
-5
0 1 2 3
4 5 6 7 (n-1)
V'_{np} (MeV)
assumed configuration
$[\pi f^{n}_{7/2} \nu g_{9/2}]$
$[\pi f^{n-1}_{7/2} f^{2}_{5/2}]$

Table 3-1. Isotopic abundance and thickness of the targets.

Nucleid	Thickness ($\mu g/cm^2$)	Enrichment (%)	
^{50}Ti	86.8	69.7	self-support
^{52}Cr	51.5	99.87	self-support
^{54}Fe	80.9	92.3	carbon backing
^{56}Fe	65.3	99.93	carbon backing

Table 4-I. Summary of the present $^{54}Fe(\alpha,d)^{56}Co$ reaction and comparison with previous (d,α) and $(^3He,p)$ works.

No.	Present a) Ex. (MeV)	L (α,d)	σ(α,d) (μb)	N	previous works b) (assumed config)	Ex. (MeV)	L (d,α)	c) ^{3}L (^{3}He,p)	J^π (proposed)	J^π (best)	d) Theory Ex. (MeV)	J^π	configuration $\|p_{3/2}\rangle$	$\|p_{1/2}\rangle$	$\|f_{5/2}\rangle$
1.	0.000	4	30± 7	220	$f_{7/2}p_{3/2}$	0.000	(4)	——	4^+	4^+	0.00	4^+	0.921	+0.325	-0.218
2.	0.157	2+4	60± 8	74	$f_{7/2}p_{3/2}$	0.157	2	2	3^+	3^+	0.216	3^+	0.936	-0.268	+0.227
3.	0.576	4	238±20	95	$f_{7/2}p_{3/2}$	0.576	4	4	(5^+)	5^+	0.408	5^+	0.926		-0.377
4.	0.830	——	——			0.830	(4)	——	4^+		0.840	4^+	0.574	-0.567	+0.734
5.	1.00	2+4	182±16			0.970	2	2	2^+		0.984	2^+	0.158		+0.987
						1.009	4	——	5^+		1.264	5^+	0.377		+0.926
						1.114	(2+4)	——	3^+		1.139	3^+	-.304	-0.295	+0.905
6.		——	——												
						1.450	——	0	0^+	0^+					
7.		——	~ 0												
8.	1.718	0	329±27	1300	$f_{7/2}f_{5/2}$	1.720	0	0+2	1^+	1^+	3.495	1^+			1.000
				190	$p_{3/2}p_{3/2}$										
9.	1.92	2	318±25	410	$f_{7/2}p_{1/2}$	1.930	2	2	(3^+)		1.905	3^+	0.176	+0.917	+0.358
10.	2.06	2	33± 7			2.060	2	2	$1^+,2^+,3^+$						
11.	2.29					2.283	6	——	7^+						
		2	211±20			2.293	——	2	$1^+,2^+,3^+$						
12.	2.37	6	57± 9	120	$f_{7/2}f_{5/2}$	2.372	6	——	6^+	6^+	2.324	6^+			1.000

Table 4-I. (continued)

	Present					Previous works					Theory[d]		
No.	Ex. (MeV)	L (α,d)	σ(α,d)[a] (μb)	N	(assumed config)	Ex. (MeV)	L[b] (d,α)	L[c] (^{3}He,p)	J^π (proposed)	J^π (best)	Ex. (MeV)	J^π	configuration $\|p_{3/2}\rangle$ $\|p_{1/2}\rangle$ $\|f_{5/2}\rangle$
13.	2.47	(4)	52± 8	102	$f_{7/2}p_{1/2}$	2.469	(4,3)	4	$3^+,4^+,5^+$		2.636	4^+	-.115 +0.757 +0.643
14.	2.73	0	52± 8			2.730	0	——	1^+	1^+			
15.	2.79	——	30± 8			2.773	——	——					
16.	3.07	0	172±30			3.074	2	2	1^+	1^+			
17.	3.18	<3				3.178	(2)	2	$1^+,2^+,3^+$				
						3.638			8^+				
						4.180			9^+				
18.	4.99	7	148±35	120	$f_{7/2}g_{9/2}$	4.991	——	——	———	8^-			
19.	5.08	——				5.081							
						5.275	——	——	10^+				
20.	5.31	——				5.337	——	strong					
21.	5.47	——											

a) Integrated from 14° to 105° $\quad \sigma(\alpha,d)=2\pi \int_{14°}^{105°} (d\sigma/d\omega)_{CM} \sin(\theta_{CM})\, d\theta_{CM}.$

b) Schneider et al. ref.14)

c) Laget et al. ref. 26)

d) Horie and Ogawa ref.54)

Table 5-I. Spectroscopic factors and transformation coefficients from j-j to L-S coupling scheme of the $^{54}Fe(\alpha,d)^{56}Co$ reaction with the $[\pi(\ell_p j_p)\nu(\ell_n j_n)]_{L,J}$ transfer.

Orbits of transferred two-nucleon $(\ell_p j_p)(\ell_n j_n)$	Transferred angular momentum L	J	Transformation coefficient from j-j to L-S coupling scheme	Spectroscopic factor for the (α,d) reaction S(fm^3)
$f_{7/2}$ $p_{3/2}$	2	2	-0.6172	0.1156
	2	3	0.6389	0.1239
	4	3	-0.1429	0.0094
	4	4	-0.2182	0.0220
	4	5	1.0000	0.4625
$f_{7/2}$ $p_{1/2}$	2	3	0.7377	0.1652
	4	3	0.1237	0.0071
	4	4	0.6455	0.1491
$f_{7/2}$ $f_{5/2}$	0	1	0.5714	0.1930
	2	1	0.3912	0.0310
	2	2	0.7071	0.1012
	2	3	0.4830	0.0473
	4	3	0.3799	0.0373
	4	4	0.7071	0.1294
	4	5	0.3655	0.0345
	6	5	0.2456	0.0629
	6	6	0.7071	0.5210
$f_{7/2}$ $g_{9/2}$	1	1	0.5271	0.0622
	1	2	0.5118	0.0586
	3	2	-0.3564	0.0169
	3	3	0.1992	0.0053
	3	4	0.7182	0.0687

Table 5-I. continued

Orbits of transferred two-nucleon $(\ell_p j_p)(\ell_n j_n)$	Transferred angular momentum L	J	Transformation coefficient from j-j to L-S coupling scheme	Spectroscopic factor for the (α,d) reaction S(fm^3)
$f_{7/2}$ $g_{9/2}$	5	4	-0.2254	0.0107
	5	5	0.1054	0.0023
	5	6	0.8648	0.1576
	7	6	-0.0915	0.0081
	7	7	-0.0476	0.0022
	7	8	1.0000	0.9647
$p_{3/2}$ $p_{3/2}$	0	1	0.6086	1.3204
	2	1	-0.2722	0.1650
	2	3	1.0000	2.2269
$f_{5/2}$ $f_{5/2}$	0	1	-0.3194	0.2402
	2	1	0.6999	0.3966
	2	3	-0.2291	0.0535
	4	3	0.8009	0.6544
	4	5	-0.0963	0.0096
	6	5	0.9318	3.6184

Table 5-II. Optical potential parameters used in the present DWBA calculations.

Channel		V(MeV)	W(MeV)	W_D(MeV)	a(fm)	a_I(fm)	r_0(fm)	r_I(fm)	r_C(fm)	reference
alpha	A1	169.8	25.1		0.494	0.494	1.445	1.445	1.30	57)
	A2	182.0	14.5		0.724	0.564	1.200	1.67	1.30	14)
d	D1	111.3		18.04	0.886	0.736	1.038	1.307	1.038	59)
	D2	88.5		16.5	0.629	0.860	1.200	1.110	1.105	14)
t, ^{3}He	T	170.0	16.5		0.752	0.817	1.160	1.498	1.30	65)
bound state										
d	F1	adjusted			0.55		1.27		1.30	
	F2	adjusted			0.55		1.35		1.30	
p		adjusted			0.65		1.25		1.30	
n		adjusted			0.65		1.25			

$D_0^2(\alpha,t) = D_0^2(\alpha,{}^3He) = 24.0 \times 10^4$ MeV^{2}fm^3 55)

$D_0^2(t,d) = 5.06 \times 10^4$ MeV^{2}fm^3 66)

$D_0^2({}^3He,d) = 4.42 \times 10^4$ MeV^{2}fm^3 66)

Optical potential has a form of

$$V(r) = -V(e^x+1)^{-1} - i(W-4W_D\frac{d}{dx'})(e^{x'}+1)^{-1} + V_C(r,r_C) \text{ , with } x=(r-r_0A^{1/3})/a \text{ and } x'=(r-r_IA^{1/3})/a_I.$$

Table 7-I. Summary of the low-lying high spin states. Excitation energies and total cross sections are presented. Theoretical cross sections were obtained by assuming the final states have pure configurations of $[\pi f_{7/2}^{n} \nu p_{3/2}^{m}]_{5^+}$.

Nucleus	Ex. (MeV)	$\sigma_{exp.}$ [a] (μb)	σ_{DWBA} [a][b] (μb)	σ_{DWBA} [a][b][c] (μb)	(n-l)
^{52}V	0.020 ± 0.020	1500 ± 200	1060	1350	6
^{54}Mn	0.363 ± 0.010	540 ± 70	540	——	4
^{56}Co	0.576 ± 0.010	210 ± 30	230	——	2
^{58}Co	0.020 ± 0.020	135 ± 20	100	120	2

a) Total cross section here defined is

$$\sigma = 2\pi \int_{14^\circ}^{82^\circ} (d\sigma/d\omega)_{CM} \sin(\theta_{CM})\, d\theta_{CM} \quad .$$

b) Normarization factor of the (α,d) reaction N=100 is already multiplied.

c) Cross sections of the unresolved multiplets were estimated by assuming that they have pure $[\pi f_{7/2}^{n} \nu p_{3/2}^{m}]_J$ configurations. For ^{52}V ; $J^\pi = 2^+$ and 3^+ and for ^{58}Co ; $J^\pi = 2^+$ and 4^+.

Table 7-II. Experimental results for the higher excited high spin states. Excitation energies and total cross sections are presented. DWBA cross sections were obtained by assuming that the final states have pure $[\pi f_{7/2}^{n} \nu g_{9/2}]_{8^-}$ or $[\pi f_{7/2}^{n-1}(0^+)\pi f_{5/2}\nu f_{5/2}]_{5^+}$ configuration. States with these configurations are expected to lie at 4 MeV or more high excitation energies.

Nucleus	Ex.(MeV)	$\sigma_{exp.}$ [a] (μb)	$\sigma_{DWBA}(8^-)$ [a,b] (μb)	$\sigma_{DWBA}(5^+)$ [a,b] (μb)	(n-1)
^{52}V	4.32 ± 0.03	790 ± 120	580	350	6
^{54}Mn	4.72 ± 0.02	360 ± 50	280	270	4
^{56}Co	4.99 ± 0.02	130 ± 25	105	190	2
^{58}Co	3.75 ± 0.03	145 ± 30	125	230	2

a) Total cross section here defined is

$$\sigma = 2\pi \int_{14^\circ}^{82^\circ} (d\sigma/d\omega)_{CM} \sin(\theta_{CM})\, d\theta_{CM} \quad .$$

b) Normarization factor of the (α,d) reaction N=100 has been already multiplied.

Table 7-IV. Neutron and proton single particle informations obtained from experimentally observed levels of odd-mass nuclei. Energy centroids, summed spectroscopic factors and binding energies for $p_{3/2}$, $p_{1/2}$, $f_{5/2}$ and $g_{9/2}$ neutron and $f_{7/2}$ and $f_{5/2}$ proton orbits are shown.

neutron

orbit	$p_{3/2}$			$p_{1/2}$			$f_{5/2}$			$g_{9/2}$		
Nucl.	$\overline{Ex}$ (MeV)	$\Sigma S_{\ell j}$	$\varepsilon'_\nu(\ell j)$ (MeV)	$\overline{Ex}$ (MeV)	$\Sigma S_{\ell j}$	$\varepsilon'_\nu(\ell j)$ (MeV)	$\overline{Ex}$ (MeV)	$\Sigma S_{\ell j}$	$\varepsilon'_\nu(\ell j)$ (MeV)	$\overline{Ex}$ (MeV)	$\Sigma S_{\ell j}$	$\varepsilon'_\nu(\ell j)$ (MeV)
^{49}Ca [a)]	0.00	1.03	-5.14	2.03	1.33	-3.11	3.95	0.89	-1.19	4.02	0.31	-1.12
^{51}Ti [b)]	0.40	1.13	-5.98	1.90	1.24	-4.48	3.45	0.94	-2.94	3.76	0.58	-2.62
^{53}Cr [b)]	0.80	1.10	-7.14	1.98	1.18	-5.96	2.25	0.90	-5.69	3.72	0.74	-4.22
^{55}Fe [b)]	0.93	1.10	-8.36	2.09	1.20	-7.20	1.24	0.90	-8.05	3.81	0.50	-5.49
^{57}Fe [c)]	0.64	0.83	-7.00	2.01	1.13	-5.63	1.19	0.91	-6.45	2.45	0.45	-5.19

proton

orbit	$f_{7/2}$			$f_{5/2}$		
Nucl.	$\overline{Ex}$ (MeV)	$\Sigma S_{\ell j}$	$\varepsilon'_\pi(\ell j)$ (MeV)	$\overline{Ex}$ (MeV)	$\Sigma S_{\ell j}$	$\varepsilon'_\pi(\ell j)$ (MeV)
^{49}Sc [a)]	0.00	1.00	-9.62	4.77	1.54	-4.85
^{51}V [d)]	0.00	0.91	-8.06	5.15	0.54	-2.91
^{53}Mn [e)]	0.00	0.47	-6.56	5.20	1.21	-1.36
^{55}Co [f)]	0.00	0.21	-5.05	4.85	1.00	-0.20
^{57}Co [g)]	0.00	0.20	-6.02	3.50	0.88	-2.52

a) Nuclear Data Sheet B4

b) D.C.Kocher and W.Haeberli ref. 71)

c) J.A.Thomson, ref. 72)

d) Nuclear data Sheets 23, D.J.Pullen et al. ref. 73) S.Gales et al. ref. 74)

e) D.D.Armstrong et al.ref. 75), S.Gales et al.ref.76)

f) S.Fortier et al. ref. 77)

g) Nuclear Data Sheets 20

Table 7-III. Experimentally obtained two-particle residual interaction energies ($V'^{pn}(j_1 j_1 J)$) for higher excited states. Assumed configurations are $[\pi f_{7/2}^{n} \nu g_{9/2}]_{J=8^-}$ and $[\pi f_{7/2}^{n-1}(0^+) \pi f_{5/2} \nu f_{5/2}]_{J=5^+}$. Also the binding energies of proton and neutron in an orbit (ℓj) used in the calculations are listed.

Nucleus	Ex.(MeV)	$\varepsilon'_\pi(f_{7/2})$ (MeV)	$\varepsilon'_\nu(g_{9/2})$ (MeV)	$V'^{pn}(8^-)$ (MeV)	$\varepsilon'_\pi(f_{5/2})$ (MeV)	$\varepsilon'_\nu(f_{5/2})$ (MeV)	$V'^{pn}(5^+)$ (MeV)
^{50}Sc	(4.42) [a]	-9.62	-1.12	———	-4.85	-1.19	———
^{52}V	4.32±0.03	-8.06	-2.62	-0.38	-2.91	-2.94	-5.18
^{54}Mn	4.72±0.02	-6.56	-4.22	-0.02	-1.36	-5.69	-3.75
^{56}Co	4.99±0.02	-5.05	-5.49	+0.39	-0.20	-8.05	-1.91
^{58}Co	3.75±0.03	-6.02	-5.19	+0.17	-2.52	-6.45	-2.07

a) data taken from the work by C.Moazed et al. ref.18)

Table 7-V. Comparison between the experimental and theoretical single particle, p-n residual interaction and average p-n interaction energies.

single particle energy	present (MeV)	δ-force (MeV)	Horie and Ogawa[54] (MeV)	Kuo and Brown[79] (MeV)
$\varepsilon_\pi(f_{7/2})$	-9.60	——	——	——
$\varepsilon_\pi(f_{5/2})$	-4.75	——	——	——
$\varepsilon_\nu(p_{3/2})$	-4.90	——	-5.14	——
$\varepsilon_\nu(p_{1/2})$	-3.13	——	-3.12	——
$\varepsilon_\nu(f_{5/2})$	-1.15	——	-1.19	——
$\varepsilon_\nu(g_{9/2})$	-1.10	——	——	——
<u>average p-n interaction</u>				
$\bar{V}^{pn}(f_{7/2}p_{3/2})$	-0.58		-0.61	-0.53
$\bar{V}^{pn}(f_{7/2}p_{1/2})$	-0.69		-0.72	-0.60
$\bar{V}^{pn}(f_{7/2}f_{5/2})$	-1.14		-1.04	-0.91
$\bar{V}^{pn}(f_{7/2}g_{9/2})$	-0.73	-0.69	——	——
$\bar{V}^{pn}(f_{7/2}s_{1/2})$	——		——	-0.53
$\bar{V}^{pn}(f_{7/2}d_{5/2})$	——		——	-0.51
$\bar{V}^{pn}(f_{7/2}d_{3/2})$	——		——	-0.79
<u>p-n residual interaction of stretched configuration</u>				
$V^{pn}(f_{7/2}p_{3/2}\ 5^+)$	——		-1.02	-0.98
$V^{pn}(f_{7/2}p_{1/2}\ 4^+)$	——		-0.78	-0.50
$V^{pn}(f_{7/2}f_{5/2}\ 6^+)$	——		-1.36	-1.50
$V^{pn}(f_{7/2}g_{9/2}\ 8^-)$	-0.76	-1.42	——	——
$V^{pn}(f_{7/2}s_{1/2}\ 4^-)$	——		——	-0.65
$V^{pn}(f_{7/2}d_{5/2}\ 6^-)$	——		——	-1.04
$V^{pn}(f_{7/2}d_{3/2}\ 5^-)$	——		——	-0.94
<u>p-p interaction of T=1</u>				
$V_0^{pp}(f_{7/2}f_{7/2})$	-2.52		——	-1.81
$E_0^{pp}(f_{7/2}f_{7/2})$	2.21		——	——